

AD-A121 178

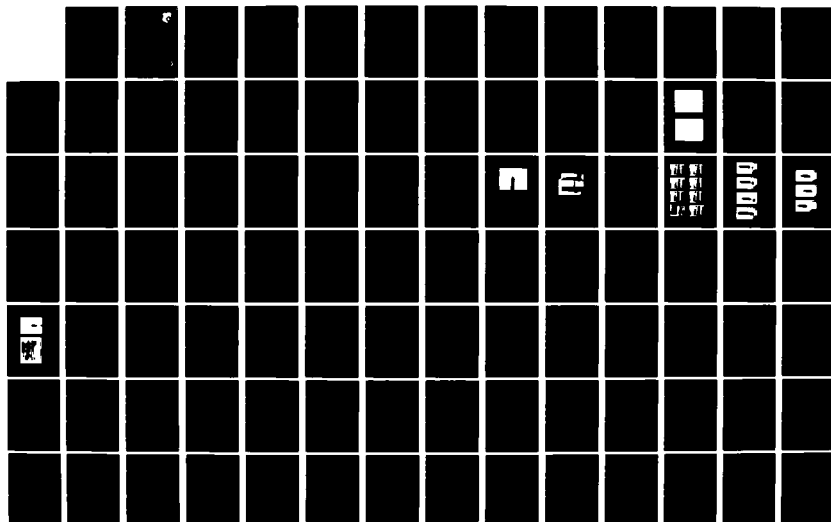
A STUDY OF THE J-INTEGRAL METHOD USING POLYCARBONATE  
(U) SYSTEMS RESEARCH LABS INC DAYTON OH RESEARCH  
APPLICATIONS DIV H L BERNSTEIN AUG 82 AFMAL-TR-82-4080  
F33615-79-C-5025

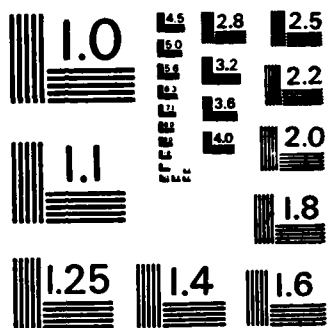
1/2

UNCLASSIFIED

F/G 11/9

NL





MICROCOPY RESOLUTION TEST CHART  
NATIONAL BUREAU OF STANDARDS - 1963 - A

12

AFWAL-TR-82-4080

A STUDY OF THE J-INTEGRAL METHOD  
USING POLYCARBONATE

Henry L. Bernstein



Research Applications Division  
Systems Research Laboratories, Inc.  
2800 Indian Ripple Road  
Dayton, Ohio 45440

August 1982

Technical Report for Period April 1976 - May 1981

Approved for public release; distribution unlimited.

MATERIALS LABORATORY  
AIR FORCE WRIGHT AERONAUTICAL LABORATORIES  
AIR FORCE SYSTEMS COMMAND  
WRIGHT-PATTERSON AIR FORCE BASE, OHIO 45433

DTIC  
ELECTE  
NOV 08 1982  
S D  
E

82 11 08 002

ADA121170

RECEIVED COPY

NOTICE

When Government drawings, specifications, or other data are used for any purpose other than in connection with a definitely related Government procurement operation, the United States Government thereby incurs no responsibility nor any obligation whatsoever; and the fact that the Government may have formulated, furnished, or in any way supplied the said drawings, specifications, or other data, is not to be regarded by implication or otherwise as in any manner licensing the holder or any other person or corporation, or conveying any rights or permission to manufacture use, or sell any patented invention that may in any way be related thereto.

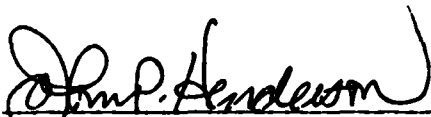
This report has been reviewed by the Office of Public Affairs (ASD/PA) and is releasable to the National Technical Information Service (NTIS). At NTIS, it will be available to the general public, including foreign nations.

This technical report has been reviewed and is approved for publication.



THEODORE NICHOLAS  
PROJECT ENGINEER  
METALS BEHAVIOR BRANCH

FOR THE COMMANDER



JOHN P. HENDERSON, CHIEF  
METALS BEHAVIOR BRANCH

"If your address has changed, if you wish to be removed from our mailing list, or if the addressee is no longer employed by your organization, please notify AFWAL/MLLN, W-PAFB, OH 45433 to help us maintain a current mailing list".

Copies of this report should not be returned unless return is required by security considerations, contractual obligations, or notice on a specific document.

Unclassified

SECURITY CLASSIFICATION OF THIS PAGE (When Data Entered)

REPORT DOCUMENTATION PAGE		READ INSTRUCTIONS BEFORE COMPLETING FORM
1. REPORT NUMBER AFWAL-TR-82-4080	2. GOVT ACCESSION NO. A121170	3. RECIPIENT'S CATALOG NUMBER
4. TITLE (and Subtitle) A STUDY OF THE J-INTEGRAL METHOD USING POLYCARBONATE		5. TYPE OF REPORT & PERIOD COVERED Technical Report April 1976 - May 1981
		6. PERFORMING ORG. REPORT NUMBER
7. AUTHOR(s) Henry L. Bernstein		8. CONTRACT OR GRANT NUMBER(s) F33615-76-C-5191 F33615-79-C-5025
9. PERFORMING ORGANIZATION NAME AND ADDRESS Research Applications Division Systems Research Laboratories, Inc. 2800 Indian Ripple Rd., Dayton, OH 45440		10. PROGRAM ELEMENT, PROJECT, TASK AREA & WORK UNIT NUMBERS Prog. Elements 62102F, 61102F; Projects 7351, 2307; Task Areas 735106, 2307P1; Work Units 73510690, 2307P112
11. CONTROLLING OFFICE NAME AND ADDRESS Materials Laboratory (AFWAL/MLLN) Air Force Wright Aeronautical Laboratories Wright-Patterson Air Force Base, OH 45433		12. REPORT DATE August 1982
14. MONITORING AGENCY NAME & ADDRESS (if different from Controlling Office)		13. NUMBER OF PAGES 137
		15. SECURITY CLASS. (of this report)  Unclassified
		15a. DECLASSIFICATION/DOWNGRADING SCHEDULE
16. DISTRIBUTION STATEMENT (of this Report)  Approved for public release; distribution unlimited.		
17. DISTRIBUTION STATEMENT (of the abstract entered in Block 20, if different from Report)		
18. SUPPLEMENTARY NOTES		
19. KEY WORDS (Continue on reverse side if necessary and identify by block number) Polycarbonate J-Integral Tearing Modulus Fracture of Plastics Non-Linear Fracture Mechanics		
20. ABSTRACT (Continue on reverse side if necessary and identify by block number) In this experimental program the crack-growth resistance of a model material, polycarbonate, was investigated using the J-integral method. Deeply cracked, three-point-bend specimens having crack lengths ranging from 0.6 to 0.8 of the specimen width and thicknesses ranging from 1 to 0.125 in. were tested. The J-integral was found to provide a good measure of crack initiation and growth in polycarbonate. Over these ranges, no effect of thickness or crack length on the fracture behavior was found. The J-integral value of the fracture toughness was 9 psi-in. at the beginning of crack growth, 25 psi-in. at 2% crack growth, and 41 psi-in.		

DD FORM 1 JAN 73 1473 EDITION OF 1 NOV 65 IS OBSOLETE

Unclassified

SECURITY CLASSIFICATION OF THIS PAGE (When Data Entered)

20. Abstract continued.

at pop-in. The crack growth followed an exponential relation with J. Data in the literature on other materials also obeyed an exponential relation. This relation was used to evaluate  $J_{IC}$  and to extend the application of the tearing modulus.

# FOREWORD

The work described in this report was performed at the Metals Behavior Branch, Metals and Ceramics Division, Materials Laboratory, Air Force Wright Aeronautical Laboratories (AFWAL/MLLN), under Contracts F33615-76-C-5191 and F33615-79-C-5025. The contracts were administered under the direction of AFWAL by Dr. Theodore Nicholas (MLLN). The programs were conducted by the Research Applications Division, Systems Research Laboratories, Inc., Dayton, OH, with Dr. Noel Ashbaugh as the Principal Investigator.

The author would like to thank Dr. Noel Ashbaugh of SRL for his encouragement and many valuable discussions, Dr. Theodore Nicholas of AFWAL/MLLN for his support, Mr. Richard Klinger of SRL for his assistance in running the tests, Mr. George Mornhinweg of SRL for preparing the specimens, Messrs. Doug Deaton and Dale Silver of SRL for assistance in reducing the data, and Mrs. Judith Paine for typing the manuscript.

Accession For	
NTIS GRA&I	<input checked="" type="checkbox"/>
DTIC TAB	<input type="checkbox"/>
Unannounced	<input type="checkbox"/>
Justification	
By	
Distribution/	
Availability Codes	
Dist	Avail and/or Special
A	



## TABLE OF CONTENTS

Section	Page
1 INTRODUCTION	1
2 EXPERIMENTAL CONSIDERATIONS	9
Material	9
J-Integral Test Method and Test Matrix	19
Crack-Length Measurement	23
3 RESULTS AND DISCUSSION	33
Load-Displacement Behavior of the Specimen	33
Crack-Growth Behavior	38
Fracture Criteria	48
4 CONCLUSIONS	59
REFERENCES	60
APPENDIX A: LOAD-DISPLACEMENT CURVES	64
APPENDIX B: J VS. CRACK GROWTH FOR POLYCARBONATE	79
APPENDIX C: DATA IN THE LITERATURE ON J VALUES AND CRACK GROWTH FOR VARIOUS MATERIALS	119



# LIST OF FIGURES

Figure		Page
1	"Dogbone" Tensile Specimen.	10
2	Stress-Strain Curve of Polycarbonate Specimen T-3.	13
3	Strain-Rate Effects upon Tensile Properties of Polycarbonate at Room Temperature.	15
4	Diamond-Shaped Flaw in Tensile Specimen (a) surface (b) depth. Maximum surface length is 0.138 in. and is perpendicular to the tensile axis.	16
5	Fatigue Crack Growth of Polycarbonate in the T-S Direction.	18
6	Three-Point-Bend Specimen.	20
7	Photograph of Crack and Craze Regions through the Side.	27
8	Photograph of Crack and Craze Regions through the End of Specimen 6.	28
9	Series of Photographs (Positive Images) Showing Crack Growth Observed through the End of Specimen 6.	30
10	Series of Photographs Showing Crack Growth in Specimen 10.	31
11	Typical Load-Displacement Curves.	34
12	Estimates of Extent of Yielding in Specimens at Maximum Load.	37
13	Master Plot of J as a Function of Apparent Crack Growth (Some of the Data May include Craze Length).	40
14	Plot of J as a Function of Crack Extension.	42
15	Plot of J as a Function of Crack Extension and Craze.	43
16	Fracture Surfaces.	47
17(a)	Tearing Modulus as a Function of Crack Growth from Exponential and Linear Fits of J vs $\Delta a$ .	
(b)	Tearing Modulus as a Function of J from Exponential and Linear Fits of J vs $\Delta a$ .	56

## LIST OF TABLES

Table		Page
1	Tensile-Test Results	11
2	Summary of Thickness, Initial Crack Length, and Crack-Growth Behavior	21
3	Compliance and Limit Loads	35
4	Fracture Criteria	50

## SECTION 1

### INTRODUCTION

The purpose of this investigation was to study experimentally the initiation and crack growth of cracks under monotonic loading using the J-integral method. Polycarbonate (PC) was used as a model material in the experiments because it is both ductile and transparent. The study was conducted in the regime of large plastic strains where linear-elastic fracture mechanics (LEFM) is invalid and non-linear fracture-mechanics (NLFM) concepts must be used. The J-integral was studied because it is the most promising of these concepts.

Crack growth under large plastic strains is an important engineering problem. Some materials are extremely ductile and can, therefore, withstand large amounts of plastic strain before the initiation of crack growth. Whenever the plastic zone size at the crack tip becomes of the same order of magnitude as other in-plane geometrical dimensions, LEFM is invalid. Thus, the fracture and safety of structures made from such ductile materials can only be determined using NLFM.

The J-integral for two-dimensional problems which was proposed by Rice<sup>1</sup> is a path-independent integral around a crack tip for a non-linear elastic material. The integral derived earlier by Eshelby<sup>2</sup> is defined for a crack parallel to the x-axis as

$$J = \int_{\Gamma} \left( W dy - \vec{T} \cdot \frac{\partial \vec{u}}{\partial x} ds \right) \quad (1)$$

where  $\Gamma$  is a path starting at the lower crack surface and extending in a counterclockwise direction around the crack tip to the upper surface;  $W$  is the strain-energy density;  $\vec{T}$  is the traction vector along the path; and  $\vec{u}$  is the displacement vector along this path. The value  $J$  of the J-integral has been shown by McClintock<sup>3</sup> to characterize the stress and strain field about the crack tip for a power-law hardening material

$$\sigma_{ij} = A \left( \frac{J}{A I r} \right)^{\frac{n}{n+1}} \bar{\sigma}_{ij}(\theta) \quad (2a)$$

$$\epsilon_{ij} = \left( \frac{J}{A I r} \right)^{\frac{n}{n+1}} \bar{\epsilon}_{ij}(\theta) \quad (2b)$$

where A and n are constants in the power-law-hardening equation:  $\bar{\sigma} = A(\bar{\epsilon}_p)^n$ , where  $\bar{\sigma}$  and  $\bar{\epsilon}_p$  are the equivalent stress and equivalent plastic strain, respectively; I is a function<sup>4</sup> of n; r is the radial distance from the crack tip; and  $\bar{\sigma}_{ij}(\theta)$  and  $\bar{\epsilon}_{ij}(\theta)$  are functions of the angular distance from the crack tip. Equations (2a) and (2b) are based upon the crack-tip model of Hutchinson<sup>5</sup> and Rice and Rosengren<sup>6</sup> which shows that the product of stress and strain has a  $1/r$  singularity. The crack-tip analysis is valid as long as no unloading occurs at the crack tip, such as that which takes place when the crack grows. However, this analytical restriction does not preclude experimental attempts to use the J-integral after crack growth has begun. The J-integral may sufficiently characterize the stress and strain fields of the growing crack.

Under conditions of LEFM, the value of J is equivalent to the strain-energy release rate, G. J and G are related to the stress-intensity factor K by

$$J = G = K^2/E \text{ for plane stress} \quad (3a)$$

$$J = G = (1-\nu^2)K^2/E \text{ for plane strain} \quad (3b)$$

where E is the elastic modulus and  $\nu$  is Poisson's ratio.

A method of measuring the value of the J-integral experimentally was developed by Begley and Landes;<sup>7</sup> this method was based upon the following definition of J:

$$J = - \frac{\partial U}{\partial a} \quad (4)$$

where  $U$  is the potential energy per unit thickness and  $a$  is the crack length. The first method which they proposed was a graphical data-reduction scheme requiring the use of multiple specimens. The end result was a graph of  $J$  vs. load-point displacement. Later, they proposed a second method<sup>8</sup> based upon an estimation formula for  $J$  from the fully plastic behavior<sup>9</sup> of the specimen. With this second method, a graph of  $J$  vs. amount of crack growth,  $\Delta a$ , was developed; this graph was called a J-Integral Resistance Curve. From this curve, the value of  $J$  at the beginning of crack growth ( $J_{IC}$ ) could be determined. It has been shown by Griffis and Yoder<sup>10</sup> and by Landes, et al.,<sup>11</sup> that these two methods of measuring  $J$  are equivalent.

Crack growth takes place when the sharp fatigue precrack forms a blunt crack tip followed by fracture of the material ahead of the tip.<sup>12</sup> This crack-tip blunting advances the crack length and is, therefore, included in the amount of crack growth,  $\Delta a$ . The relation between  $J$  and the amount of crack growth caused by blunting,  $\Delta a_B$ , has been given by a formalized blunting line,<sup>8</sup>

$$\Delta a_B = \frac{J}{2\sigma_f} \quad (5)$$

where  $\sigma_f$  is the flow stress--usually defined as the average of the yield and ultimate stresses. Some controversy exists over the factor of 2 in Eq. (5).<sup>13</sup> The initiation of crack growth is said to have taken place when the measured amount of crack growth is greater than  $\Delta a_B$ . The value of  $J$  at this point is called  $J_{IC}$ , the fracture toughness of the material. It is thought to be a material property and is related to  $K_{IC}$  through Eq. (3b).

The J-integral has been used with success as a parameter to characterize the initiation of crack growth in a number of materials.<sup>7-8, 10, 14-24</sup> An ASTM standard is being developed for the measurement of the J-integral at the initiation of crack growth.<sup>14-15</sup>

The value of  $J_{IC}$  has been found to be independent of specimen size as long as a minimum size is exceeded:

$$B, a, b \geq \alpha \frac{J_{IC}}{\sigma_f} \quad (6)$$

where  $B$  is the specimen thickness;  $a$  is crack length;  $b$  is the remaining ligament;  $\alpha$  is a constant; and  $\sigma_f$  is the flow stress. The size criterion is governed by  $\alpha$  which has a value somewhere between 25 and 50, depending upon the material.

Many materials have much more resistance to fracture than indicated by  $J_{IC}$ . In order to utilize this additional fracture toughness in engineering design, a method called the Tearing Instability Theory has been proposed by Paris, et al.<sup>25</sup> This method is based upon structural compliance and the J-integral resistance curve. When the elastic recovery of the structure caused by crack growth cannot be absorbed by the plasticity around the crack tip, it must be absorbed by additional crack growth, in which case unstable crack growth takes place. Otherwise, the crack grows in a stable manner. The theory defines a material parameter called the tearing modulus,  $T$ , for characterizing the stable crack-growth behavior as

$$T = \frac{E}{\sigma_f} \frac{2}{da} \frac{dJ}{da} \quad (7)$$

where  $E$  and  $\sigma_f$  have been defined previously and  $dJ/da$  is the slope of the J-integral resistance curve. This slope is found from a linear approximation of the resistance curve, in the early stages of crack growth.

Polycarbonate (PC) was used as a model material because it is transparent and ductile. The transparency allowed the crack length to be measured as the crack grew, making it possible to generate a J-integral resistance curve for each specimen. With opaque materials, such as metals, each specimen yields only one data point unless special crack-length-measurement techniques are employed. Thus, six or more specimens are usually required to generate this curve. The ductility of PC meant that crack growth

could be studied under large plastic strains, which was the object of the research. The specific type of PC used was Lexan.

Crack growth in PC, and in most other polymers, occurs by the formation of a crazed zone ahead of the crack tip, followed by the rupture of the craze. As the craze breaks, the crack grows and a new craze forms. Reviews on the subject of crazing have been conducted by Kambour,<sup>26</sup> Brown,<sup>27</sup> and Kinloch,<sup>28</sup> as well as others; and crazing in PC has been studied by Fraser and Ward<sup>29</sup> and by Mills.<sup>30</sup> Crazing in polymers is a form of plastic deformation, the other type of plastic deformation being shearing. Crazing occurs by reorienting the molecular chains over a narrow, but sometimes long, region such that the chains, or fibrils, span the narrow gap. Between the fibrils is an open space, or void; therefore, crazing in polymers is similar to void formation in metals. Thus, the crazed region ahead of the crack tip in polymers may be analogous to the process zone ahead of the crack tip in metals. The craze cannot be considered as a crack because it carries a portion of the load. The micromechanics of craze formation, growth, and rupture are not well understood. Various theories--sometimes conflicting--have been proposed to explain the various aspects of crazing, but few are universally accepted.

Parvin and Williams<sup>31-32</sup> found in Markrolon PC that crack growth began at a value of  $2.24 \text{ MPa}\sqrt{\text{m}}$  ( $2040 \text{ psi}\sqrt{\text{in.}}$ ); and pop-in took place at  $4.00 \text{ MPa}\sqrt{\text{m}}$  ( $3640 \text{ psi}\sqrt{\text{in.}}$ ), with final fracture also occurring at this value of K. They used single-edge-notched specimens of dimension 150 by 50 mm (5.91 by 1.97 in.) with thicknesses of 3 mm (0.118 in.) and 5 mm (0.197 in.), having crack lengths ranging from 8 to 2 mm (0.315 to 0.079 in.). The crack tip was sharpened either by machining with a fly cutter of root radius  $< 0.5 \mu\text{m}$  (0.02 mils) or by razor blade. The specimens were pulled in tension, and net section yield with necking took place before fracture. Thus, the value of K at pop-in may not be accurate because the size of the plastic zone is not small with respect to the crack length. This problem does not appear to be present for the value of K at the beginning of crack growth. No effect of specimen thickness,

displacement rate of 0.05 and 0.5 cm/min. (0.02 to 0.2 in./min.), or the notch-sharpening technique employed was observed on these values of K.

Brinson<sup>33</sup> made a study of the plastic zone size about the crack tip in PC using photoelasticity and the Dugdale Model. He used a center-cracked panel (CCP) specimen of  $1.5 \times 4.0 \times 0.020$  in., containing a slit 0.015 in. high and 0.125 in. long. The slit had an 0.010-in.-long notch at each end and a root radius no larger than 0.005 in. Good agreement was found between the measured plastic zone size and that predicted by the Dugdale Model. From the data the value of G at which crack growth began was ~ 5 psi-in., and fracture occurred at 68 psi-in.

Mills<sup>30</sup> also studied the plastic zone size using photoelasticity and found good agreement between the data from experimental measurements and the predictions of the Dugdale model. He studied two other polymers in addition to a Merlon M-39 PC. He used a CCP specimen  $200 \times 75$  mm ( $7.87 \times 2.95$  in.) having crack lengths (2a) ranging from 10 to 20 mm (0.394 to 0.787 in.) and thicknesses of 0.5 to 6 mm (0.020 to 0.240 in.). Two types of yielding in the plastic zone were observed. For specimens 0.5-mm (0.020-in.) thick, shearing at a 45-deg. angle took place at the crack tip, whereas crazing occurred for specimens 1.5- to 6-mm thick (0.059 to 0.240 in.). (No data were reported between 0.5 and 1.5 mm). The shape of the crack front became semi-elliptical as the crack grew through the craze. At some point, the crack would grow rapidly and either fracture the specimen or arrest after forming two 45-deg. shear lips.

In a study of fatigue-crack retardation in PC, Banasiak<sup>34-35</sup> measured a value of  $3300 \text{ psi}\sqrt{\text{in.}}$  for  $K_{IC}$ . The sheet of PC used was the same as in the present study, but a different direction of crack growth was studied; Banasiak used the T-L direction, whereas the T-S direction was used in the present study. These directions are defined in ASTM Standard E399 for measuring  $K_{IC}$ .



Fraser and Ward<sup>29</sup> made a study of crazing and fracture of PC over the temperature range 22.5 to  $-70^{\circ}\text{C}$  and also analyzed their results by means of the Dugdale Model. They used a compact-tension specimen  $50 \times 46.7 \text{ mm}$  ( $1.97 \times 1.84 \text{ in.}$ ) (crack length was unreported). A sharp notch was made with a razor blade after the specimen was cooled to the temperature of liquid nitrogen,  $-210^{\circ}\text{C}$ . The craze shape was studied by machining out the section of the specimen containing the craze and crack tip and mounting it in a special apparatus. This apparatus wedged open the crack in order to permit photographs of an interference fringe pattern in the craze to be made. From these fringes, the height of the craze was calculated. Only one test of Lexan PC was made at room temperature ( $22.5^{\circ}\text{C}$ ), and this specimen was 6.48-mm (0.255-in.) thick. At the point where the crack began growing into the craze, the craze length was  $101.5 \mu\text{m}$  (4.00 mils); the crack-opening displacement was  $5.8 \mu\text{m}$  (0.23 mils); the craze stress was 58 MPa; and  $G$  was  $0.37 \text{ kJ/m}^2$ . These last two values were calculated from the Dugdale Model. The fracture toughness was found to be  $4.6 \text{ kJ/m}^2$ . The Dugdale Model yielded a good description of the craze length.

Key, Katz, and Parker<sup>36</sup> reported a  $K_{IC}$  value for PC of  $3290 \text{ psi}\sqrt{\text{in.}}$ . This value is in good agreement with the values given above.

The fracture properties of PC can be given in terms of  $J$  or  $G$ . Equation (3b) is used to calculate  $J$  from  $K$ ;  $E$  is taken to be 322,000 psi and  $\nu$  is 0.38. The plane-strain version is used because in all of the results (except for those of Brinson<sup>33</sup>), the thickness is sufficient to produce plane strain, as evidenced by the formation of crazes. Values of  $J$  at the beginning of crack growth range from 2.11 psi-in. as reported by Fraser and Ward<sup>29</sup> to 11.1 psi-in. by Parvin and Williams.<sup>31-32</sup> The low value may be due to the very sensitive crack-growth detection technique used. An intermediate value of  $\sim 5 \text{ psi-in.}$  could be obtained from Brinson's data, but the thickness of 0.020 in. is in the range of shear yielding reported by Mills.<sup>30</sup> The value of  $G_{IC}$  found by Fraser and Ward was 26.3 psi-in. and that found by Banasiak was 28.9 psi-in., giving an

average value of 27.6 psi-in. The value of J at pop-in was given as 35.2 psi-in. by Parvin and Williams, but large-scale plasticity makes this measurement questionable.

## SECTION 2

### EXPERIMENTAL CONSIDERATIONS

#### MATERIAL

The material used in the experimental program was polycarbonate (PC). PC was chosen as a model material because it is transparent and ductile. The transparency was of prime importance because it enabled the crack length to be continuously recorded during the test. Thus, a single specimen could be used to generate the J-integral resistance curve. With opaque materials, such as metals, it is necessary to use multiple specimens or special crack-length-detection techniques such as unloading compliance<sup>37</sup> on a single specimen to generate this curve. Of the available transparent materials, PC was chosen because of its good ductility, which made possible the attainment of fully plastic behavior before fracture. Other transparent materials, such as Plexiglass or glass, are brittle and fracture in the elastic regime.

The PC used was a standard-grade, unshrunk, 1-in.-thick sheet of Lexan.<sup>34</sup> Neither the detailed history of the sheet nor the molecular weight was known. The sheet appeared to have been made by laminating two 0.5-in.-thick sheets together. No influence of the lamination upon the mechanical properties was observed, and the longitudinal (L) and transverse (T) directions in the plane of the plate could not be determined. The crack-growth tests were conducted in such a way as to avoid the effects of the lamination.

The tensile properties of the PC were measured using the dogbone-shaped specimen shown in Fig. 1. All tests were run on a screw-driven Instron machine under displacement control. The results of the tensile tests are given in Table 1. The 0.2% offset yield stress and the ultimate stress were calculated using the original area of the specimen, whereas the necked area was used for calculation of the true stress at fracture. The 0.2% offset yield strength is a common measure of the yield strength of metals; however, in plastics, the ultimate stress as given in Table 1 is often

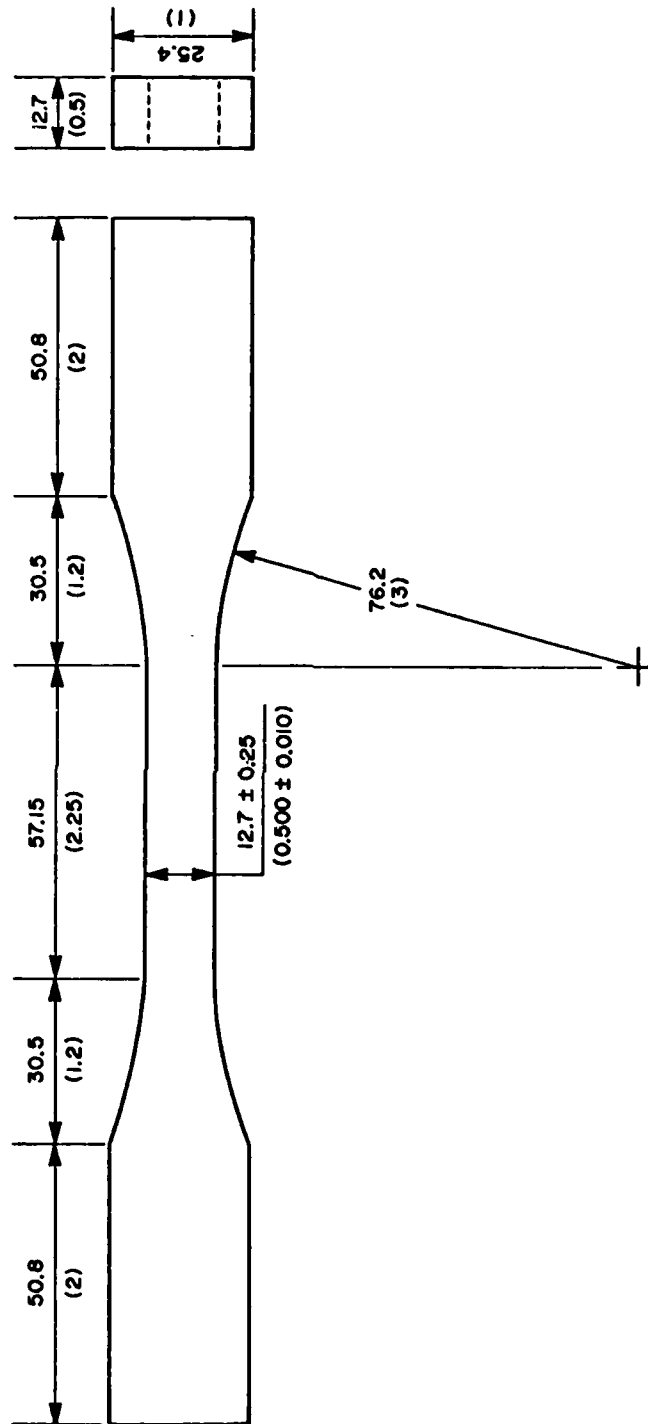


Figure 1. "Dogbone" Tensile Specimen [dimensions in mm (in.)].

Table 1  
TENSILE-TEST RESULTS

SPECIMEN NO.	DISPLACEMENT RATE mm/min. (in./min.)	ELASTIC MODULUS MPa (psi)	0.2% OFFSET YIELD STRESS MPa (psi)	ULTIMATE STRESS MPa (psi)	TRUE STRESS AT FRACTURE MPa (psi)	REDUCTION IN AREA %
T3	50.8 (2.0)	2158 (313,000)	41.78 (6,060)	66.81 (9,690)	79.36 (11,510)	38.6
T2	5.08 (0.2)	2165 (314,000)	39.65 (5,750)	64.40 (9,340)	71.56 (10,380)	35.4
T4	1.27 (0.05)	2241 (325,000)	39.58 (5,740)	65.50 (9,500)	84.71 (12,290)	40.0
T1	0.508 (0.02)	2310 (335,000)	35.92 (5,210)	62.06 (9,000)	76.51 (11,100)	36.3
Average		2220 (322,000)	39.23 (5,690)	64.68 (9,380)	78.05 (11,320)	37.6

used for the yield strength. These measures of the yield stress are more fully discussed in ASTM Standard D638 for the tensile testing of plastics. The average value of the 0.2% offset yield stress was 39.23 MPa (5,690 psi); the ultimate stress, 64.68 MPa (9,380 psi); the true stress at fracture, 78.05 MPa (11,320 psi); the elastic modulus, 2220 MPa (322,000 psi); and the percent reduction in area, 37.6%. With the exception of the yield stress, these values compare well with those reported in a text on PC.<sup>38</sup> The text values are 8,000 to 9,000 psi for the yield stress, 9,000 to 10,500 psi for the ultimate stress, 320,000 psi for the elastic modulus, and 60 to 100% for the elongation. In addition, a value of 0.38 is given for Poisson's ratio. The values in the text appear to have been measured at a displacement rate of 0.2 in./min., but it is uncertain how the yield stress was measured. Therefore, the discrepancy between the yield stresses may be due to the use of different measurement techniques. The elongation of 60 to 100% corresponds to a percent reduction in area of 37.5 to 50% under the assumption that constant volume deformation occurs. Ashbaugh<sup>39</sup> also measured the tensile properties of PC using the same material as that in the present study. He used 0.5- and 0.25-in.-diam. tensile bars having gage lengths of 2 and 1 in., respectively; special care was taken to ensure good alignment of the specimen. The displacement rate was 0.75 in./min. A consistent value of 353,000 psi was measured for the elastic modulus, 6,400 psi for the 0.2% offset yield strength, 10,500 psi for the ultimate stress, 78% for the elongation, and 44% for the reduction in area. These values are all higher than those measured in the present study. The higher elastic modulus could be due to Ashbaugh's superior alignment, and the higher yield and ultimate stresses due to this alignment in conjunction with the higher displacement rate. Although a universal joint was used at one end of the dogbone specimen in the present study, good alignment was difficult to obtain.

A typical stress-strain curve for PC is shown in Fig. 2. The curve is similar to that for non-ferrous metals up to the maximum load. At this point, a neck forms in the gage length and the load drops.

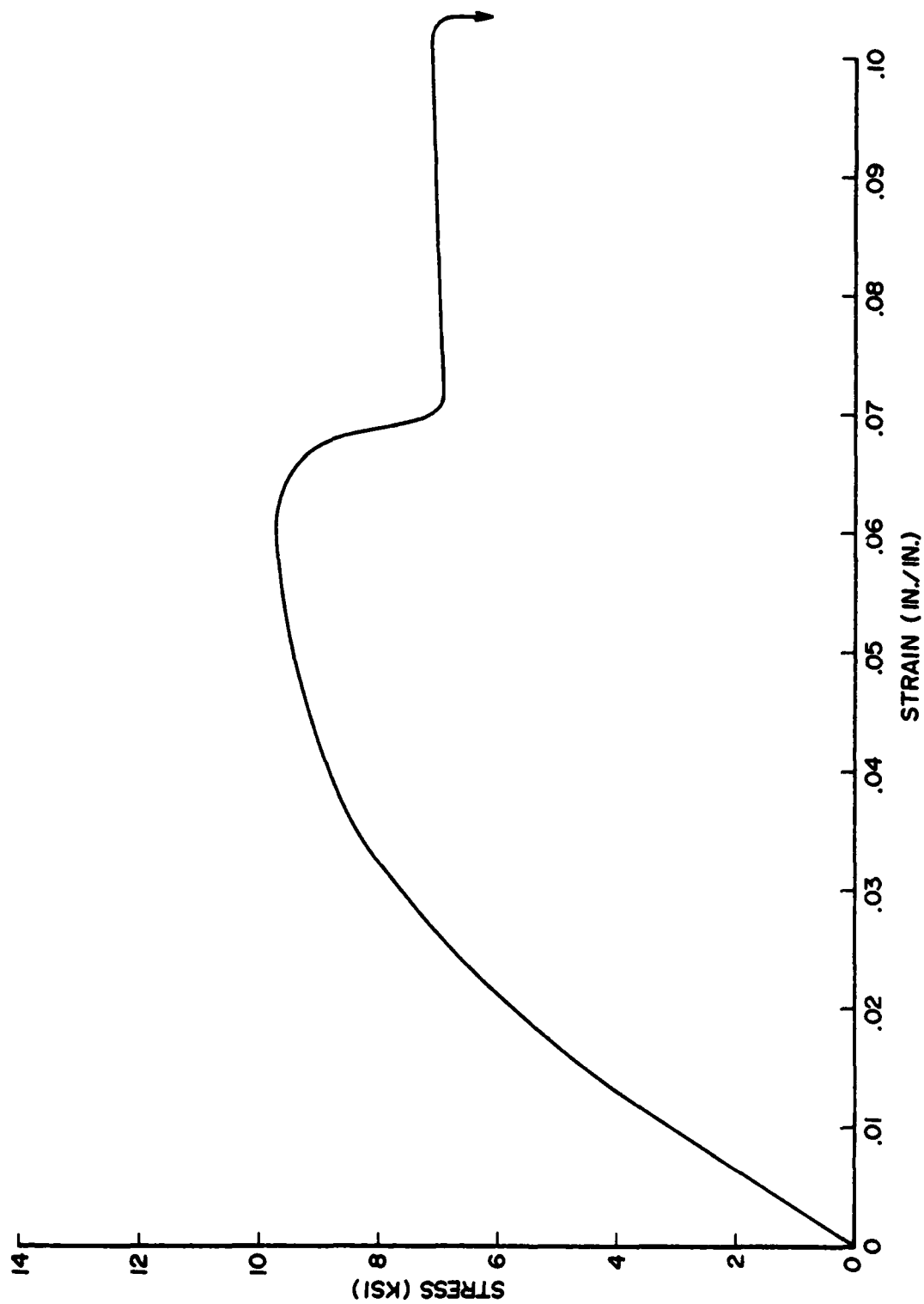


Figure 2. Stress-Strain Curve of Polycarbonate Specimen T-3.

The load remains at this value for the remainder of the test until fracture occurs (actually, the load slowly rises, but it never approaches the maximum). The load remains at this value because the neck travels up and down the gage length, at a constant stress, thereby absorbing the imposed displacement. PC forms new necked material rather than further deforming the original neck, as occurs with metals, because of its strain-hardening properties. Even under the much higher stresses, the necked PC has more resistance to plastic flow than the unnecked PC.

The stress-strain behavior of PC has been compared to that of steel because an upper and lower yield point appears to exist in PC. However, the so-called upper and lower yield points in PC are caused by necking, whereas in steel, they are formed by a different physical phenomenon. Necking in steel takes place at the ultimate stress, which is higher than the upper yield stress. Therefore, the author believes that the use of PC to model the deformation behavior of steel is unjustified, based solely upon the similar shape of their stress-strain curves.

The tensile properties of the PC exhibited some strain-rate sensitivity over the two decades of displacement rate at which the tests were run. As shown in Fig. 3, both the ultimate and yield stresses increased as the displacement rate increased; but, paradoxically, the material was stiffer at the lower rates. The reason for the elastic modulus becoming larger at the lower rates is not known, but experimental error cannot be ruled out. Ashbaugh found no rate dependence of the elastic modulus for rates of 0.75 and 0.05 in./min. Over the range of strain rate, the elastic modulus, ultimate stress, and yield stress varied by 3.5, 4 and 8%, respectively, from their average values.

Fracture in PC took place when a diamond-shaped surface flaw formed and grew until it intersected a corner of the specimen, at which point unstable fracture occurred. Figure 4 is a photograph of such a flaw. These flaws were thought to originate at machining defects; however,



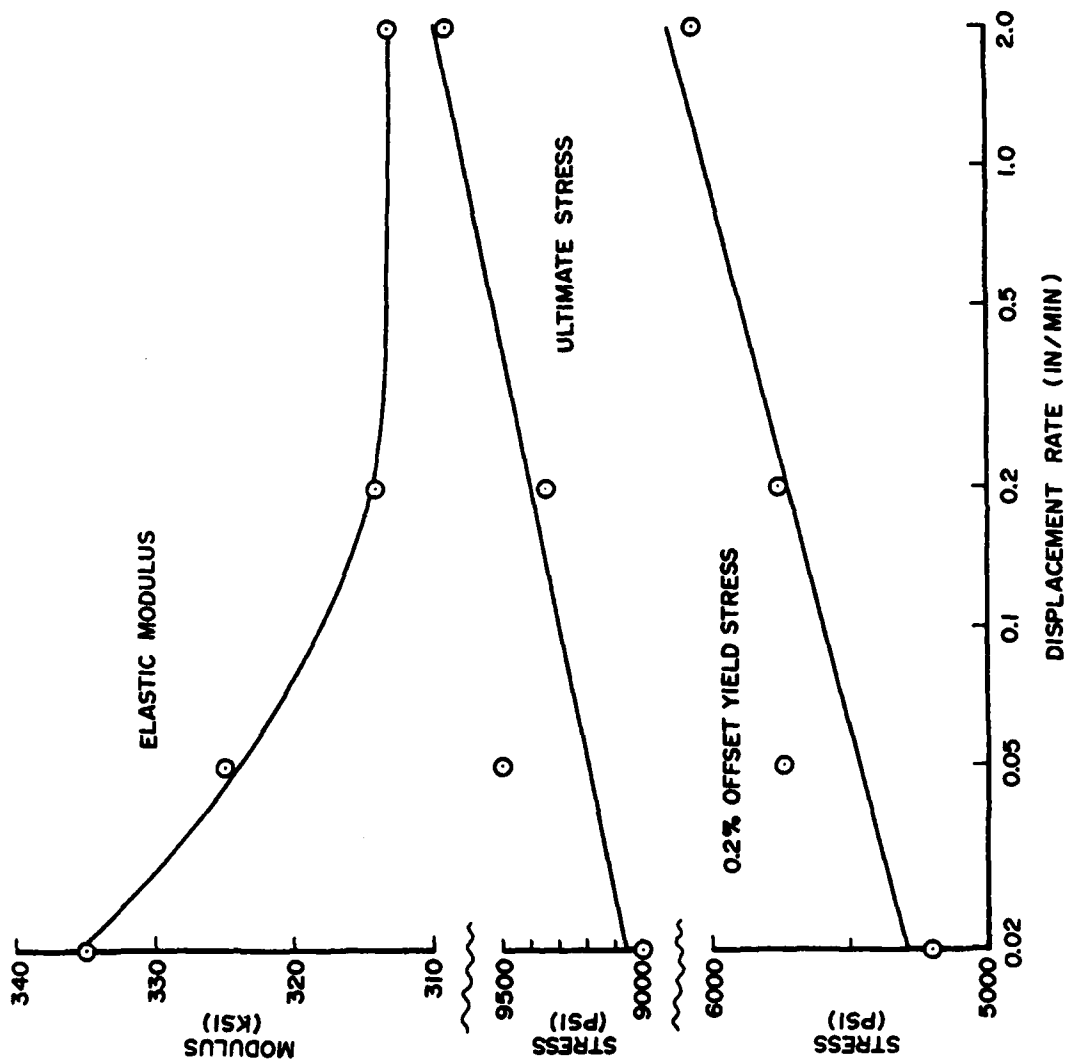


Figure 3. Strain-Rate Effects upon Tensile Properties of Polycarbonate at Room Temperature.

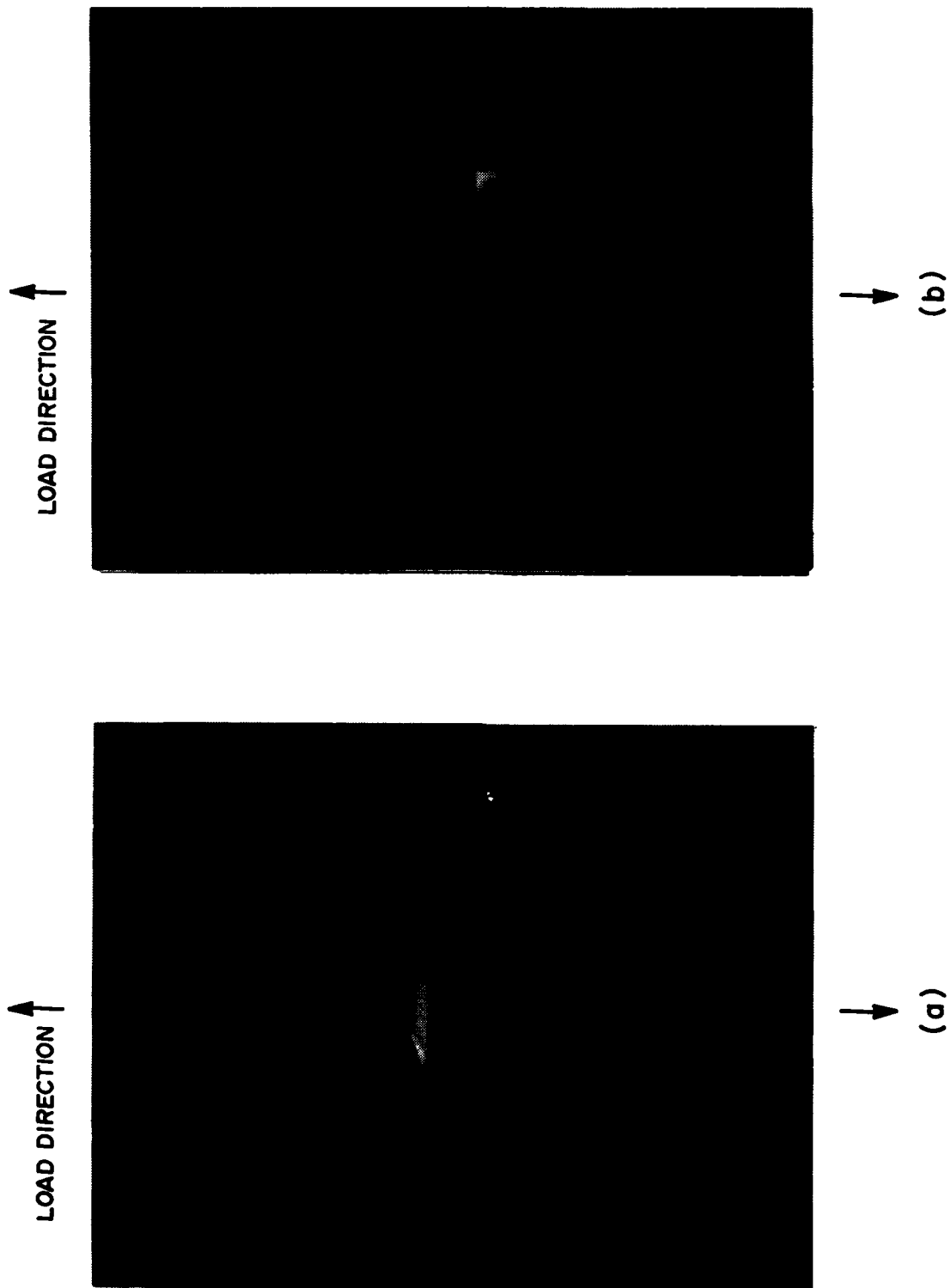


Figure 4. Diamond-Shaped Flaw in Tensile Specimen (a) Surface, (b) Depth. Maximum surface length is 0.138 in. and is perpendicular to the tensile axis.

this same type of failure mechanism was observed by Cornes, et al.,<sup>40</sup> who report that a narrow, diamond-shaped craze (similar in shape to that produced by a Knoop's Hardness Indenter)  $\sim 120 \times 17 \text{ mm}$  ( $4.7 \times 0.7$  mils) in size, formed in Merlon M 39 PC tensile specimens. These crazes grow until they break down and a crack or cavity forms. This crack then grows until unstable fracture takes place. Machining defects could still be responsible for the flaws in Fig. 4, since they provide a site for craze initiation and growth.

Since failure in the tensile tests was dependent upon the initiation and growth of flaws, the percent elongation of the specimens was dependent upon the location and severity of these nascent flaws. Thus, a wide variation in elongation was measured but not reported in Table 1. The reduction in area provided a much better measure of ductility than elongation.

One three-point-bend fatigue-crack-growth (FCG) test with  $R = 0.1$  was made on a 1-in.-thick specimen. The crack growth was in the T-S direction. This differs from most other FCG data for PC which are taken in the T-L or L-T orientation. The crack growth took place in the same half of the thickness as that in which the fracture toughness tests were conducted. Thus, the lamination halfway into the plate was avoided. The crack length was measured through the length of the specimen with a traveling microscope. The crack was measured along the surfaces, at the quarter points. The average of the three quarter points was used as the crack length.

The FCG data are presented in Fig. 5. Also included are the FCG data generated by Banasiak<sup>34-35</sup> on the same sheet of PC as that used in the present study--but in the T-L orientation. It can be seen that Banasiak's data are higher in value by about one-half a decade but follow the same trend. His data are in good agreement with those published by Manson, et al.,<sup>41</sup> for PC in the T-L or L-T orientation.

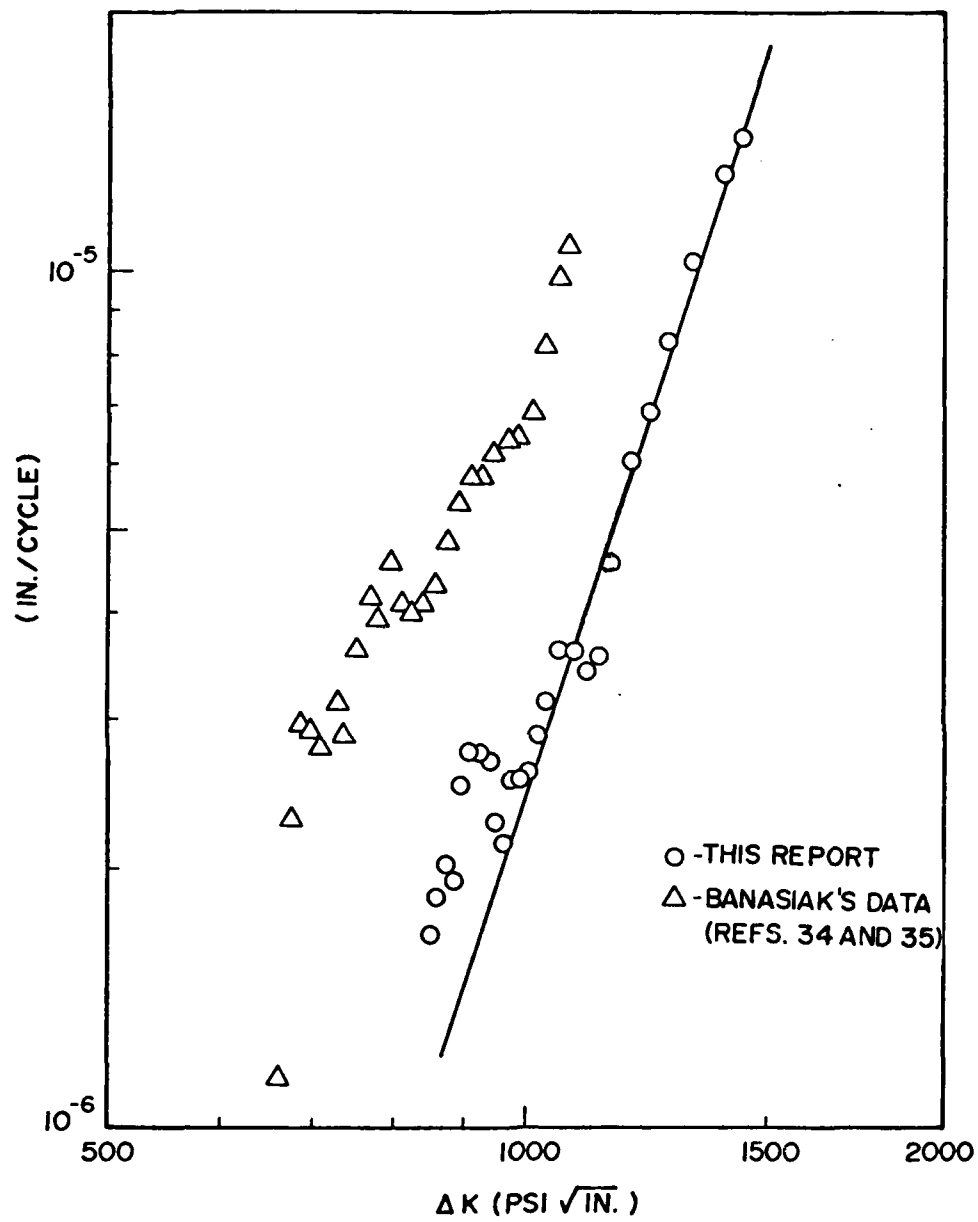


Figure 5. Fatigue Crack Growth of Polycarbonate in the T-S Direction.

These data show that FCG in the T-S orientation is lower than in the T-L direction. The data can be approximated by the expression

$$da/dN = 1.38 \times 10^{-20} (\Delta K)^{4.76} \quad (8)$$

where  $da/dN$  is in in./cyc. and  $\Delta K$  in  $\text{psi} \sqrt{\text{in.}}$ .

#### J-INTEGRAL TEST METHOD AND TEST MATRIX

The J-integral tests were conducted on three-point-bend specimens having the same planer dimensions (see Fig. 6), except for crack length. Crack lengths ranged from 0.54 to 0.81 in. and thicknesses of 0.125, 0.25, 0.5, and 1 in. were tested. Specimen crack lengths are given in Table 2. Two of the specimens had notch lengths of 0.25 rather than 0.5 in., but no influence upon the fracture behavior was observed. All specimens had the same orientation within the plate, and the crack was grown in the thickness direction, T-S. The specimens were oriented in this way in order to avoid possible effects of either the lamination in the middle of the plate or the plate surfaces. Since the initial crack length for all specimens was  $> 0.5$  in. and the notches were machined on the same surface of the plate, the cracks grew in essentially the same region of the plate and the lamination was avoided. The location of the specimens within the plate was not recorded. The specimens were tested in the as-machined condition, with the sides and ends being polished to permit the crack to be observed easily.

Typically three crack lengths and four thicknesses were tested in order to evaluate the effects of size upon the J-integral. Specimen 22, having a 0.55-in. crack length was used in an attempt to obtain a  $K_{IC}$  value according to ASTM Standard E399. Deeply cracked specimens having crack lengths greater than one-half the specimen width were used in order to obtain crack growth under large plastic strains. Extreme difficulty was encountered in testing specimens thinner than 0.125 in. at the small loads required.

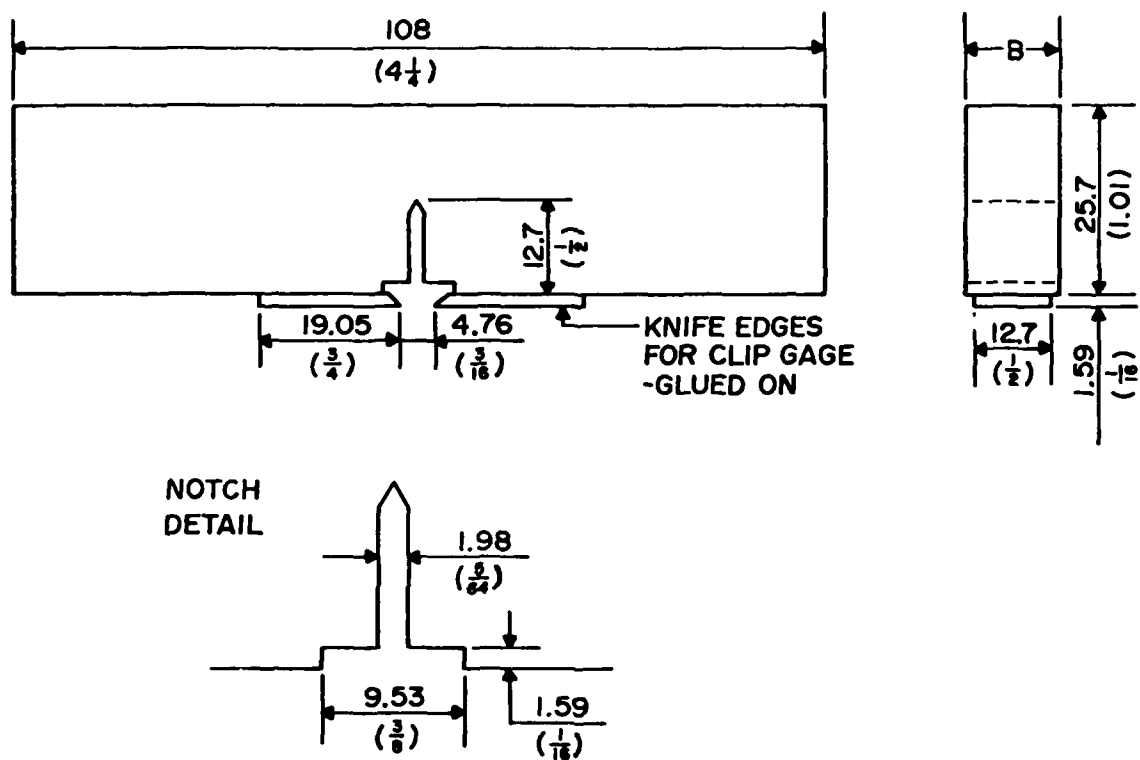


Figure 6. Three-Point-Bend Specimen [dimension in mm (in.)].

Table 2

SUMMARY OF THICKNESS, INITIAL CRACK LENGTH, AND CRACK-GROWTH BEHAVIOR

SPECIMEN NO. (a)	B THICKNESS (in.)	a <sup>INITIAL</sup> (in.)	TYPE OF FRACTURE (c)	J = mΔa + b		log J = m log Δa + b		CRACK-GROWTH BEHAVIOR (d)
				m	b	m	b	
23 (b)	1.014	0.543	U	1.949	2.86	0.915	0.436	G
2 (b)	0.998	0.706	U	0.846	7.46	0.699	0.495	C
22	0.990	0.777	U	0.510	29.93	0.202	1.341	0
4	0.500	0.700	U	0.629	17.57	0.473	0.873	G
6	0.498	0.693	PS	0.786	7.10	0.767	0.370	C
24	0.495	0.802	U	0.965	10.69	0.661	0.629	G
12	0.248	0.587	PS	1.103	9.33	0.611	0.703	G,C
13	0.250	0.688	PS	1.432	8.05	0.812	0.523	G
10	0.250	0.790	S	0.986	10.60	0.640	0.664	G,C
15	0.125	0.591	PR	1.311	8.30	0.729	0.595	G,C
20	0.123	0.705	PR	0.758	9.79	0.636	0.595	C
14	0.124	0.793	S	0.774	29.13	0.399	1.139	0
21	0.122	0.814	S	0.974	12.58	0.508	0.845	G,C

(a) W = 1.01 in.

(b) Notch depth = 1/4 in.; all others 1/2 in.

(c) U = unstable; PS = pop-in and stable at max. load; PR = pop-in and stable on rising load;

S = smooth, no pop-in

(d) G = crack growth only; C = crack + craze growth; 0 = "outliers"

Although the tests were carried out over a period of three years, no effect of test data on the experimental results was observed. The specimens were kept in desiccators prior to the tests, even though PC is not sensitive to the humidity of laboratory air.<sup>38</sup>

The specimens were fatigue precracked on a 300-kg Schenck machine, under three-point bending. In general, a span of 2.25 in. was used, although for some of the thinner specimens, a shorter span was needed. The maximum stress-intensity factor for the final 50 mils of precracking was between 800 and 2,000  $\text{psi}\cdot\sqrt{\text{in.}}$  for the specimens. The loading on the Schenck machine was achieved by a rotating shaft and an adjustable eccentric, set for a given maximum displacement.

The J-integral tests were conducted in a screw-driven Instron machine which controlled the displacement rate of the center tup of the three-point-bend loading fixture. A clip gage, attached to the bottom of the specimen across the crack mouth, was used to measure the crack-mouth opening. The clip gage had a small spring force to minimize the application of any additional loading--especially to the thinner specimens. The base and rollers of the fixture and the tup were made of steel. Two LVDT's, one on each side of the specimen, measured the load-point displacement, i.e., the relative displacement between the tup and the rollers. The LVDT body was attached to an aluminum support bar which rested on the rollers, and the spring-loaded plunger of the LVDT contacted the base of the tup.

Although the crack-mouth opening (COD) was measured during the test as a function of load, these data did not provide significant insight in this investigation. Generally the amount of plasticity was too great for obtaining meaningful  $K_{IC}$  values. The COD appeared to follow an approximately linear relationship with the load-point displacement.

Excellent alignment of the specimen in the test fixture was obtained by use of two plexiglas plates. Each plate had two holes which fitted



on bases at the end of the rollers. A line was scribed on the plates, equi-distant from these holes. By sighting down the lines, the tup and the crack in the specimen could be positioned evenly between the rollers.

All tests were conducted at a displacement rate of 0.02 in./min. A single rate was used in order to avoid introduction of the effect of strain rate into the data base. This rate was chosen because it permitted the crack growth to be photographed manually. A rate faster than 0.05 in./min. would have prohibited manual photography. In addition, Parvin and Williams<sup>31-32</sup> found no difference in the fracture properties for rates of 0.5 and 0.05 cm/min. (0.2 and 0.02 in./min.).

Data obtained during the test included load vs. time, load-point displacement vs. load, and COD vs. load as well as photographs of the crack front as the test progressed. The load at which each photograph was taken was marked on the load-vs.-time record as the test progressed.

The value of the J-integral was calculated using a formula for a three-point-bend specimen with a fully plastic remaining ligament<sup>9</sup>

$$J = \frac{2A}{Bb} \quad (9)$$

where A is the area under the load-displacement curve, B is the thickness; and b is the remaining ligament. It has been shown by Landes, et al.,<sup>11</sup> that Eq. (9) is accurate to within a few percent for an elastic ligament and by Ernst, et al.,<sup>42</sup> that it agrees well with more detailed calculations which take into account the effect of crack growth upon the value of J. The area under the load-displacement curve was measured by means of a digitizing board connected to a minicomputer. A trapezoidal integration formula was programmed into the minicomputer for computing the area.

#### CRACK-LENGTH MEASUREMENT

The crack was photographed using a 35-mm single-lens reflex camera equipped with either a 135-mm or a 200-mm telephoto lens, a bellows

extension, and a tripod. This setup gave a magnification of approximately one. (The effective focal length was not measured.) The shutter and film advance were operated manually, which resulted in occasional shaking of the camera. The film used was either Kodak Panatomic-X print film, ASA 32, or Kodak Direct Positive Panchromatic 5246 slide film, ASA 64. Both films are black and white and contain 36 exposures per roll.

Two methods of viewing the crack were employed. In the first method, the crack was viewed through the length of the specimen, with illumination from the opposite end of the specimen. This method was used for all but four of the tests--Specimens 10, 12, 15, and 21. The method had the disadvantage that two images\* of the crack front were produced. In the second method, the crack was viewed such that the line-of-sight of the camera formed a 45-deg. angle with the side of the specimen. The crack was illuminated by a light source on each side of the specimen. The sources were located in such a way that a line between them passed through the plane of the crack and was perpendicular to the line-of-sight of the camera. The material did not exhibit a double image when viewed in this manner.

A high-intensity white light was used for illumination. Color separation of the light by the cracked PC specimen was not observed in the viewfinder; therefore, no attempt was made to use monochromatic light since it would not have sharpened the image appreciably. A cursory attempt was made to use polarized light by placing a polarizing filter between the light source and the specimen; however, no improvement in image quality was observed.

The film, after development, was mounted into slide holders and projected onto paper taped to a flat surface. The image of the crack was traced onto the paper and the amount of crack growth was measured from the tracing. This procedure magnified the crack about 17 times, which minimized measurement errors. It also provided a hardcopy record of the crack. For one

---

\*The formation of two images of the crack front was thought to be the result of the birefringent property of the material.

of the specimens, positive prints having a magnification of about six were used for the measurements. As the image of the crack was being traced onto the paper, decisions were made as to which features could be attributed to the machine notch, precrack, crack tip, and crack sides. When two features might be attributable to the precrack or crack tip, both features were traced and a final decision made when the crack length had been measured from the tracing.

The crack length was measured at the three quarter points--one-fourth, one-half, and three-fourths--of the specimen thickness. It was not possible to measure the surface crack lengths because usually they could not be seen. The average of these three quarter points was used as the crack length.\* An eight-point average, as recommended in the ASTM standard now under development for the measurement of  $J_{IC}$ ,<sup>14</sup> was not used because it was too laborious. Since each of the 13 tests (no photographs were taken in one of the 14 tests) produced an average of 20 photographs, use of the eight-point average would have required 2,340 measurements as opposed to the 780 required by the three-point average. Also, it was felt that the use of the eight-point average would not alter the results significantly.

To calibrate the size of each image, a feature in the photograph having a known length was measured. When the crack was viewed through the length, the breadth of the crack (which is the specimen thickness), the machine notch, or the precrack was used. When the crack was viewed from the side, the length of the machine notch, excluding the angled portion, was used.

---

\*In some of the thinner specimens, the shear lips became sufficiently large that the one-fourth and three-fourths points contained the shear lips. When this situation arose, only the one-half point was used to determine crack length. To include the shear lips in the crack length would have resulted in lower, unrealistic values of  $\Delta a$  because the value of  $\Delta a$  which contained the shear lips would be less than a previous value of  $\Delta a$  which did not. This previous value of  $\Delta a$  did not contain shear lips because they were not yet sufficiently large to intersect the one-fourth or three-fourths points.

Two methods were used to determine the amount of crack growth. In the first or "absolute" method, the actual distance between the precrack and the crack tip was measured. Use of this method required identification of the precrack and crack tip in the photograph. In the second or "relative" method, the amount of crack growth was determined by subtracting the current length of the crack from the initial length. The initial crack length was calculated by averaging the crack lengths in the first few photographs before the initiation of crack growth. The "relative" method was used when the precrack could not be positively identified in the photographs. A method was used to measure the "relative" amount of crack growth for Specimens 14, 22, and 24 only. The "relative" method was used on specimens measured by the "absolute" method; the results were essentially the same.

The major problem associated with measuring the crack involved interpretation of the features in the photographs. No interpretation was completely satisfactory for all the tests. The principal difficulties involved identification of craze, birefringence, and "halos."

The craze zone ahead of the crack tip presented a problem in the optical measurement of the crack length. Since the optical properties of the craze are different from those of the bulk PC and the crack, an image of the craze would be expected in the photographs. In the photographs taken from the side, three distinct regions could be identified (Fig. 7). The presence of such regions in the photographs taken through the length was obscured by birefringence of the image (Fig. 8). As can be seen in Fig. 7, the dark region of the crack growth ahead of the long fatigue precrack region contained ridges similar to those in the precrack region. Ahead of the dark region there was a featureless region which was assumed to be the craze zone. The craze length and growth determined by this subdivision were reasonable. However, this interpretation of the craze zone was never verified.

When the specimen was viewed through the length, two images of the crack were observed. These images were polarized at  $90^{\circ}$  to each other because

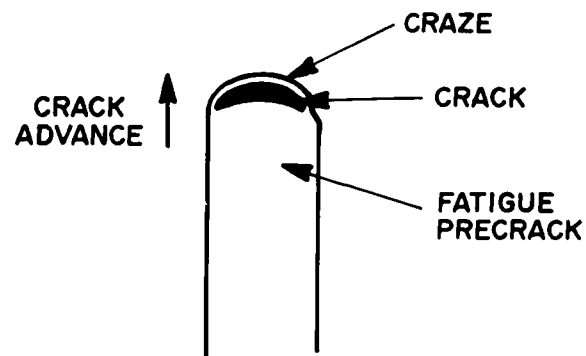
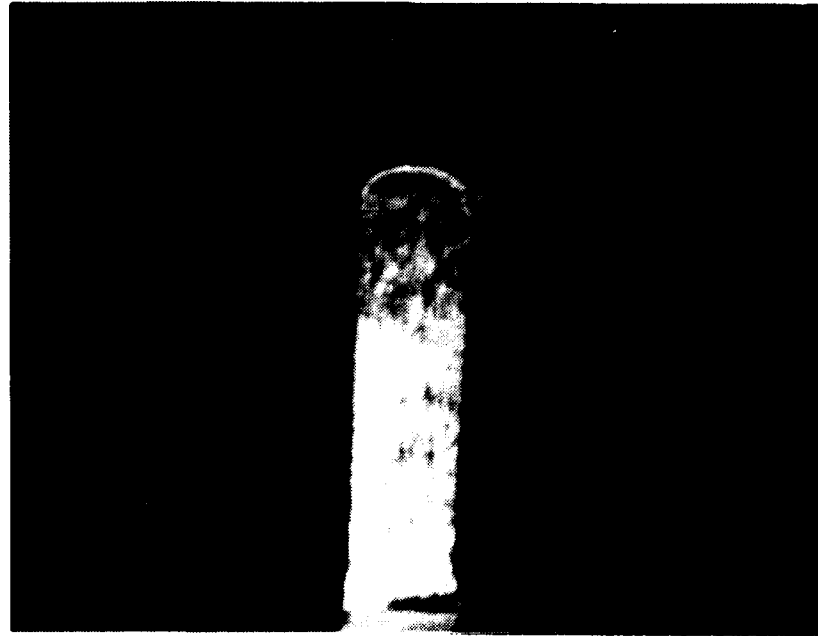


Figure 7. Photograph of Crack and Craze Regions through the Side (Specimen 10, load 17 lb.).

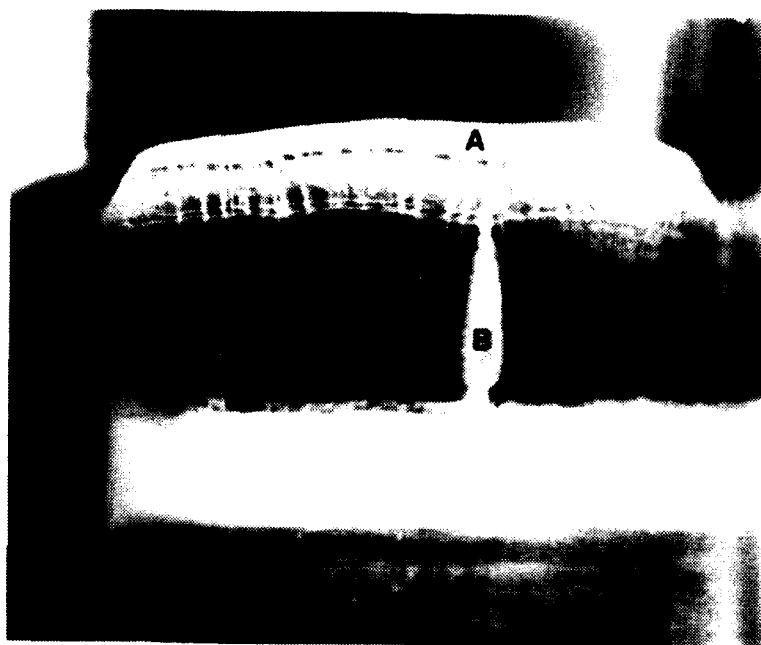


Figure 8. Photograph of Crack and Craze Region through the End of Specimen 6;(load  $\approx$  69 lb.). Area A contains growing crack and craze region. Area B is ridge connecting two portions of precrack which grew on different planes.

of the birefringence in the PC direction of crack growth. Polarization of the images was not consistent. The top images of the precrack and crack sometimes had the same angle of polarization and sometimes were  $90^\circ$  apart. Therefore, the use of a polarizer between the specimen and the camera was not possible. The distance between the two images was 17 mils or less. The crack length was measured by averaging the distance between the two images.

When the crack was viewed through the length, features called "halos" appeared above the crack front. These features were white bands of light and contained no details of the fracture surface. Under low loads, a halo would appear and grow prior to crack growth, crack growth being defined as an image ahead of the precrack containing details of a fracture surface. The halo remained ahead of the growing crack. Thus, the halo could be interpreted as the craze because it was featureless. For large crack growth, two or three sets of halos were sometimes present. Their cause was not known. To interpret them as crack extensions would have led to unreasonably large increments of crack growth; therefore, they were ignored in making crack-growth measurements.

Figures 9 and 10 are sequences of photographs showing the growth of the crack as observed through the end and through the side of the specimen, respectively. Features of these sequences of photos have been discussed previously with respect to Figs. 7 and 8.

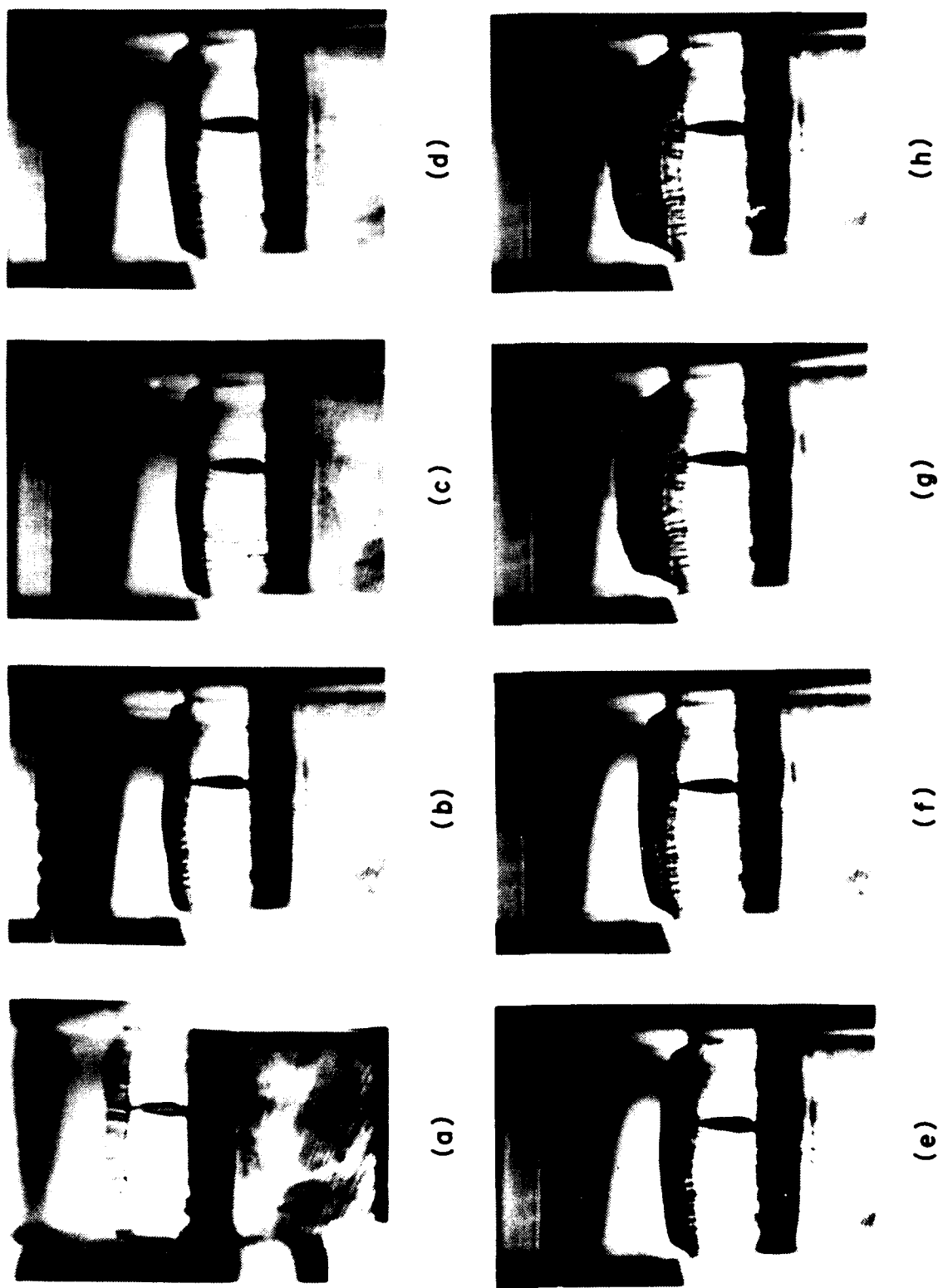
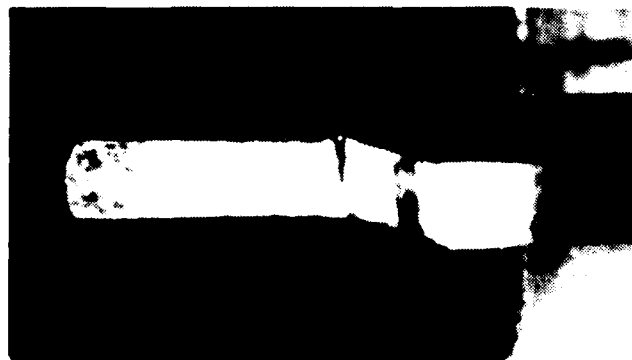


Figure 9. Series of Photographs (Positive Images) Showing Crack Growth Observed through the End of Specimen 6. (a) no load, (b) 42 lb.,  $J = 8.5$  psi-in., (c) 53 lb.,  $J = 14.4$  psi-in., (d) 65 lb.,  $J = 23.6$  psi-in., (e) 73 lb.,  $J = 32.1$  psi-in., (f) 76 lb.,  $J = 37.7$  psi-in., (g) 74 lb.,  $J = 41.7$  psi-in.; at pop-in (h) 55 lb.,  $J = 42.9$  psi-in.

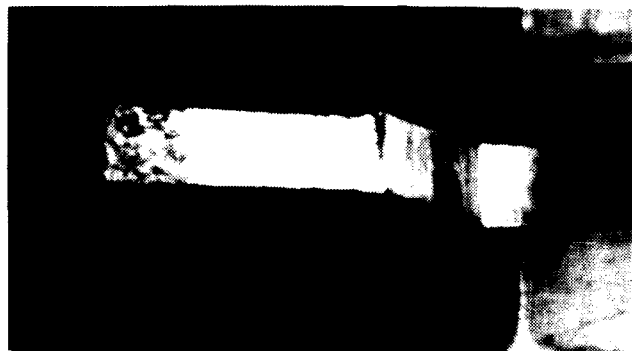




(a)



(b)

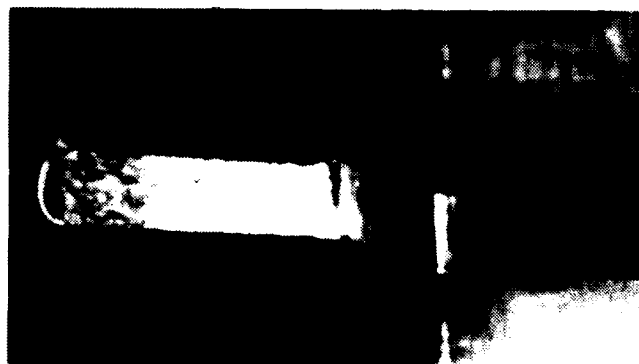


(c)

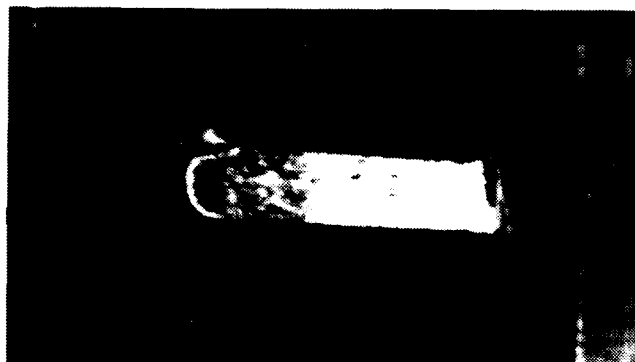


(d)

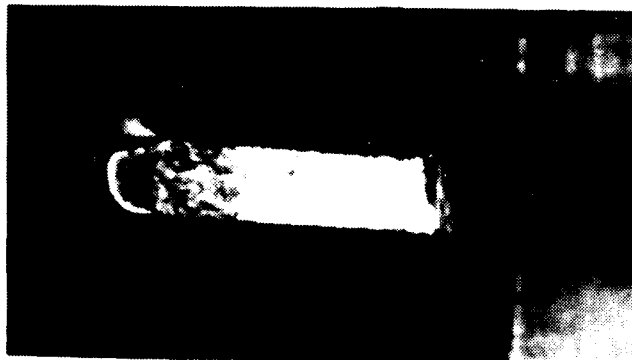
Figure 10. Series of Photographs Showing Crack Growth in Specimen 10. (a) 1.3-lb. load, (b) 9.0-lb. load,  $J = 5.1$  psi-in., (c) 12.0-lb. load,  $J = 9.4$  psi-in., (d) 16.5-lb. load,  $J = 19.7$  psi-in.



(e)



(f)



(g)

Figure 10. continued. (e) 18.8-lb. load,  $J = 28.7$  psi-in., (f) 20.2-lb. load,  $J = 38.5$  psi-in., (g) 19.8-lb. load,  $J = 46.5$  psi-in.

### SECTION 3

#### RESULTS AND DISCUSSION

##### LOAD-DISPLACEMENT BEHAVIOR OF THE SPECIMEN

In this section the load-displacement behavior of the three-point-bend specimens is discussed. Typical load-displacement behaviors of the PC are illustrated in Fig. 11. Load-displacement curves ( $P-\delta$ ) for each of the specimens can be found in Appendix A. In all specimens the crack began to grow before the maximum load was reached.

The compliance of each specimen and the maximum load in each test are given in Table 3. Also included is the Green and Hundy limit load<sup>43</sup> and the value of the quantity  $R_{sb}$ , defined in ASTM Standard E399 for measuring  $K_{IC}$ . The Green and Hundy limit load,  $P_L$ , is given by

$$P_L = \frac{1.261}{2\sqrt{3}} \sigma_y Bb^2 \quad (10)$$

and the value  $R_{sb}$  by

$$R_{sb} = \frac{6 P_M W}{Bb^2 \sigma_y} \quad (11)$$

where  $\sigma_y$  is the yield strength,  $B$  the thickness,  $b$  the remaining ligament,  $P_M$  the maximum load, and  $W$  the width.  $P_L$  is the maximum load that can be sustained by a cracked three-point-bend specimen with a span of 4 in. It is based upon the formation of a plastic hinge and the assumption that crack growth does not occur.  $R_{sb}$  is the ratio of maximum load to the load predicted from a beam analysis when the maximum stress is  $\sigma_y$ . When  $R_{sb}$  is equal to one, the outer fibers of the bend specimen are assumed to be at the yield point.

As Table 3 shows, the maximum load based upon the initial ligament length is always less than the Green and Hundy limit load because crack

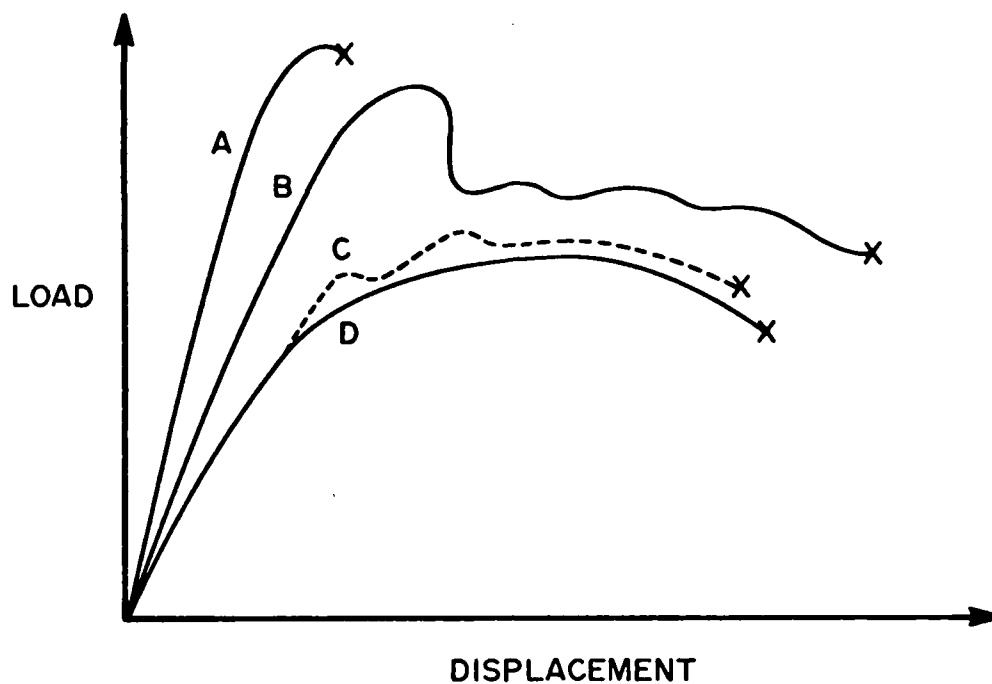


Figure 11. Typical Load-Displacement Curves: A - Thick Specimens,  
 B - Specimens of Intermediate Thickness and Crack  
 Length; C - Thin Specimens having Short Crack Lengths;  
 D - Thin Specimens having Long Crack Lengths.

Table 3

## COMPLIANCE AND LIMIT LOADS

SPECIMEN NO.	B NOMINAL (in.)	a/w INITIAL	COMPLIANCE (in./lb. $\times 10^{-4}$ )	LIMIT LOAD			R <sub>sb</sub>	
				EXPERIMENT (1b.)	GREEN & HUNDY (1b.)	EXP G&H	LOAD TO R = 1 (1b.)	R <sub>sb</sub> AT P <sub>max</sub>
23	1	0.54	1.83	293.	456.	0.64	207.	1.42
1	1	0.70	4.19	140.	185.	0.73	84.	1.67
2	1	0.70	4.08	142.	194.	0.73	88.	1.62
22	1	0.76	7.22	88.	117.	0.75	53.	1.66
4	1/2	0.69	7.96	75.	100.	0.75	45.	1.66
6	1/2	0.69	7.68	76.	104.	0.73	47.	1.62
24	1/2	0.80	17.29	39.	44.	0.89	20.	1.96
12	1/4	0.58	9.17	61.5	92.	0.67	42.	1.48
13	1/4	0.68	15.03	39.5	54.	0.73	24.	1.62
10	1/4	0.78	34.31	20.	25.	0.80	11.	1.76
15	1/8	0.59	19.17	34.5	45.	0.77	20.6	1.67
20	1/8	0.70	38.41	18.1	24.	0.75	10.7	1.68
14	1/8	0.79	76.10	9.6	12.	0.80	5.5	1.75
21	1/8	0.81	84.39	8.6	10.	0.86	4.4	1.95

growth takes place before the maximum load is reached and thus prevents the theoretical-limit load from being reached. The value of  $R_{sb}$  is always greater than one. This value indicates that the specimen yielded before the maximum load was reached. The amount of plasticity present at the maximum load was a function of crack depth. As shown in Fig. 12, the deeply cracked specimens exhibited greater plasticity and more closely approached the theoretical-limit load than the specimens with more shallow cracks. Surprisingly, with the exception of Specimen 15, there was no effect of thickness upon the amount of plasticity at the maximum load--only upon the type of fracture behavior observed, which will be discussed shortly.

Also included in Table 3 is the load required for  $R_{sb}$  to equal one. This load is the nominal elastic limit of the specimen and will be used in a section in conjunction with the crack-growth data.

The P- $\delta$  curves exhibit four types of fracture behavior--unstable (Curve A in Fig. 11), pop-in at maximum load and thereafter stable (Curve B), pop-in before maximum load and thereafter stable (Curve C), and stable with no pop-in (Curve D). For unstable fracture the crack advance becomes unstable and the specimen fractures, with one or two halves flying out of the testing machine. This behavior generally was exhibited by the 1-in.-thick specimens. Unstable crack extension characterized by pop-in at maximum load appears to be the same process as fracture except that crack arrest takes place. Once the crack arrests, further crack growth is stable. This type of behavior occurred in the 0.5- and 0.25-in.-thick specimens. Pop-in can occur before the maximum load is reached. After pop-in, the load continues to rise smoothly through the maximum load. This behavior occurred in the 0.5- and 0.25-in.-thick specimens having the shortest crack lengths. Finally, some of these thick specimens having the longest cracks exhibited a smooth P- $\delta$  response such as that which occurs in ductile metals. The type of fracture behavior relative to each specimen is given in Table 2.

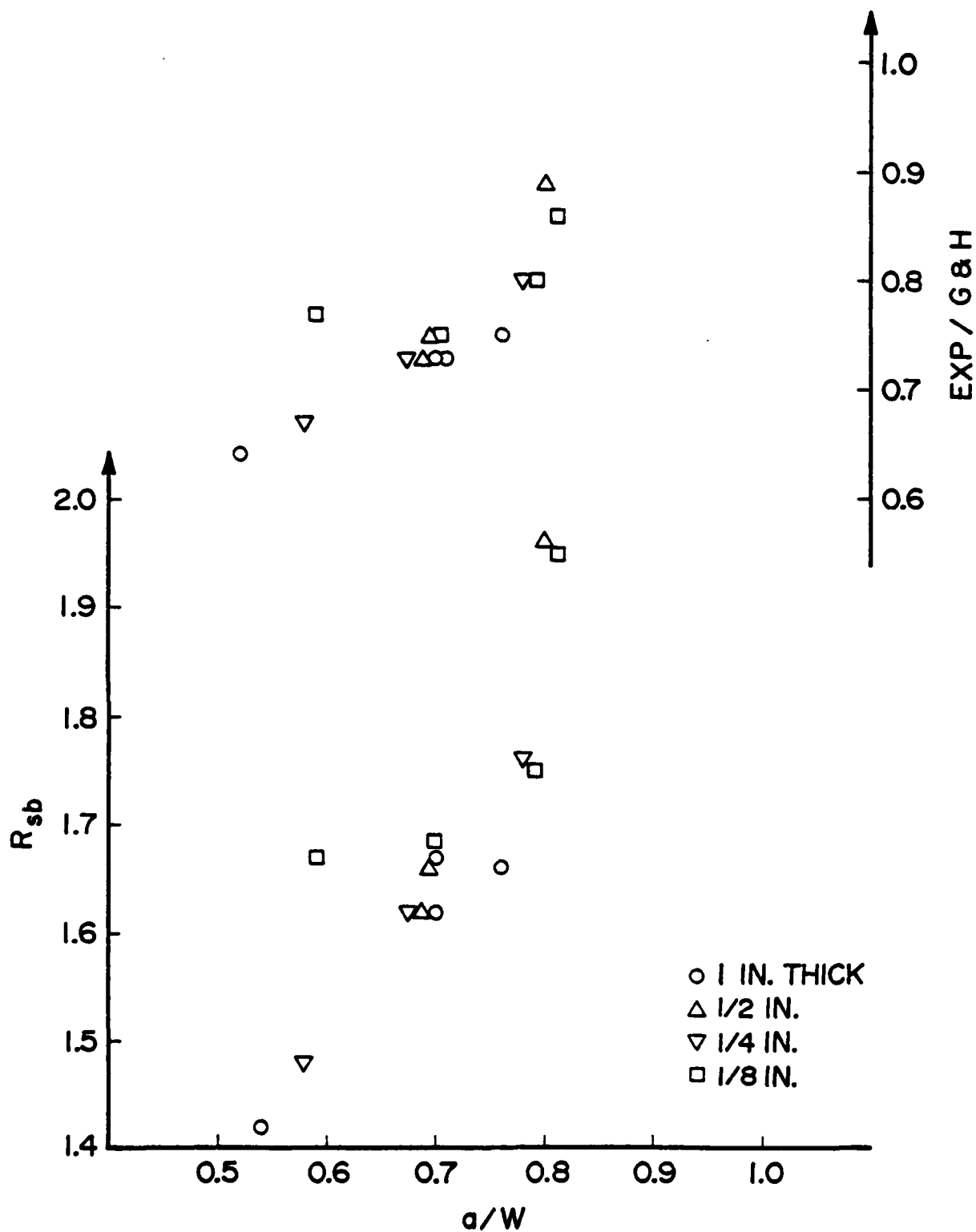


Figure 12. Estimates of Extent of Yielding in Specimens at Maximum Load.

The pop-in phenomenon was associated with rapid crack growth. The crack front would advance rapidly and then arrest. In Specimen 6, 66 mils of growth took place during pop-in. Key and Katz<sup>44</sup> studied the pop-in behavior of PC. The crack-growth behavior which they report was similar to that observed in the current experiments. However, the criterion for pop-in is a function of both the thickness and the crack length, as the present study shows. The criterion is not dependent upon thickness alone.

#### CRACK-GROWTH BEHAVIOR

Crack growth as a function of load was determined from the photographs and as a function of  $J$  through Eq. (9). For Specimens 10, 12, 15, and 21, crack length and craze length were determined from the photographs. A composite of all the data for crack growth as a function of  $J$  has been plotted using linear coordinates in Fig. 13. Tables and plots of crack growth vs.  $J$  for each specimen can be found in Appendix B.

A linear-regression line for each set of data was determined for  $J$  vs. crack growth when crack growth was 6 mils or greater, as long as subsequent growth was also greater than 6 mils. This has been recommended as the lower bound per a proposed ASTM standard for crack-growth data for  $J_{IC}$  to be fit in a least-square-error sense. The equation to which the data were fit is

$$J = m\Delta a + b \quad (12)$$

where  $\Delta a$  is in mils. The slope,  $m$ , and the  $J$ -intercept,  $b$ , of the best-fit line for each specimen are given in Table 2.

The measured values of the craze length had a maximum of about 7 mils, except for Specimen 15 which had a maximum value of 40 mils. The value of 7 mils is almost twice the 4 mils reported by Fraser and Ward,<sup>29</sup> but it is of the correct order of magnitude. The large value of 40 mils in the case of Specimen 15 occurred after a  $J$  of 40 psi-in. had been exceeded.



As can be seen from Fig. 13, the crack growth is a non-linear function of  $J$ . For small amounts of crack growth,  $J$  rises rapidly with  $\Delta a$ . As the amount of crack growth increases,  $J$  rises less sharply. Experimental data exhibiting the behavior of the predicted blunting line [Eq. (5)] were not observed. This lack of blunting is due in part to the inability to resolve such small distances ( $<1$  mil) but is caused mainly by the presence of a craze ahead of the crack tip. The craze obscured the blunted crack tip and was also responsible for the finite amount of crack extension observed at low values of  $J$ .

In the composite plot on Fig. 13, the wide scatter band was produced by data from all but two specimens. These two are called "outlier" specimens (Nos. 14 and 22). The data from the specimens forming this scatter band can be divided into two groups, based upon the crack-growth data of Specimens 10, 12, 15, and 21 in which both a crack and a craze portion could be identified. The data from the other specimens followed either the crack-growth or the crack-plus-craze growth behavior of these specimens, as shown in Figs. 14 and 15, respectively. The data which were best associated with the crack growth or crack growth plus craze length were identified in Table 2. Neither thickness nor initial crack length appeared to have an influence upon this association. This interpretation of the data is probably due to the photographic methods and lighting which were used for the test.

The term "outliers" which has been used to identify two specimens, Nos. 14 and 22, is for descriptive purposes only and is not meant to have any statistical implications. The crack-growth behavior of each of these specimens was unlike that of any other specimen. Specimen 14 exhibited an increase in  $J$  from 20 to 37 psi-in. without a corresponding increase in crack growth. This discontinuous behavior is extremely unusual and was not observed in any other test. In addition, the test condition of Specimen 14 was duplicated in the case of Specimen 21. While Specimen 21 did not exhibit the behavior of Specimen 14, its crack growth was similar to

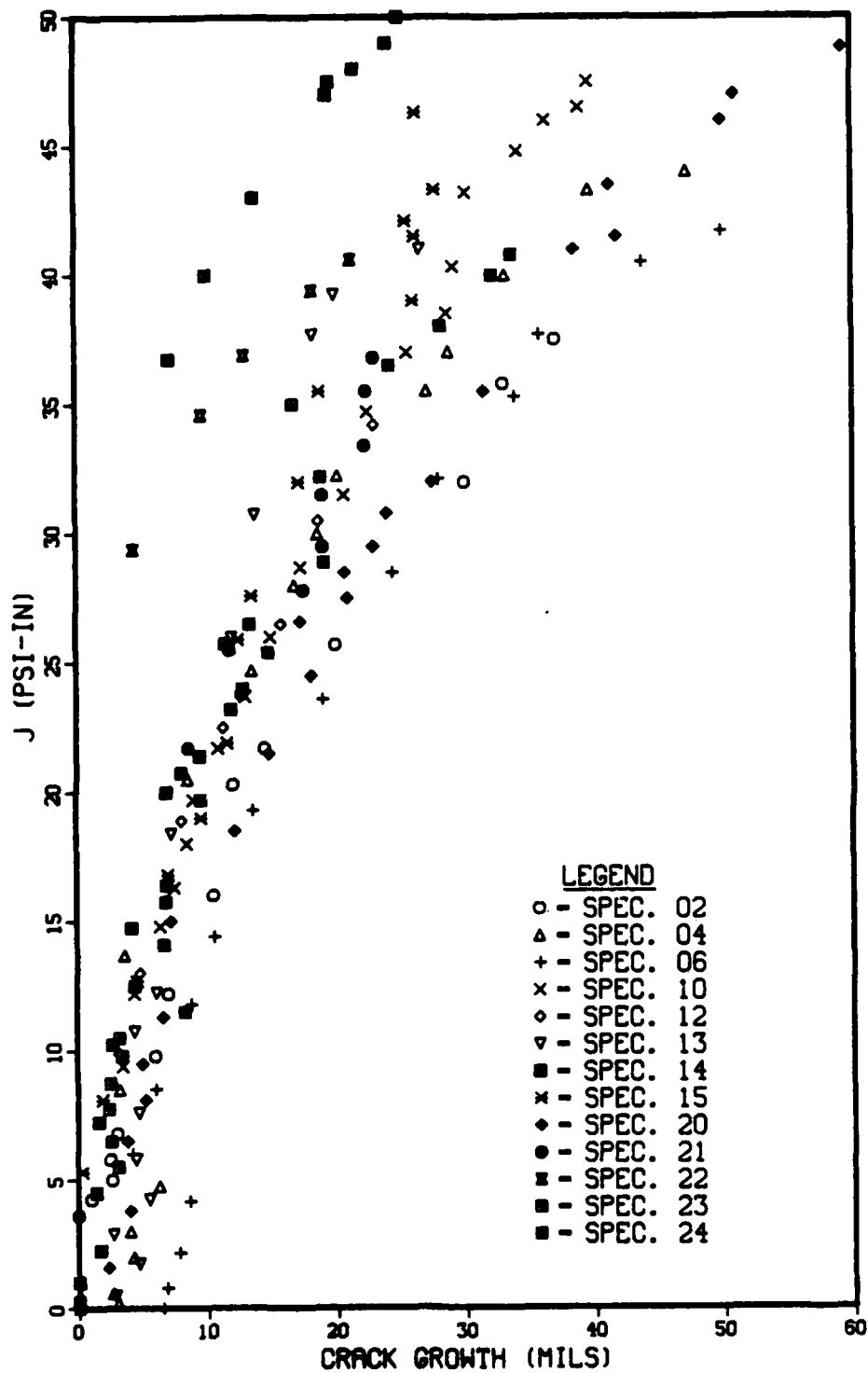


Figure 13. Master Plot of J as a Function of Apparent Crack Growth (some of the data may include craze length).

The craze had grown slowly up to this point, but afterwards grew rapidly. The reason for this behavior is not known. In the other three specimens (10, 12, 21), the craze length remained constant for the duration of the test.

Due to the fatigue-precracking procedure, a craze had formed ahead of the crack tip. (The process of fatigue-crack growth in polymers involves such formation, as discussed by Hertzberg and Manson.<sup>45-47</sup>) As the specimen was being loaded in the fracture tests, this craze opened up and gave the appearance of crack growth. This craze behavior was probably responsible for the small amounts of crack growth recorded at low values of J.

An attempt was made to apply the Dugdale Model<sup>48</sup> to the prediction of craze length. Since the model is derived for the center-cracked-panel geometry, it was necessary to modify it for the three-point-bend specimen. This modification was made by recognizing that for small plastic zones, the Dugdale yield-zone length, s, is equivalent to

$$s \cong \frac{\pi}{8} \left( \frac{K}{\sigma_y} \right)^2 \quad (13)$$

By substitution of the relation between K and J, Eq. (3b), into Eq. (13),

$$s \cong \frac{\pi}{8} \left( \frac{1}{\sigma_y} \right)^2 \frac{E}{1-\nu^2} J \quad (14)$$

it is evident that s and J are linearly related. Using the ultimate stress of 9380 psi for  $\sigma_y$ , Eq. (14) becomes

$$s \cong 1.15 J \quad (15)$$

where s is in mils. Equation (15) predicts the craze length up to 7 mils, or a J of 6.1 psi-in., reasonably well. Above this value of J, Eq. (15) predicts a longer craze length than observed. Near this value of J, crack growth begins, and it is questionable whether the model is still applicable. It also appears that with the exception of Specimen 15, the maximum craze length observed experimentally in PC is around 7 mils.

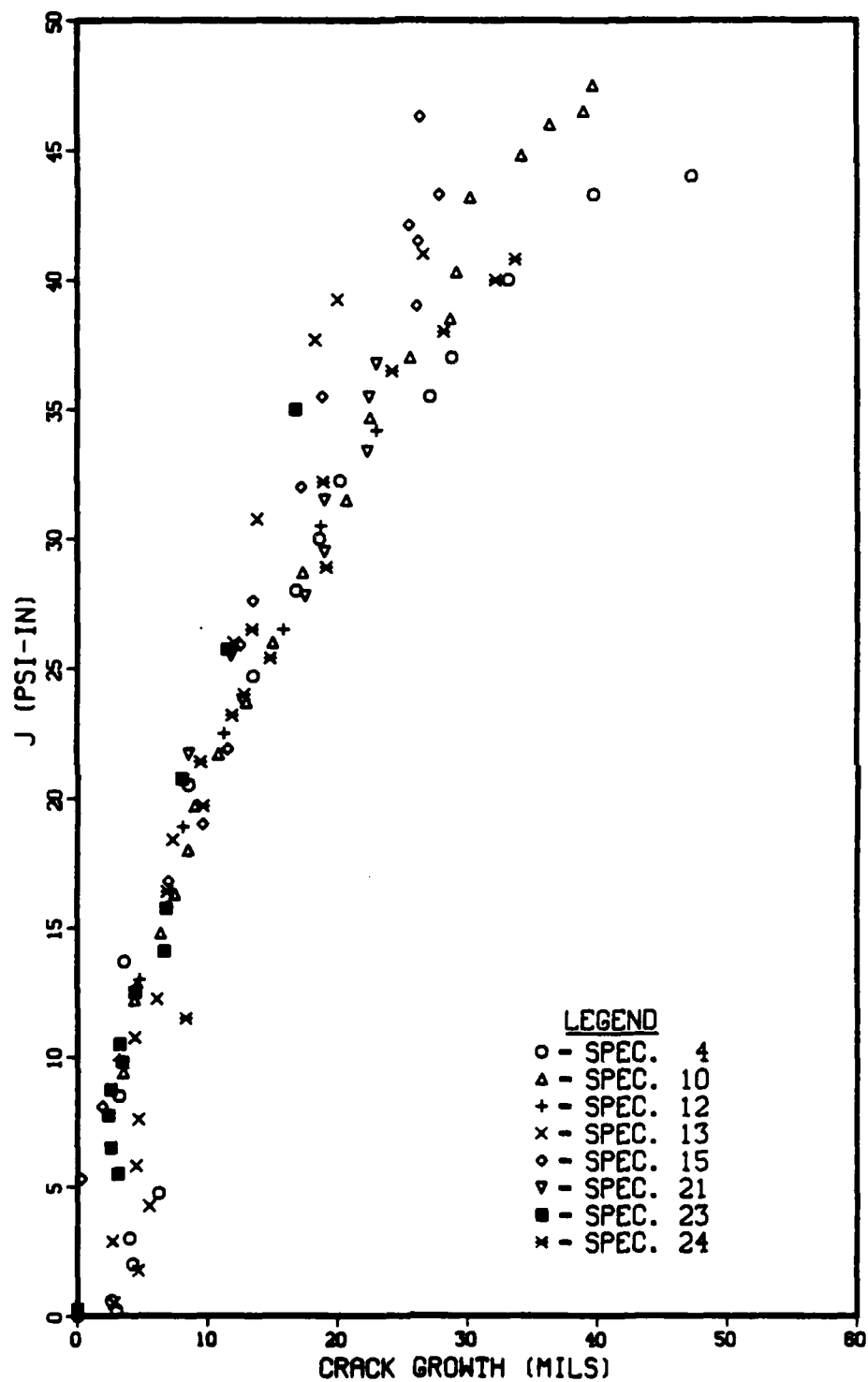


Figure 14. Plot of J as a Function of Crack Extension.

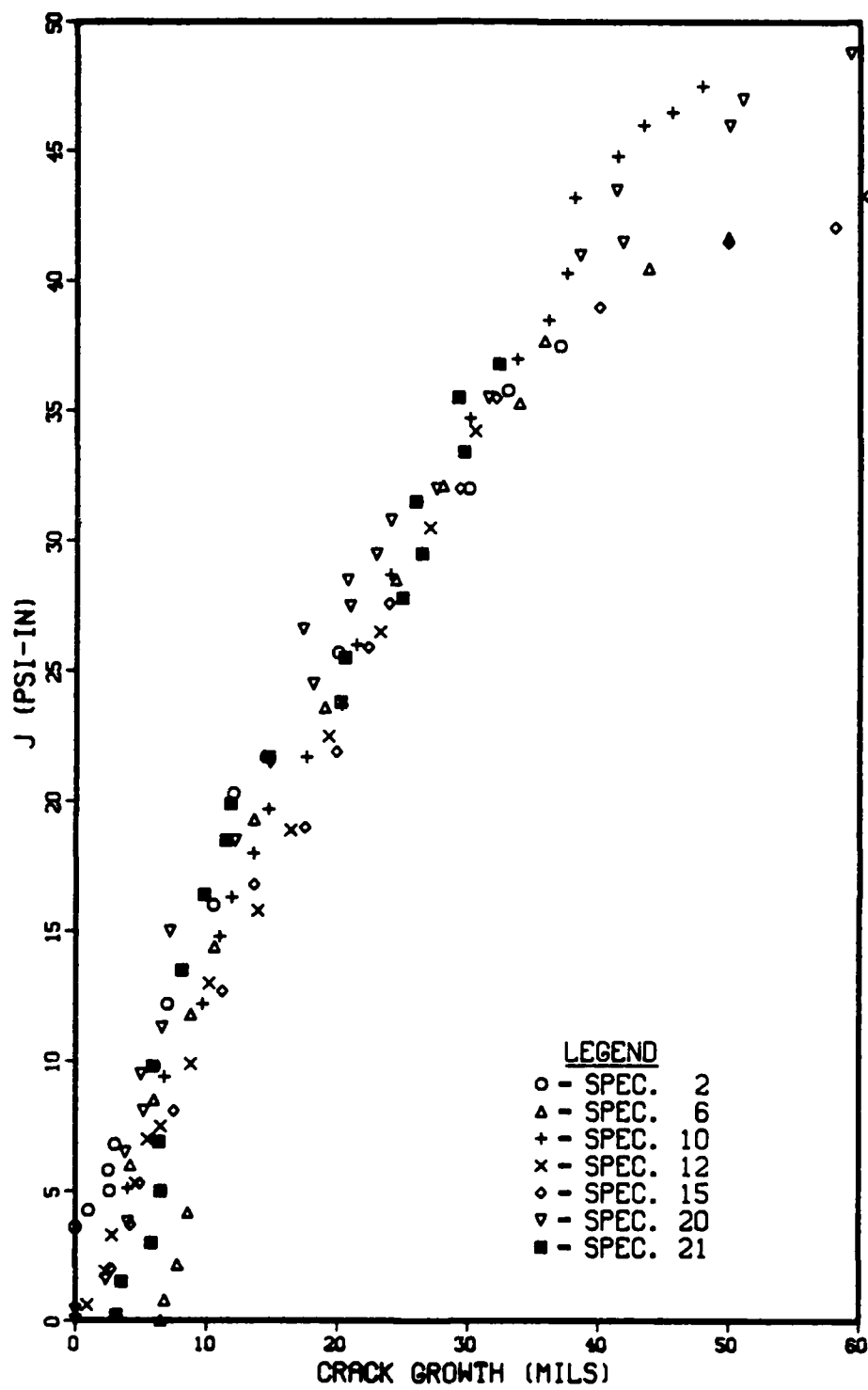


Figure 15. Plot of J as a Function of Crack Extension and Craze.

that in the other tests. Since the load-displacement record of Specimen 14 was similar to that of Specimen 21, the problem associated with Specimen 14 could be due to the measurement of crack growth. The photographs of Specimen 14 were badly overexposed and out of focus, making identification of the precrack and the crack tip extremely difficult. As a consequence, the fracture and crack-growth criteria calculated for Specimen 14 will not be used to characterize the behavior of PC.

In Specimen 22, large values of  $J$  were required to produce small amounts of crack growth. In all of the other specimens, such values of  $J$  were associated with larger amounts of crack growth. The difference in crack growth was ~ 10 mils. This large amount of growth cannot be ascribed to random errors. For some reason, ten mils of crack growth was not observed in the photographic process. Of these ten mils, seven may be due to the absence of a craze in the photographs. The source of the remainder of the discrepancy is not known, although possible.

The question which arises with respect to Specimen 22 is whether the measured crack-growth behavior is true material behavior or due to unknown photographic error. Consequently, the fracture and crack-growth criteria applied to Specimen 22 will not be used in characterizing the behavior of PC.

The initiation of crack-growth in relation to the overall deformation of the specimen is an important aspect of the crack-growth behavior of PC. The quantity  $R_{sb}$  [Eq. (11)], as discussed previously, describes the upper limit of the elastic behavior of the specimen. The load required to make  $R_{sb}$  equal to one has been given in Table 3 and indicates that the outer fibers of the specimen are at the yield point. The amount of crack growth which occurred up to these loads was between 2 and 9 mils. Some, but not all, of this crack growth is due to craze formation. This means that the crack initiates and grows a

small amount when the specimen is nominally elastic. However, the majority of crack growth takes place when the specimen is in the elasto-plastic and fully plastic regimes.

Since the crack-growth behavior of PC was non-linear, an attempt was made to linearize it by using logarithmic coordinates. Plots of  $J$  vs. crack growth using log-log coordinates are given in Appendix B. Generally, these data seemed to be closer to a straight line than when plotted using Cartesian coordinates. This behavior suggests an exponential relation between  $J$  and  $\Delta a$  of the form

$$J = C(\Delta a)^m \quad (16)$$

where  $C$  and  $m$  are material constants. Again, only data having  $\Delta a > 6$  mils, where all subsequent growth was greater than 6 mils, were used in the linear-regression fit. The values of the slope,  $m$ , and the intercept,  $\log_{10} C$ , are given in Table 2 for each specimen.

Let  $J_{init}$  be the value of  $J$  at the intersection of the blunting line, [Eq. (5),] and the exponential relation between  $J$  and  $\Delta a$ , [Eq. (16).] Then, the material constant  $C$  can be calculated as

$$C = (2\sigma_f)^m (J_{init})^{1-m} \quad (17)$$

and the crack growth behavior can be written as

$$\Delta a = \frac{J_{init}}{2\sigma_f} \left( \frac{J}{J_{init}} \right)^{1/m} \quad (18)$$

The symbol  $J_{init}$  is not to be interpreted in the same way as  $J_{IC}$ .  $J_{IC}$  is associated with a specific method<sup>14</sup> for determining  $J$  at the beginning of crack growth, and is the subject of an ASTM standard.

Since the exponential relation between  $J$  and  $\Delta a$  can be used to fit PC reasonably well, crack-growth data for other materials were gathered to determine whether they would follow this relation. Data from Paris<sup>16-25</sup>

on 5083-0 aluminum, from Shih, et al.,<sup>18</sup> and Clarke<sup>15</sup> on A533B steel, from Berger<sup>18</sup> on Ni-Cr-Mo steel, from Joyce and Gudas<sup>20</sup> on Ti-7Al-2Cb-1Ta titanium, and from Griffis and Yoder<sup>10</sup> on 7005-T6351 aluminum were examined to determine whether they obeyed this relation. These data were plotted using both logarithmic and linear coordinates, as shown in Appendix C. The non-linear crack-growth behavior, when plotted using linear coordinates, is linearized by the logarithmic coordinates for all the materials except one. This linearization is most dramatic for 5083-0 aluminum and A533B steel. It is of interest to note that the data for the A533B steel are from both analytical calculations by Shih, et al., and experimental results by Clarke and that both groups of data fit the exponential relation. The only material which did not follow this relation was the 7005-T6351 aluminum. This material followed a linear relation quite well.

This linearization of the resistance curve using logarithmic coordinates has been observed elsewhere. Takahashi, et al.,<sup>20-21</sup> have reported that this crack-growth behavior for a variety of alloy steels can be normalized to a single line with coordinates of  $\log J/J_i$  vs.  $\log \Delta a/\Delta a_i$ . The subscript "i" stands for initiation and was measured at a crack extension of 0.2 mm (0.008 in.) Carlson and Williams<sup>22</sup> found that crack-growth data for ASTM A533 steel followed an exponential relation, Eq. (16), better than a linear relation, Eq. (12). They used this exponential relation to determine a  $J_{IC}$  value which was in good agreement with the experimental observations.

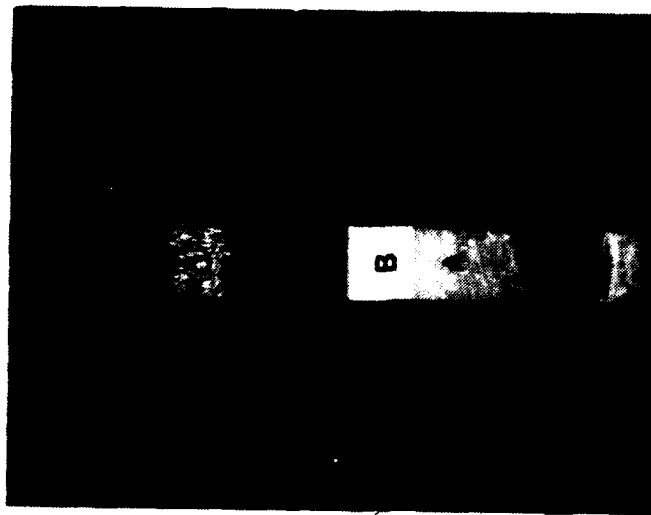
The conclusion to be drawn from these observations is that there appear to be two types of crack-growth behavior. One is a linear relation between  $J$  and  $\Delta a$ , and the other is an exponential relation.

Photographs of representative fracture surfaces are shown in Fig. 16. Fast fracture to place in the wide specimen No. 2, whereas stable crack growth without pop-in occurred in the narrow specimen, No. 14. In both cases, the crack grew in the center and was pinned at the edges,





(a)



(b)

Figure 16. Fracture Surfaces: (a) Specimen 2, 1-in. thick: (b) Specimen 14, 1/8-in. Thick. A and B are the machined notch, with B being at a 45-deg. angle. C is the fatigue precrack. Two different morphologies at C represent two different loads. D is the crack-growth portion and E the final fracture. F is the shear lip and is shown in (b).

producing a bowed crack front. The edges would eventually separate, leaving a shear lip. This lip is quite apparent in the narrow 0.25-in.-thick specimen. In the 0.125-in.-thick specimens, the crack front would be forced to a "V" shape by the shear lips. In the 1-in.-thick specimen shown in Fig. 16, the shear lips have not yet grown across the crack front when fracture occurred.

#### FRACTURE CRITERIA

In this section, criteria for characterizing the fracture behavior of PC are developed and discussed. These criteria are based upon two approaches. The first attempts to find a single value of  $J$  which describes the fracture toughness of PC, and the second attempts to describe the crack-growth behavior of PC in order to determine whether stable or unstable crack growth will take place in a structure.

The data base used to calculate the fracture criteria is made up of data from all of the PC tests except those on Specimens 14 and 22. The crack-growth behavior of these specimens was excluded because it may be the result of photographic error instead of true material behavior, as discussed in the previous subsection. The crack-growth data for Specimens 10, 12, 15, and 21 were divided into crack-growth and craze-growth groups. Only the crack-growth portion is used for fracture criteria because the craze zone is not a crack and can support load.<sup>26</sup> Use of the craze-plus-crack-length results in unreasonable values for some of the fracture criteria.

In order to find a single value of  $J$  which would characterize the fracture toughness of PC, an attempt was first made to find the value of  $J$  at the initiation of crack growth,  $J_{init}$ . This value has been used extensively in the literature for fracture toughness and is denoted by  $J_{IC}$ . An ASTM standard is being developed for its measurement. It corresponds to the linear-elastic fracture toughness,  $K_{IC}$ .

Since the PC data followed an exponential relation reasonably well, this relation was used to determine a value for  $J_{init}$ . Thus, the intersection of the crack-growth line, Eq. (16) with the blunting line, Eq. (5), was calculated. The values of  $J_{init}$  determined by this method ranged from near zero to 4.0 psi-in., as shown in Table 4. These small values of  $J$  at this intersection are due to the similarity in slopes of the crack-growth and the blunting lines. The slope of the blunting line is unity using logarithmic coordinates. When the slope of the crack-growth line approaches unity, the two lines are approximately parallel and intersect at very small values of  $J$ . From the slopes of the crack-growth lines, Table 2, it can be seen that when the slope is near one, the value of  $J_{init}$  determined by this method is very small. Consequently, this is not a suitable method for determining the value of  $J_{init}$  for PC. This method may be suitable for other materials if the slope of the crack-growth line is not near the slope of the blunting line.

Since an exponential relation failed to yield an accurate value of  $J_{init}$ , the linear relation of Eq. (11) was applied. Intersection of the linear-regression fit, Eq. (12), with the blunting line, Eq. (5), was to be the value of  $J_{init}$ . [Since the blunting line was nearly vertical, the value of the y-intercept,  $b$ , in Eq. (12) was actually used for  $J_{init}$ .] This method of determining  $J_{init}$  is nearly identical to the method used to find  $J_{IC}$  in the standard being developed by ASTM. The values of  $J_{init}$  resulting from this linear regression, as given in Table 4, range from 3 to 18 psi-in., with an average of 9.5 and standard deviation of 3.7 psi-in. denoted by  $9.5 \pm 3.7$  psi-in. Due to thickness or crack length no influence can be noted in  $J_{init}$ .

To determine whether the value of  $J_{init}$  from the linear regression could be used as an indicator of the initiation of crack growth, a value of  $J$  was estimated by examining the crack-growth data to identify the initiation of crack growth. These values are given in Table 4 under the column  $J_{init}$ -visual. The average value of  $J_{init}$  determined by this method was  $8.0 \pm 3.5$  psi-in., which agrees well with the linear value. The linear and

Table 4

## FRACTURE CRITERIA

SPECIMEN NO.	B NOMINAL (in.)	a/w INITIAL	J <sub>init</sub>			J at		T
			VISUAL (psi-in.)	LINEAR (psi-in.)	LOG (psi-in.)	$\Delta a = 2\%$ (psi-in.)	POP-IN (psi-in.)	
23	1	0.54	7.	2.9	$3 \times 10^{-8}$	25.5	42.	11.1
1	1	0.70	(a)	(a)	(a)	(a)	37.	(a)
2	1	0.70	4.	7.5	0.08	21.7	41.	4.82
22	1	0.76	(b)	29.9	24.0	38.2	42.	2.89
4	1/2	0.69	15.	17.6	4.0	25.5	43.	3.57
6	1/2	0.69	5.	7.1	0.005	19.4	42.	4.48
24	1/2	0.80	12.	10.7	0.36	28.0	42.	5.44
12 crack	1/4	.58	5.	9.3	0.91	23.0	45.	6.24
total	-	-	0.	0.71	$5 \times 10^{-4}$	14.0	-	6.30
13	1/4	0.68	10.	8.0	0.005	31.0	41.	8.11
10 crack	1/4	0.78	6.	10.6	0.56	27.3	(b)	5.50
total	-	-	0.	4.2	$7 \times 10^{-7}$	20.8	-	5.61
15 crack	1/8	0.59	5.	8.3	0.11	24.5	42.	7.43
total	-	-	0.	10.0	$1 \times 10^{-4}$	14.0	-	3.40
20	1/8	0.70	9.	9.8	0.38	20.8	38.	4.31
14	1/8	0.79	8.	29.1	13.0	45.0	(c)	4.42
21 crack	1/8	0.81	10.	12.6	3.2	27.2	(c)	5.50
total	-	-	0.	7.7	0.25	22.5	-	6.18

(a) Not measured

(b) Cannot determine

(c) No pop-in

"visual" values of  $J_{init}$  were compared for each specimen, and the linear value was on the average  $1.5 \pm 2.8$  psi-in. higher than the "visual" value. Thus,  $J_{init}$  from the linear regression provides a reliable estimate of the initiation of crack growth although the data do not follow the linear relation of Eq. (12).

These values of  $J_{init}$  are also in good agreement with those reported in the literature. Parvin and Williams<sup>31-32</sup> measured a  $J_{init}$  of 11.1 psi-in., and Fraser and Ward<sup>29</sup> report a value of 2.11 psi-in., this small value may be due to their very sensitive measurement technique.

As can be seen from the preceding paragraphs, the value of  $J$  at the initiation of crack growth is difficult to obtain. There is no physical means of determining whether a material is at the point of crack initiation. All that can be done directly is to bracket the value of  $J$  about this point. Indirect methods of determining this value must be used. These methods involve fitting a straight line, either linear or exponential, to a selected portion of the crack-growth data and extrapolating this line to an intersection with a formalized blunting line. The quantity for  $J$  which results from this method is an operational value and does not necessarily correspond to any direct physical quantity. At best, this indirect method is a means of determining  $J_{init}$  that may be useful in design calculations and serves as a reasonable estimate of the true value of  $J$  at the initiation of crack growth.

In order to avoid the difficulty of identifying when crack initiation occurs, it was decided to determine the value of  $J$  at 2% crack growth because this corresponds to the allowed amount of crack growth in ASTM Standard E399 for  $K_{IC}$ . This value of  $J$  should correspond to the value of  $K_{IC}$ , and should allow more of the intrinsic toughness of the material to be used in design. The principle advantage of this method is that the value determined corresponds to a physically known and directly measurable value of  $J$ . It should be pointed out that this value of 2% does not

represent the magic number and another value, such as 1%, could be used equally well. Also, this value of  $J$  can be found by fitting a straight line through the crack-growth data and interpolating to find the value of  $J$  at 2% crack growth. Interpolation has the advantage of being more reliable than extrapolation.

The value of  $J$  at 2% crack growth,  $J$  (2%), in PC was found by reviewing the data and estimating its value. Although this is not a quantitative procedure, the crack-growth data are closely spaced and, as a result, accurate determination can be made from the plots. The values of  $J$  (2%) ranging from 19 to 31 psi-in., with an average of  $25.0 \pm 3.5$  psi-in., are listed in Table 4. No effects of crack length or thickness upon  $J$  (2%) could be ascertained.

This value of  $J$  (2%) corresponds to a  $K$  of 3070 psi  $\sqrt{\text{in.}}$ , which is in good agreement with the  $K_{IC}$  value of 3300 psi  $\sqrt{\text{in.}}$  reported by Banasiak,<sup>34</sup> 3290 reported by Key and Katz,<sup>36</sup> and 3150 reported by Fraser and Ward.<sup>29</sup> The slightly lower value of  $J$  (2%) may be due to the difference in crack-growth direction in the present study. This good agreement between  $J$  (2%) and  $K_{IC}$  supports a position that  $J$  (2%) is a better measure of  $K_{IC}$  than  $J_{init}$ . The value of  $K$  which corresponds to  $J_{init}$  is 1735 psi  $\sqrt{\text{in.}}$ , which is 46% lower than the value of  $K_{IC}$  reported in the literature.

In order to determine whether the use of  $J$  (2%) would have wider applicability, this method was applied to the ASTM Round-Robin test results on A533B steel.<sup>14</sup> As pointed out previously, the crack-growth behavior of this material followed an exponential relation. Consequently, the value of  $J$  (2%) was found by interpolating an exponential fit to the data, although a linear fit was also interpolated. The value of  $J$  (2%) was found separately for each of the twelve participating laboratories. The average value of  $J$  (2%) was  $336 \pm 23 \text{ kJ/m}^2$  for the linear fit and  $330 \pm 16 \text{ kJ/m}^2$  for the exponential fit, corresponding to a  $J_{init}$  value of  $270 \pm 23 \text{ kJ/m}^2$  for the linear fit and  $190 \pm 39 \text{ kJ/m}^2$  for the

exponential fit. Thus, the value of  $J$  (2%) yields a reproducible number with less scatter than that for  $J_{init}$ , and it allows more of the toughness of the material to be used as a fracture criterion. Also,  $J$  (2%) is insensitive to the type of fit enjoyed, whereas  $J_{init}$  is extremely sensitive to the type of fit.

One difficulty with the use of either  $J_{init}$  or  $J$  (2%) in engineering design is that the material frequently has much more resistance to fracture than either of these values would seem to indicate. For PC, the value of  $J$  at the maximum load withstood by the specimen is given in Table 4. These values are at least four times greater than those of  $J_{init}$  and at least two times greater than those of  $J$  (2%). In order to utilize the available toughness of the material for design purposes, two approaches can be taken. One involves the use of the value of  $J$  at pop-in and the other, the use of the relation between crack growth and  $J$  in a stability analysis. It has been shown that the value of  $J$  at maximum load is not a material parameter but is dependent upon the specimen geometry.<sup>23</sup>

The value of  $J$  at pop-in for PC is given in Table 4. When unstable fracture occurred, the value of  $J$  at the fracture point was used as the pop-in value. The average value of  $J$  at pop-in was  $41.0 \pm 2.2$  psi-in. Specimen thickness and crack length had no effect upon this value. This value is in good agreement with a value of 35.2 psi-in. measured by Parvin and Williams.<sup>32</sup> For those specimens in which pop-in did not occur, the value of  $J$  at maximum load closely corresponded to the value of  $J$  at pop-in. However,  $J$  at pop-in may be due to the type of specimen employed. Tests should be made with either a single-edge-notch specimen pulled in tension or a center-cracked panel before  $J$  at pop-in is used to characterize the fracture toughness of PC. (Although Brinson<sup>33</sup> tested center-cracked panels, the thickness employed was in the plane-stress regime.) It should be noted that in other materials, the value of  $J$  at maximum load cannot be used to characterize fracture toughness because the value of  $J$  is dependent upon specimen geometry.<sup>23-24</sup> However, it is not known whether this geometrical dependence holds for  $J$  at pop-in

since other materials usually do not exhibit the type of pop-in behavior exhibited in PC. (The physical cause for the pop-in behavior in PC is not known.)

The second method for utilizing the available toughness of the material involves characterization of the crack-growth behavior as a function of  $J$ . Then the stability of crack growth in a structure can be calculated. A method proposed for this stability calculation is the Tearing Instability Theory of Paris, et al.<sup>25</sup> As discussed in the Introduction, a linear relation between crack growth and  $J$  is used to approximate the crack-growth behavior. This relation is expressed in terms of the tearing modulus,  $T$ , defined as

$$T = \frac{E}{\sigma_0} \frac{dJ}{da} \quad (7)$$

where  $E$  is the elastic modulus,  $\sigma_0$  the flow stress, and  $dJ/da$  the slope of the linear  $J$ - $\Delta a$  curve. This modulus is a linear approximation to the  $J$ - $\Delta a$  curve, which is made at the early stages of crack growth. As discussed in previous paragraphs, the crack-growth behavior of PC and many other materials does not follow a linear relation with  $J$ , but rather an exponential relation. Although this exponential behavior does not invalidate the concept of the tearing modulus as a linear approximation, it appears that the applicability of the concept can be extended to a larger range of crack-growth behavior. If the exponential relation between  $J$  and  $\Delta a$ , Eq. (16), is differentiated and used for  $dJ/da$ , then the tearing modulus would take on the form

$$T = \frac{E}{\sigma_0} C m (\Delta a)^{(m-1)} \quad (19a)$$

or

$$T = \frac{E}{\sigma_0} (C)^{1/m} m (J)^{\frac{m-1}{m}} \quad (19b)$$



where Eq. (19b) is derived by using Eq. (16) to replace  $\Delta a$  with  $J$ . Equation (19b) enables the calculation of a value of  $J$  at which instability occurs in a given geometry. Equation (19) can be used to account for the continuously decreasing slope of the linear  $J$ - $\Delta a$  curve, which means that stability of the structure decreases with crack growth.

The value of the tearing modulus in Table 4 for PC was computed from the straight-line fit to the crack-growth data used to find the linear value of  $J_{init}$ . The flow stress was taken to be the average of the yield and ultimate stresses. The values of  $T$  ranged from 3.57 to 11.1, with an average of  $6.05 \pm 2.14$ . There were discernible effects of thickness or crack length upon  $T$ . The values of  $\log C$  and  $m$  for the exponential formulation of the tearing modulus, Eq. (19a) or (19b), have been given in Table 2 as  $b$  and  $m$ , respectively under the columns for  $\log J$ . The values of the slope,  $m$ , range from 0.473 to 0.915, with an average of  $0.677 \pm 0.128$ ; the value of the intercept,  $b$ , ranges from 0.436 to 0.873, with an average of  $0.611 \pm 0.157$  (excluding the "outlier" Specimens 14 and 22). No effects of thickness or crack length were evident from these values. Thus, the exponential relationship between  $J$  and  $\Delta a$  is

$$J = 438.5 (\Delta a)^{0.677} \quad (20)$$

where  $\Delta a$  is in inches. Differentiating Eq. (20) and substituting into Eqs. (19a) and (19b) result in the following equations for the tearing modulus,  $T_{log}$ :

$$T_{log} = 1.684 (\Delta a)^{-0.323} \quad (21a)$$

$$T_{log} = 30.67 (J)^{-0.477} \quad (21b)$$

where  $\Delta a$  is in inches. The results of Eqs. (21a) and (21b) are plotted in Fig. (17a) and (17b), along with the tearing modulus from the linear behavior,  $J = b + m\Delta a$ . These figures show that the linear tearing modulus is a good average of the logarithmic modulus, except at small values of  $J$  or  $\Delta a$ , where crack-tip blunting and not crack growth is occurring. Since

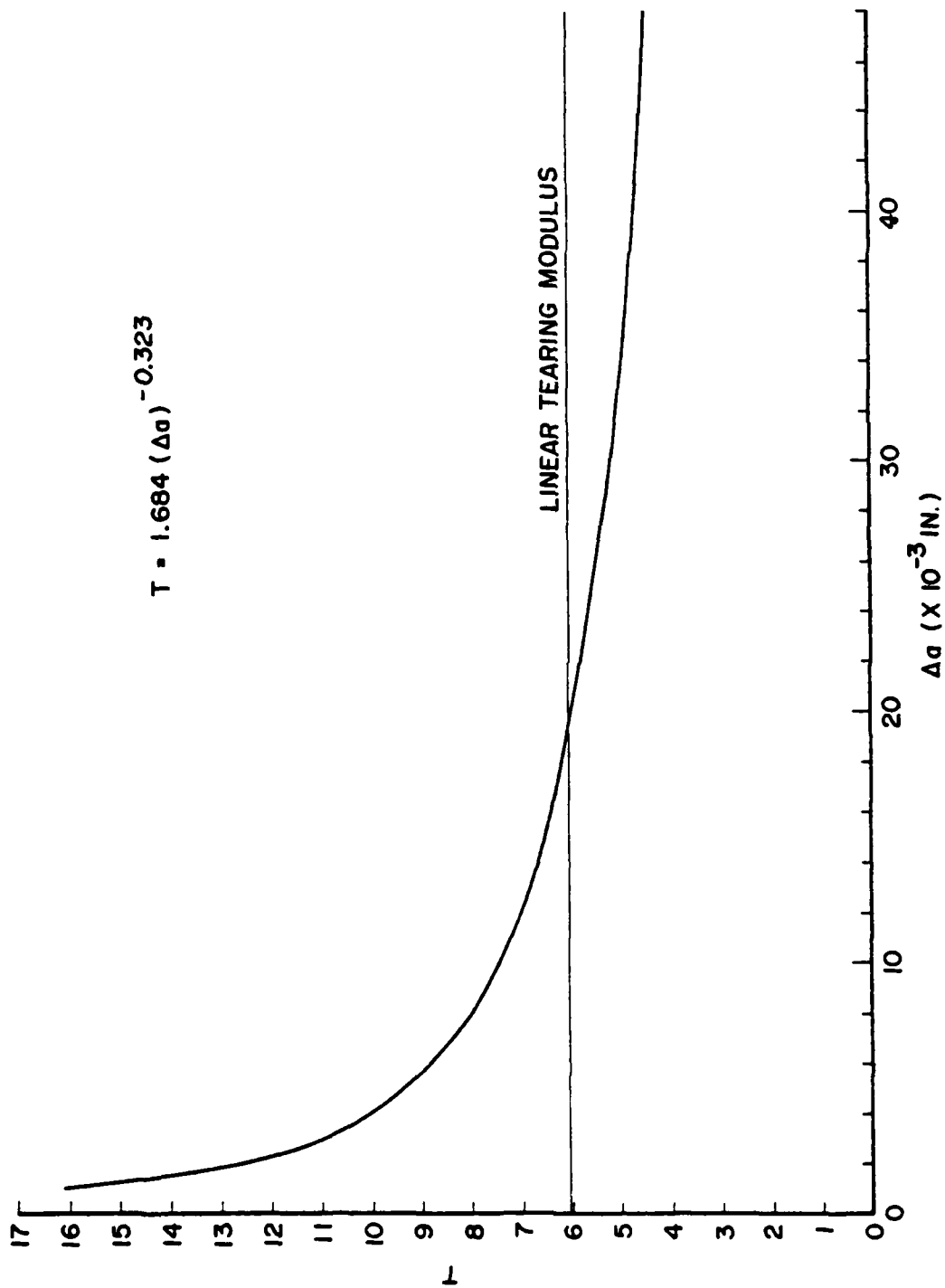


Figure 17(a). Tearing Modulus as a Function of Crack Growth from Exponential and Linear Fits of  $J$  vs  $\Delta a$ .  $T = 1.684 (\Delta a)^{-0.323}$ .

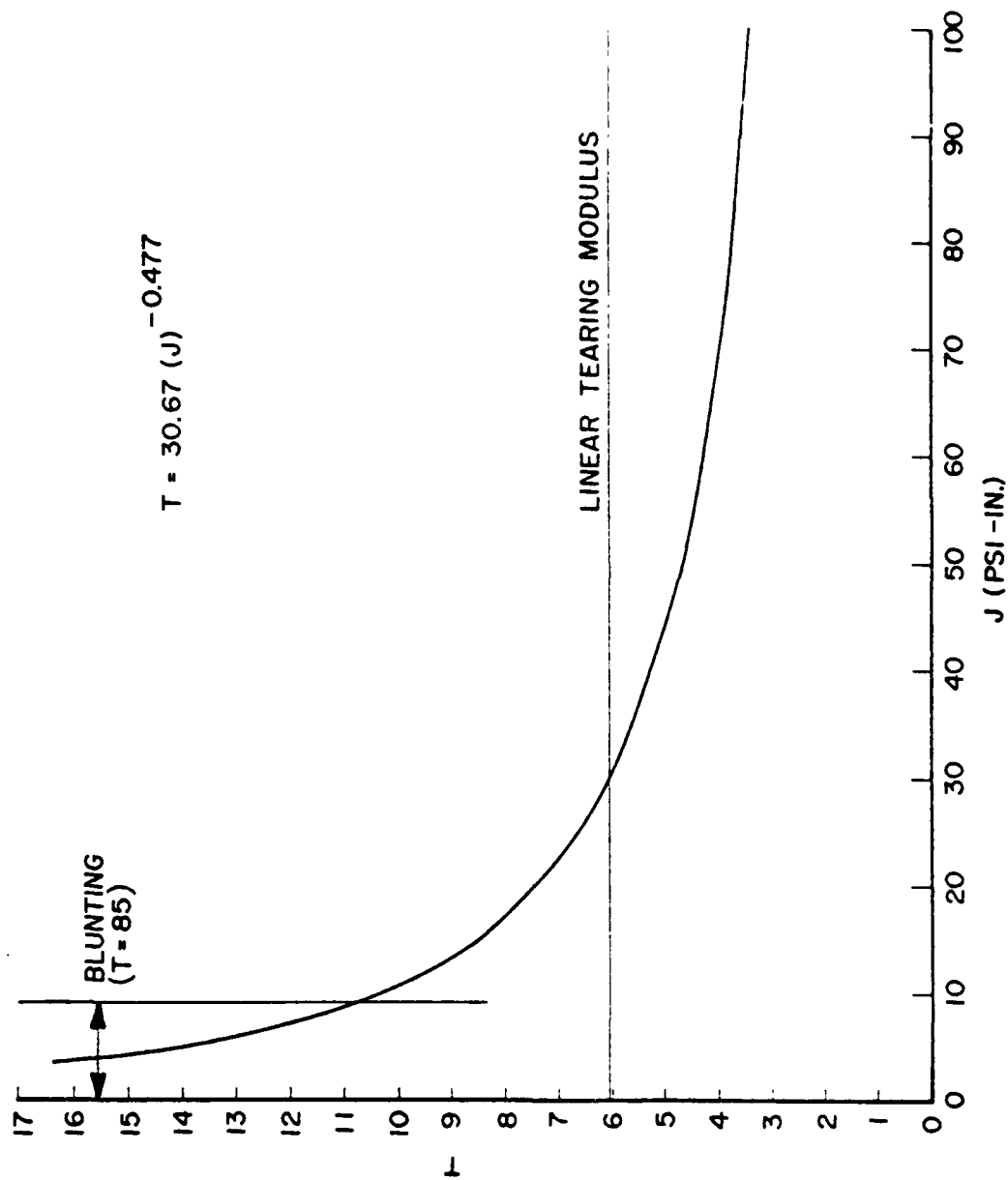


Figure 17(b). Tearing Modulus as a Function of J from Exponential and Linear Fits of J vs  $\Delta a$ .  $T = 30.67 (J)^{-0.477}$ .

the blunting behavior is formalized as a linear relation between  $J$  and  $\Delta a$ , the use of the linear tearing modulus would be appropriate in this regime. The value of  $T$  for crack-tip blunting is 85.5, which indicates a very high resistance to instability. (The use of  $T$  in the blunting regime is somewhat questionable since it is associated with crack extension.)

In the Introduction, a minimum specimen size above which  $J_{init}$  is invariant with respect to specimen dimensions was discussed. The size limitation was given by Eq. (6) in which a constant  $\alpha$  controls the size and usually varies from 25 to 50. Since the fracture criteria for PC showed no dependence upon thickness or crack length, the minimum dimension of 0.125 in. should be used in Eq. (5). Using this number,  $\alpha$  is less than or equal to 105 for  $J_{init}$ , 38 for  $J$  (2%), and 23 for  $J$  at pop-in.

SECTION 4  
CONCLUSIONS

1. a) The value of J at the initiation of crack growth in PC was found to be ~ 9 psi-in.  
b) The value of J at 2% crack growth in PC was found to be 25 psi-in.  
c) The value of J at pop-in for PC was found to be 41 psi-in.  
d) No effect of thickness or crack length upon the above values was observed.

2. The crack growth in PC was characterized by an exponential function of J

$$J = 438.5 (\Delta a)^{0.677}$$

where a is in inches and J is in psi-in. An exponential relation between J and crack growth was observed for other materials in the literature.

3. a) The value of the tearing modulus for a linear fit to J vs.  $\Delta a$  was found to be 6.05.  
b) A tearing modulus for exponential behavior,  $J = C (\Delta a)^m$ , for PC was found to be

$$T_{\log} = 1.684 (\Delta a)^{-0.323}$$

or

$$T_{\log} = 30.67 (J)^{-0.477}$$

where  $\Delta a$  is in inches and J is in psi-in. (T is nondimensional).

- c) No effect of thickness or crack length upon either of these moduli was observed.
  - d) The linear tearing modulus provided a reasonable approximation to the behavior of the logarithmic tearing modulus.
4. The J-integral provided a reasonable characterization of the non-linear fracture behavior of PC.

# REFERENCES

1. J. R. Rice, J. Appl. Mech. 35, 379 (June 1968).
2. J. D. Eshelby in Solid State Physics (F. Seitz and D. Turnbull, Eds.), Vol. 3 (Academic Press, New York, 1956), pp. 79-144.
3. F. A. McClintock, in Fracture (H. Liebowitz, Ed.), Vol. 3 (Academic Press, New York, 1971), pp. 47-225.
4. P. D. Hilton and J. W. Hutchinson, Eng. Frac. Mech. 3, 435 (1971).
5. J. W. Hutchinson, J. Mech. Phys. Solids 16, 13 (1968).
6. J. R. Rice and G. F. Rosengren, J. Mech. Phys. Solids 16, 1 (1968).
7. J. A. Begley and J. D. Landes, "The J-Integral as a Fracture Criterion," in Fracture Toughness, ASTM-STP 514 (American Society for Testing and Materials, Philadelphia, PA, 1972), pp. 1-20.
8. J. D. Landes and J. A. Begley, "Test Results from J-Integral Studies: An Attempt to Establish a  $J_{IC}$  Testing Procedure," in Fracture Analysis, ASTM-STP 560 (American Society for Testing and Materials, Philadelphia, PA, 1974), pp. 170-186.
9. J. R. Rice, P. C. Paris and J. G. Merkle, "Some Further Results of J-Integral Analysis and Estimates," in Progress in Flaw Growth and Fracture Toughness Testing, ASTM-STP 536 (American Society for Testing and Materials, Philadelphia, PA, 1973), pp. 231-245.
10. C. A. Griffis and G. R. Yoder, "Initial Crack Extension in Two Intermediate-Strength Aluminum Alloys," J. Eng. Mater. Tech., 152 (April 1976).
11. J. D. Landes, H. Walker, and G. A. Clark, "Evaluation of Estimation Procedures Used in J-Integral Testing," in Elastic-Plastic Fracture, ASTM-STP 668 (American Society for Testing and Materials, Philadelphia, PA, 1979), pp. 266-287.
12. B. A. Fields, J. Pressure Vessel Tech., 81 (February 1976).
13. W. J. Mills, J. Test. Eval. 9(1), 56 (January 1981).
14. G. A. Clarke, J. Test Eval. 8(5), 213 (September 1980).
15. G. A. Clarke, J. D. Landes, and J. A. Begley, J. Test. Eval. 8(5), 221 (September 1980).
16. G. Argy, P. C. Paris, and F. Shaw, "Fatigue Crack Growth and Fracture Toughness of 5083-0 Aluminum Alloy," in Properties of Materials for Liquefied Natural Gas Tankage, ASTM-STP 579 (American Society for Testing and Materials, Philadelphia, PA, 1975), pp. 96-137.

17. C. F. Shih, H. G. deLorenzi, and W. R. Andrews, "Studies on Crack Initiation and Stable Crack Growth," in Elastic-Plastic Fracture, ASTM-STP 668 (American Society for Testing and Materials, Philadelphia, PA, 1979), pp. 65-120.
18. C. Berger, H. P. Keller, and D. Munz, "Determination of Fracture Toughness with Linear-Elastic and Elastic-Plastic Methods," in Elastic-Plastic Fracture, ASTM-STP 668 (American Society for Testing and Materials, Philadelphia, PA, 1979), pp. 378-405.
19. A. J. Joyce and J. P. Gudas, "Computer Interactive  $J_{IC}$  Testing of Naval Alloys," in Elastic-Plastic Fracture, ASTM-STP 668 (American Society for Testing and Materials, Philadelphia, PA, 1979), pp. 458-468.
20. H. Takahashi, M. A. Khan, and M. Suzuki, J. Test. Eval. 8(2), 63 (March 1980).
21. H. Takahashi, M. A. Khan, and M. Suzuki, J. Test. Eval. 9(1), 14 (January 1981).
22. K. W. Carlson and J. A. Williams, "A More Basic Approach to the Analysis of Multiple Specimen R-Curves for Determination of  $J_C$ ," in Fracture Mechanics, ASTM-STP 743 (American Society for Testing and Materials, Philadelphia, PA, 1981), pp. 503-524.
23. J. D. Landes and J. A. Begley, "Recent Development in  $J_{IC}$  Testing," Westinghouse Research Labs Scientific Paper 76-1E7-JINTF-P3 (Westinghouse Research Labs., Pittsburgh, PA, May 1976).
24. F. Zaverl, Jr., "The Influence of Specimen Dimensions on a  $J_M$  Fracture Toughness Test," T. & A. M. Report No. 394 (Dept. of Theoretical and Applied Mechanics, University of Illinois, Urbana, IL., September 1974).
25. P. C. Paris, H. Tada, A. Zahoor, and H. Ernst, "The Theory of Instability of the Tearing Mode of Elastic-Plastic Crack Growth," in Elastic-Plastic Fracture, ASTM-STP 668 (American Society for Testing and Materials, Philadelphia, PA, 1979), pp. 5-36.
26. R. P. Kambour, J. Polymer Sci.: Macromolecular Rev. 7, 1 (1973).
27. N. Brown, "Methods of Studing Crazing," in Methods of Experimental Physics, Vol. 16C (Academic Press, New York, 1980), pp. 233-273.
28. A. J. Kinloch, Metal Sci. 14 (8,9), 305 (1980).
29. R. A. W. Fraser and I. M. Ward, Polymers 19(2), 220 (February 1978).

30. N. J. Mills, Eng. Frac. Mech. 6, 537 (1974).
31. M. Parvin and J. G. Williams, Int. J. Frac. 11 (6), 963 (December 1975).
32. M. Parvin and J. G. Williams, J. Mater. Sci. 10, 1883 (1975).
33. H. F. Brinson, Exp. Mech. 10, 72 (February 1970).
34. D. H. Banasiak, "Fatigue Crack Growth and Retardation Using Transparent Polycarbonate," Master's Thesis, Air Force Institute of Technology, Wright-Patterson Air Force Base, Ohio, June 1973.
35. D. H. Banasiak, A. F. Grandt, Jr., and L. T. Montulli, J. Appl. Polymer Sci. 21, 1297 (1977).
36. P. L. Key, Y. Katz and E. R. Parker, "An Application of Fracture Mechanics to Glassy Plastics," UCRL-17911 (University of California Radiation Laboratory, Livermore, CA, February 1968).
37. G. A. Clarke, W. R. Andrews, P. C. Paris, and D. W. Schmidt, "Single Specimen Tests for  $J_{IC}$  Determination," in Mechanics of Crack Growth, ASTM-STP 590 (American Society for Testing and Materials, Philadelphia, PA, 1976), pp. 27-42.
38. W. F. Christopher and D. W. Fox Polycarbonates (Reinhold Publishing Corp., New York, 1962).
39. SRL Quarterly Progress Report for period 18 June 1980 through 18 September 1980 under Air Force Contract F33615-79-C-5025 (Systems Research Laboratories, Inc., Dayton, OH, October 1980).
40. P. L. Cornes, K. Smith, and R. N. Haward, J. Polymer Sci. 15, 955 (1977).
41. J. A. Manson, R. W. Herzberg, S. L. Kim, and W. C. Wu "Fatigue Crack Propagation in Polycarbonate," in Toughness and Brittleness of Plastics (R. D. Deanin and A. M. Crugnola, Eds.), Advances in Chemistry Series, Vol. 154 (American Chemical Society, Wash., D.C., 1976) (from a symposium held in September 1974).
42. H. A. Ernst, P. C. Paris and J. P. Landes, "Estimations on J-Integral and Tearing Modulus T from a Single Specimen Test Record," Westinghouse R&D Center Scientific Paper 80-1D3-JINTF-P3, (Westinghouse R&D Center, Pittsburgh, PA, May 1980).
43. A. P. Green and B. B. Hundy, "Initial Plastic Yielding in Notch Bend Tests," J. Mech Phys. Solids 4, 128 (1956).
44. P. L. Key and Y. Katz, "On the Pop-In Mode of Fracture," Int. J. Frac. Mech. 5(1), 63 (March 1969).



- 45 J. A. Manson and R. W. Hertzberg, "Fatigue Failure in Polymers," CRC Critical Reviews in Macromolecular Science (Chemical Rubber Co., Cleveland, OH, August, 1973), pp. 433-500.
- 46 R. W. Hertzberg, J. A. Manson and W. C. Wu, "Structure of Polymers and Fatigue Crack Propagation," in Progress in Flaw Growth and Fracture Toughness Testing, ASTM-STP 536 (American Society for Testing and Materials, Philadelphia, PA, 1973), pp. 391-403.
- 47 R. W. Hertzberg and J. A. Manson, Fatigue of Engineering Plastics, (Academic Press, New York, 1980).
- 48 D. S. Dugdale, J. Mech. Phy. Solids 8, 100 (1960).

APPENDIX A  
LOAD-DISPLACEMENT CURVES

Load-displacement response of the PC specimens is given in the following curves. The amount of crack extension in mils which was measured from the photographs is noted at various load and displacement points on the curves.

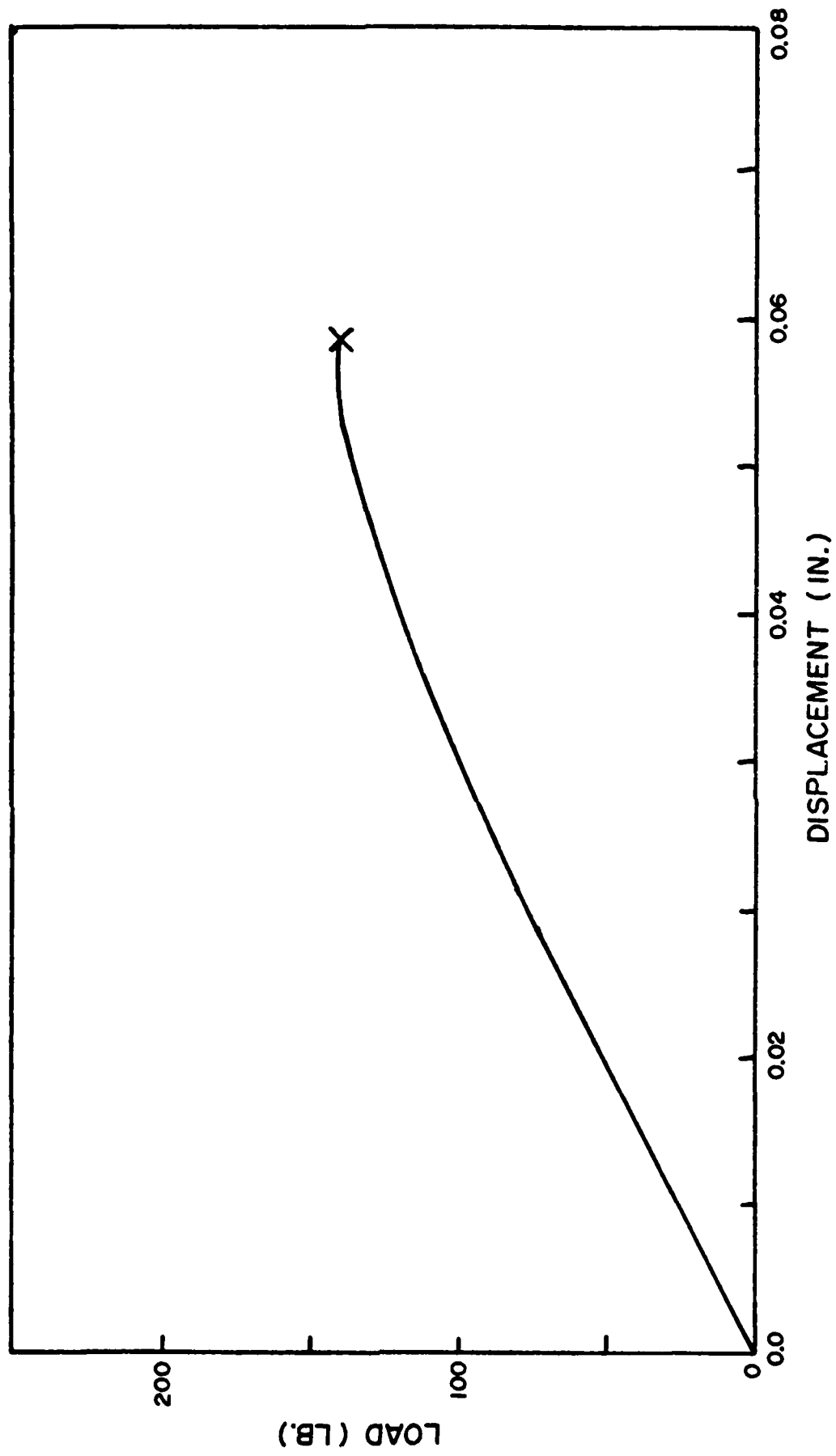


Figure A1. Load-Displacement Behavior of Specimen No. 1.

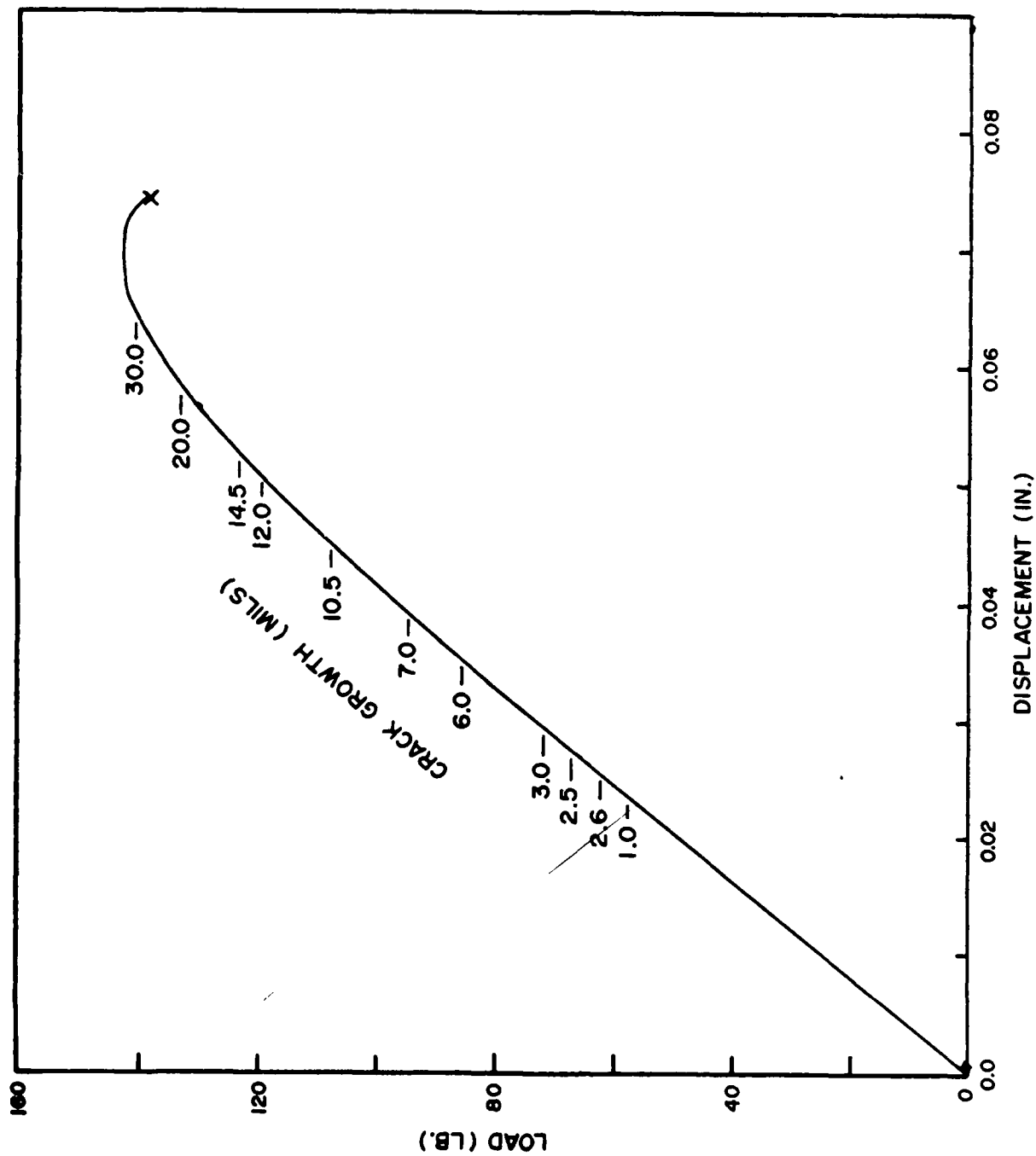


Figure A2. Load-Displacement Behavior of Specimen No. 2.

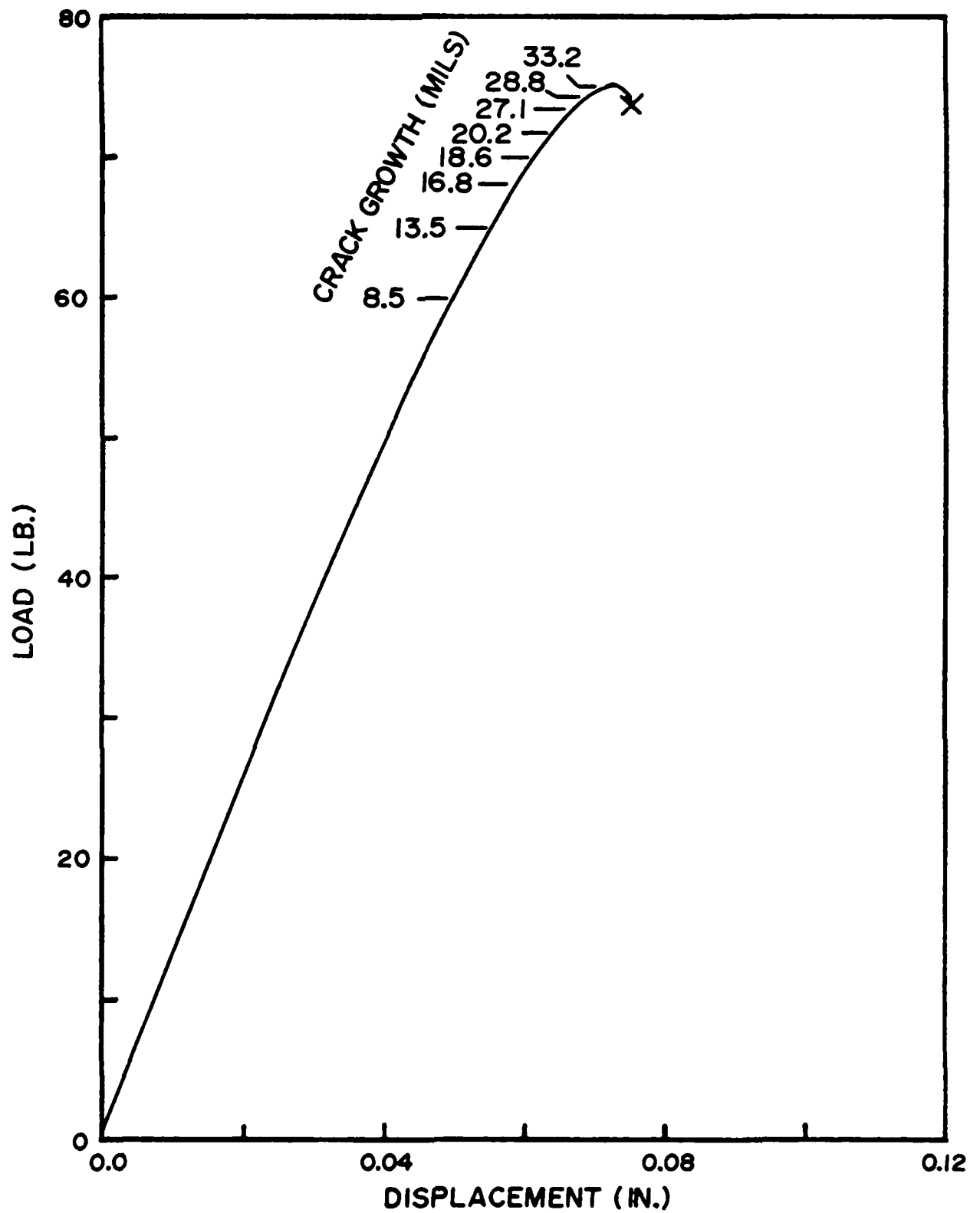


Figure A3. Load-Displacement Behavior of Specimen No. 4.

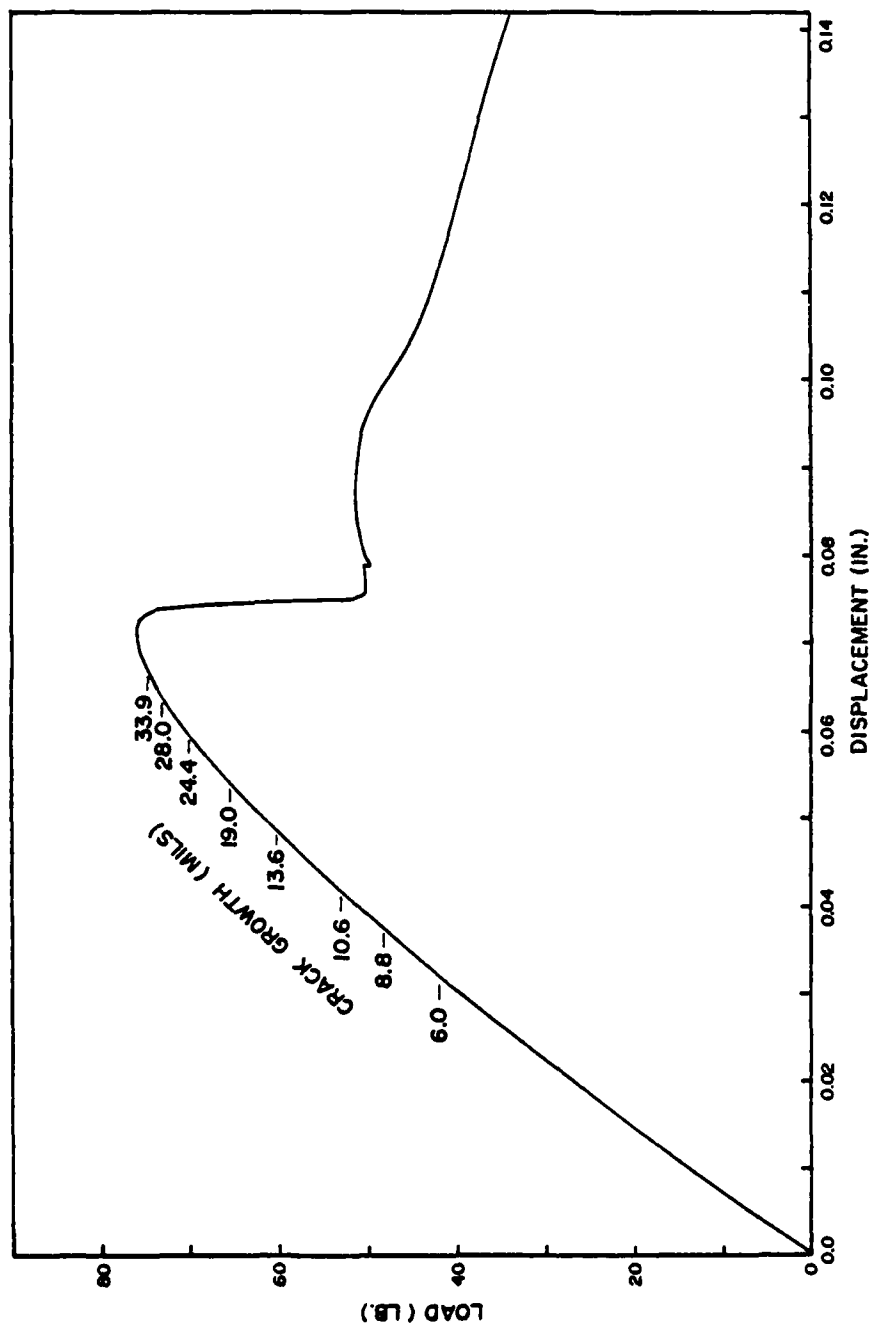


Figure A4. Load-Displacement Behavior of Specimen 6.

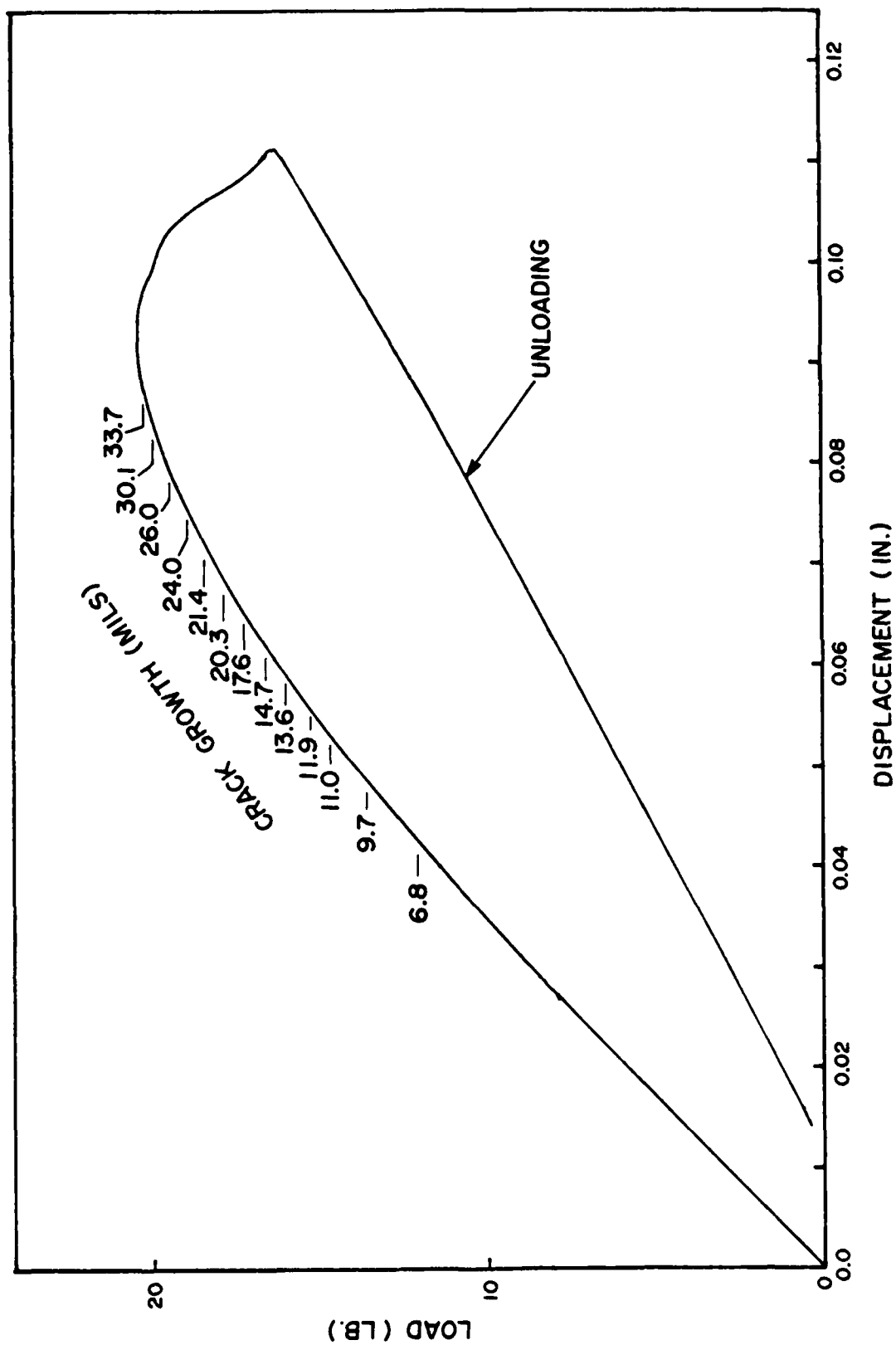


Figure A5. Load-Displacement Behavior of Specimen No. 10.

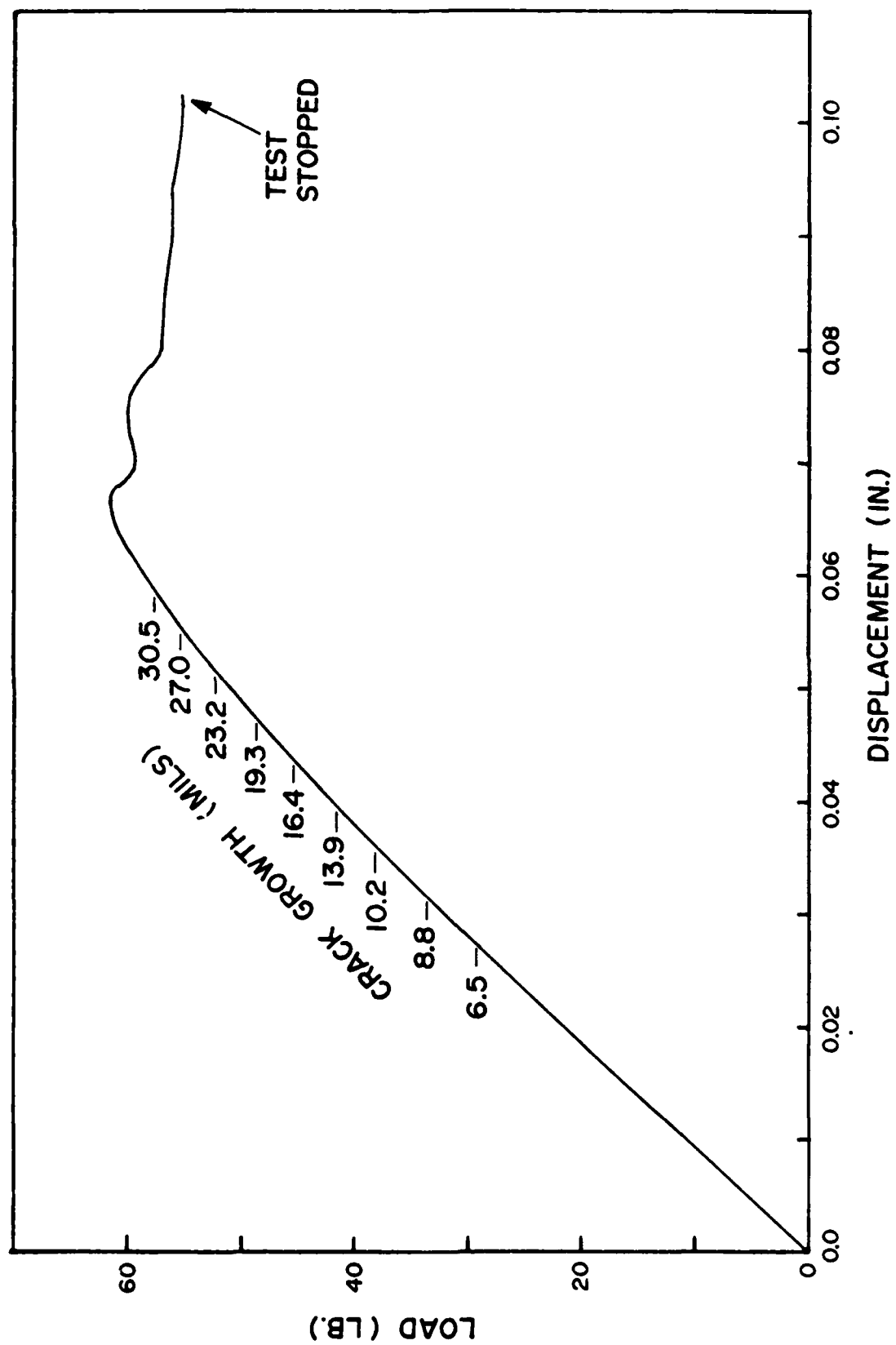


Figure A6. Load-Displacement Behavior of Specimen No. 12.



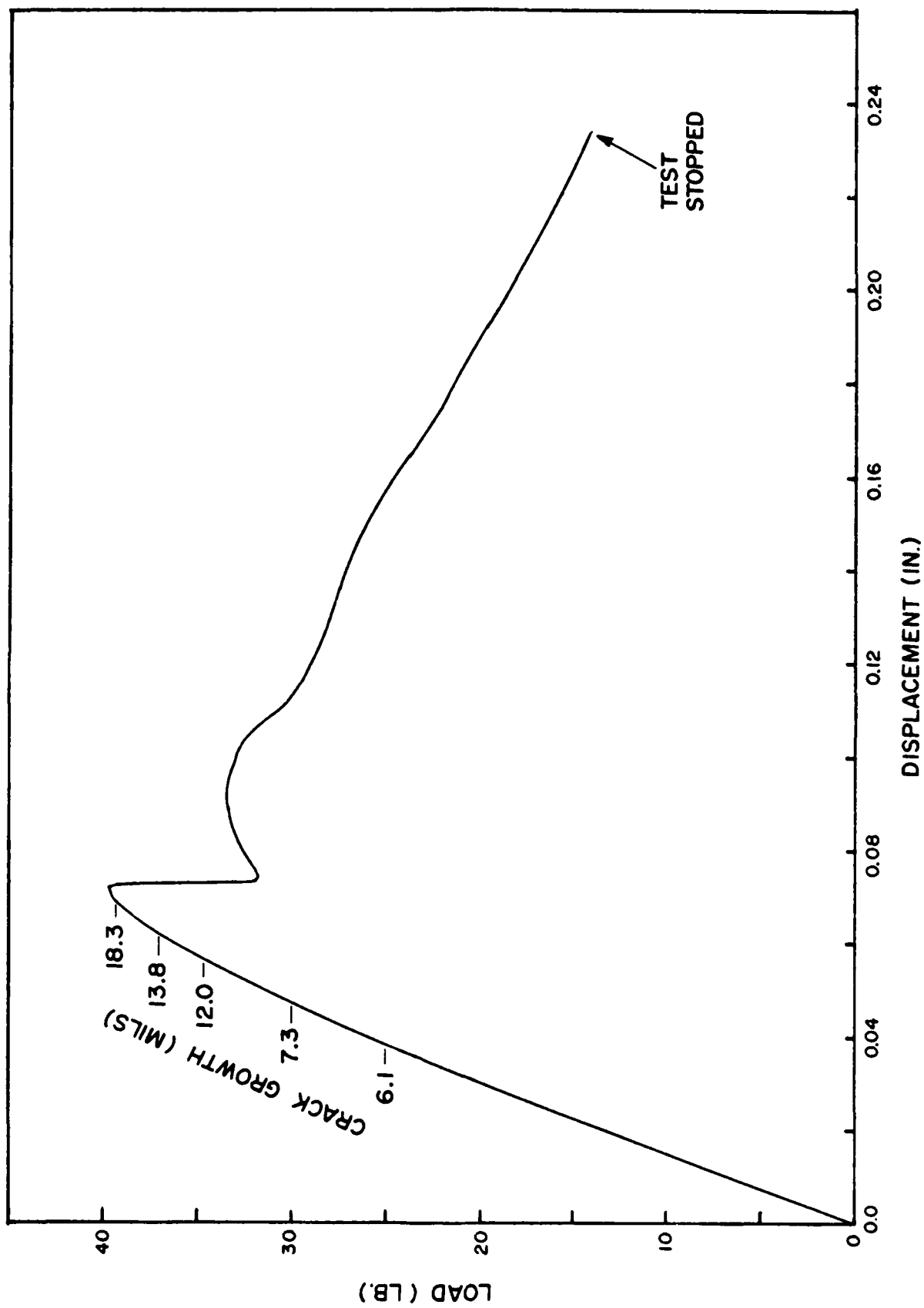


Figure A7. Load-Displacement Behavior of Specimen No. 13.

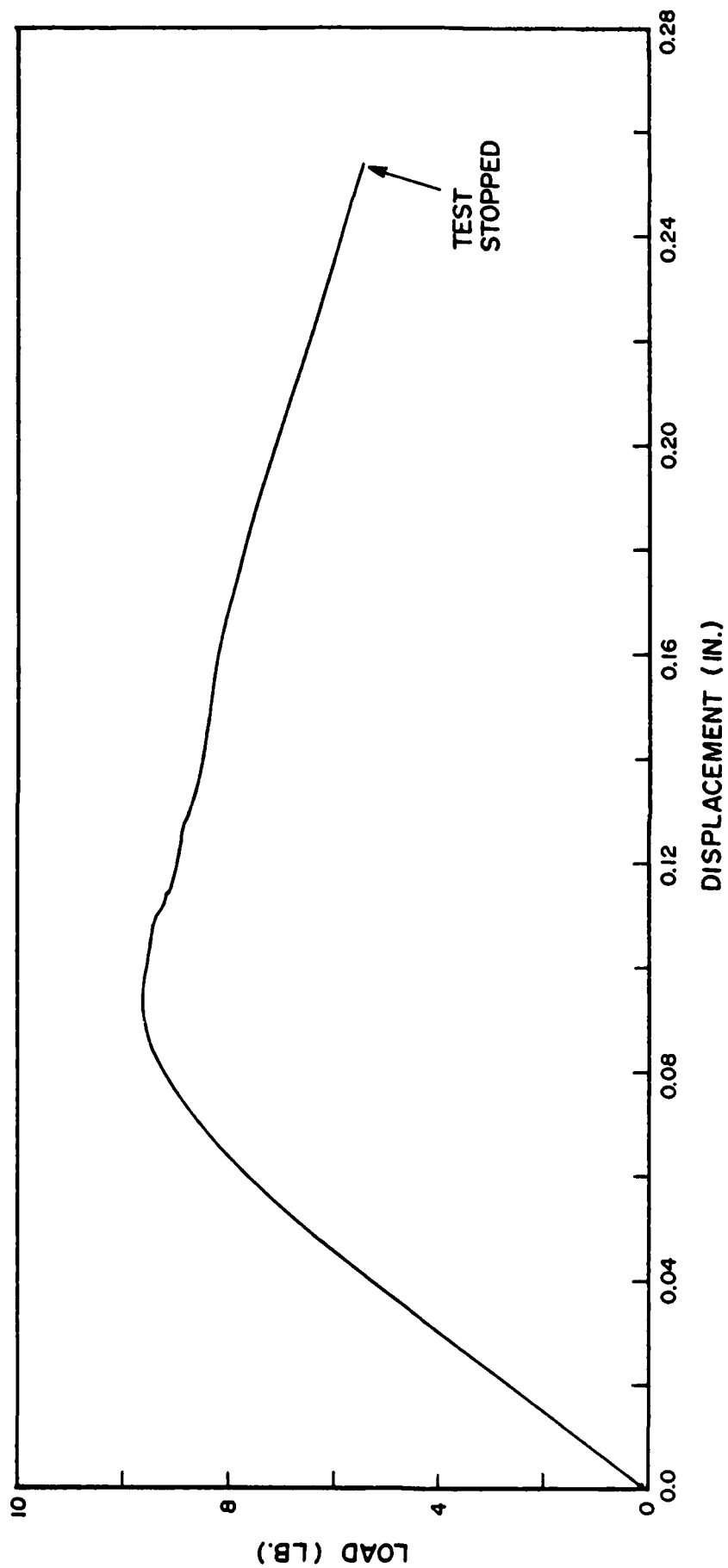


Figure A8. Load-Displacement Behavior of Specimen No. 14.

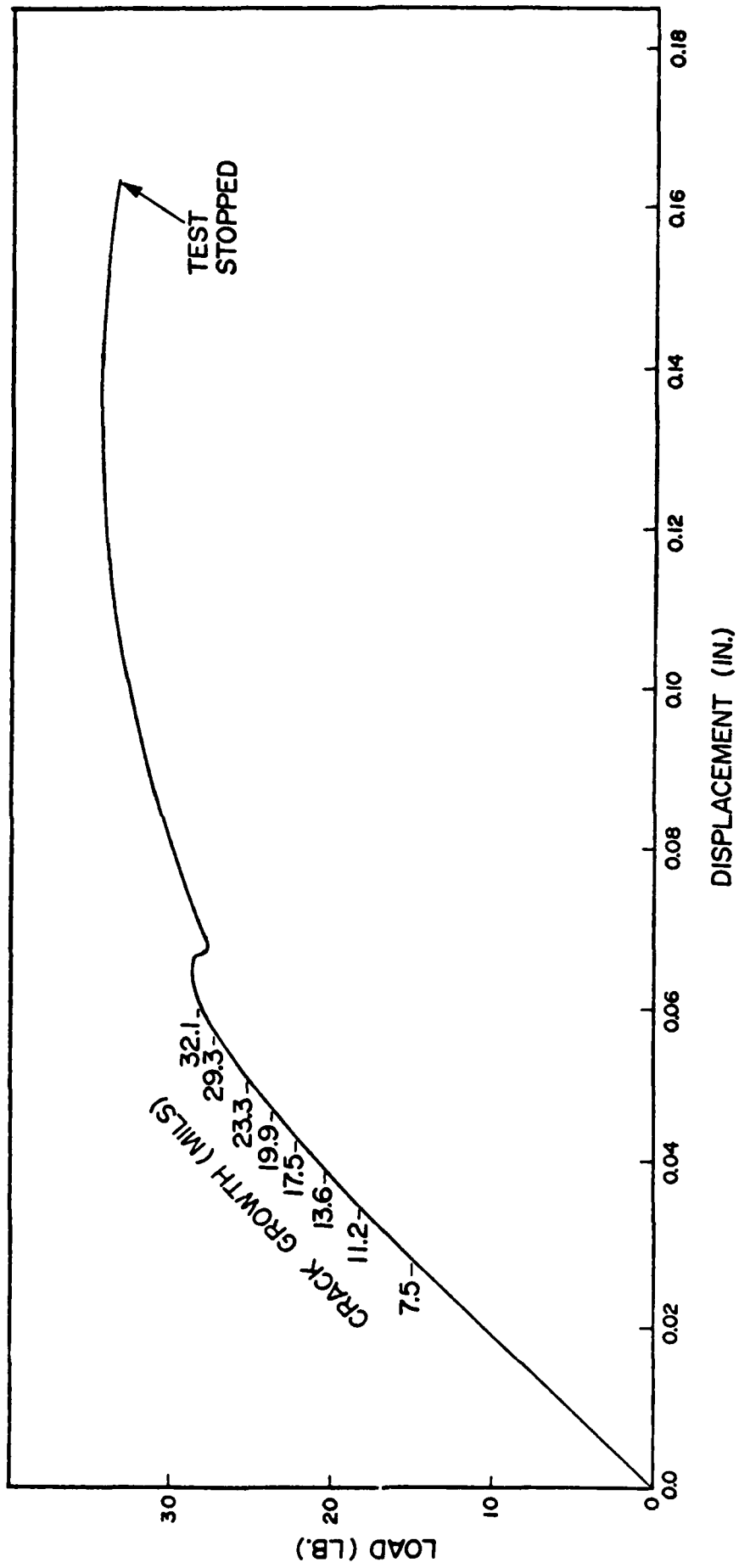


Figure A9. Load-Displacement Behavior of Specimen No. 15.

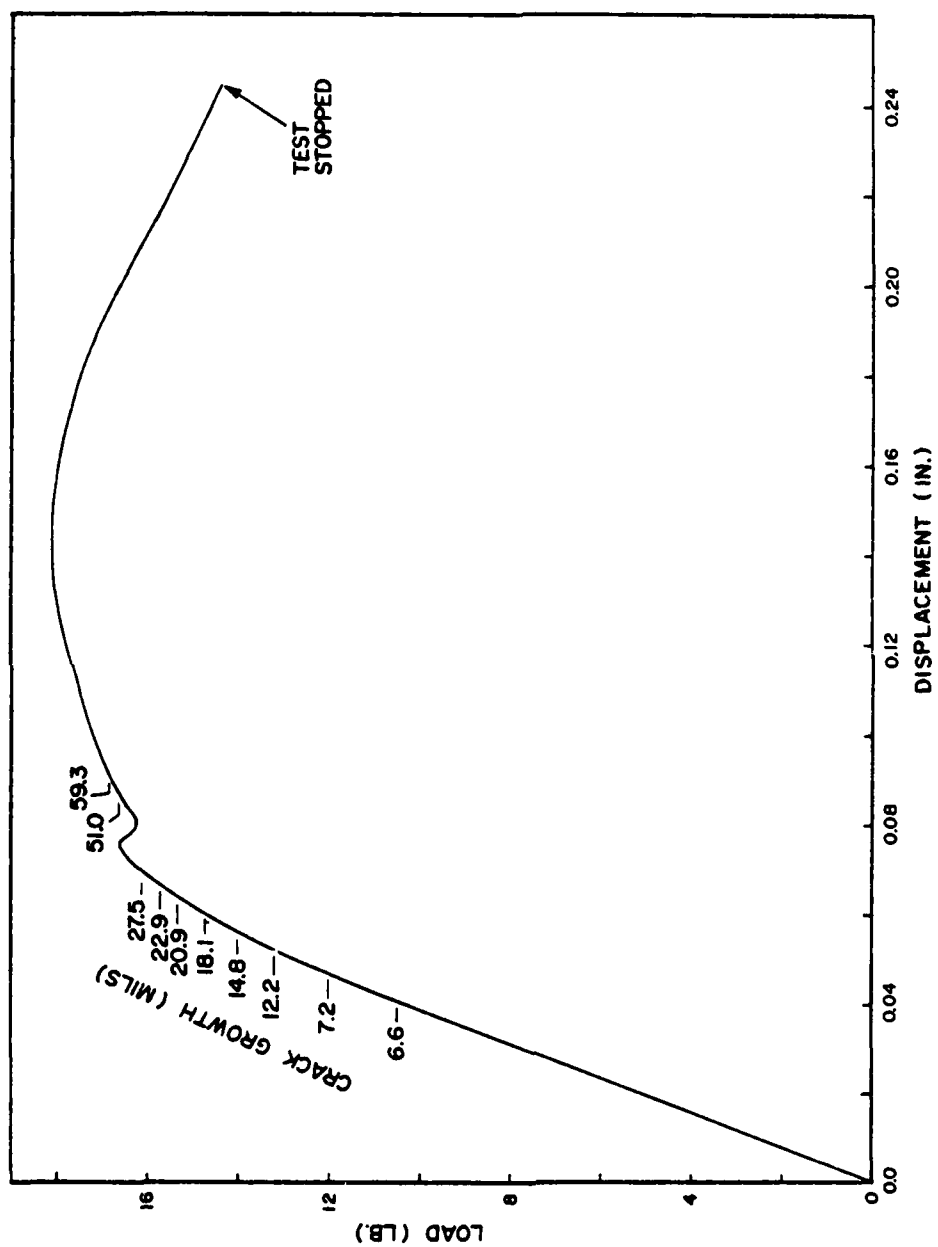


Figure A10. Load-Displacement Behavior of Specimen 20.

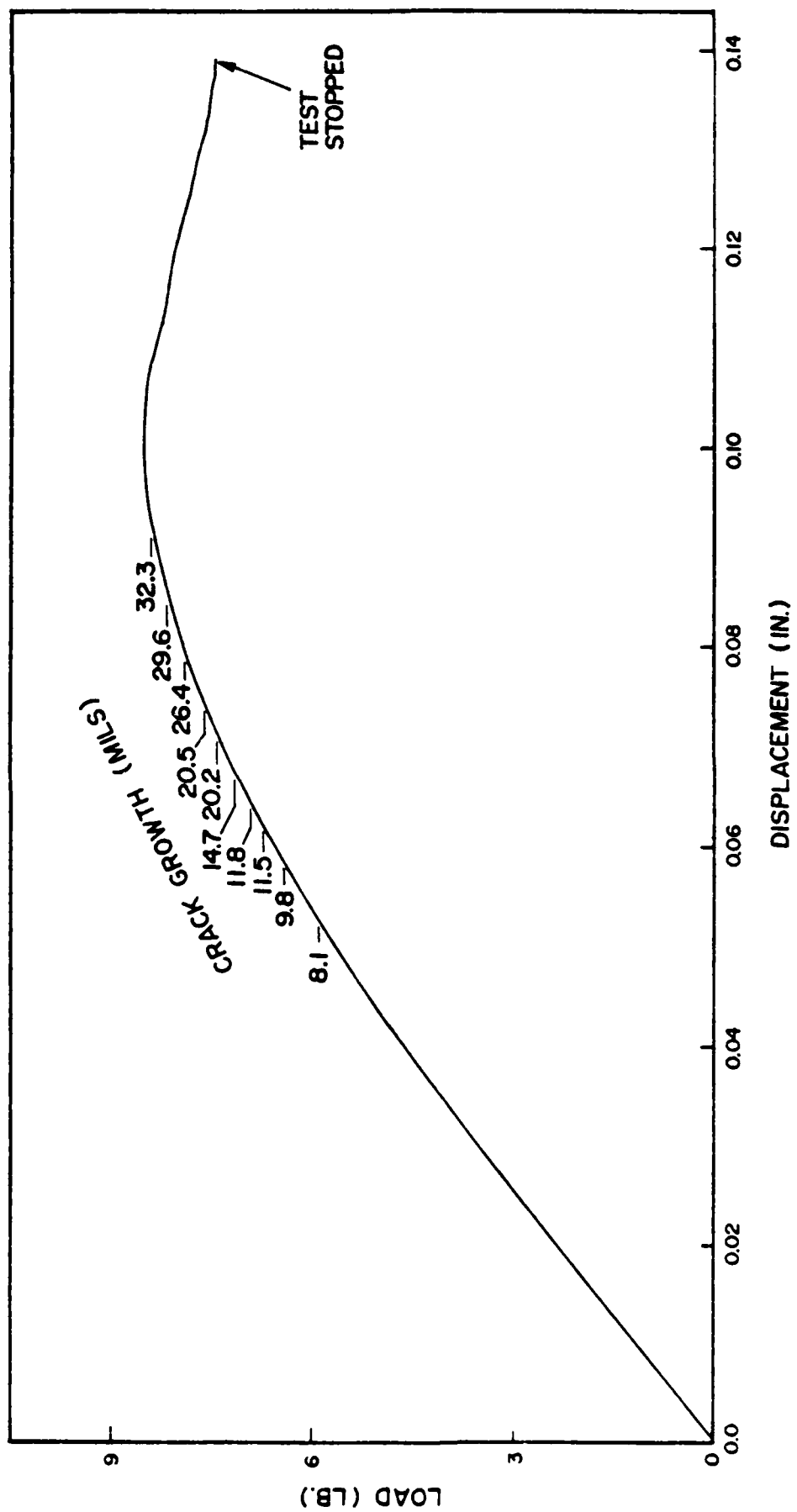


Figure A11. Load-Displacement Behavior of Specimen No. 21.

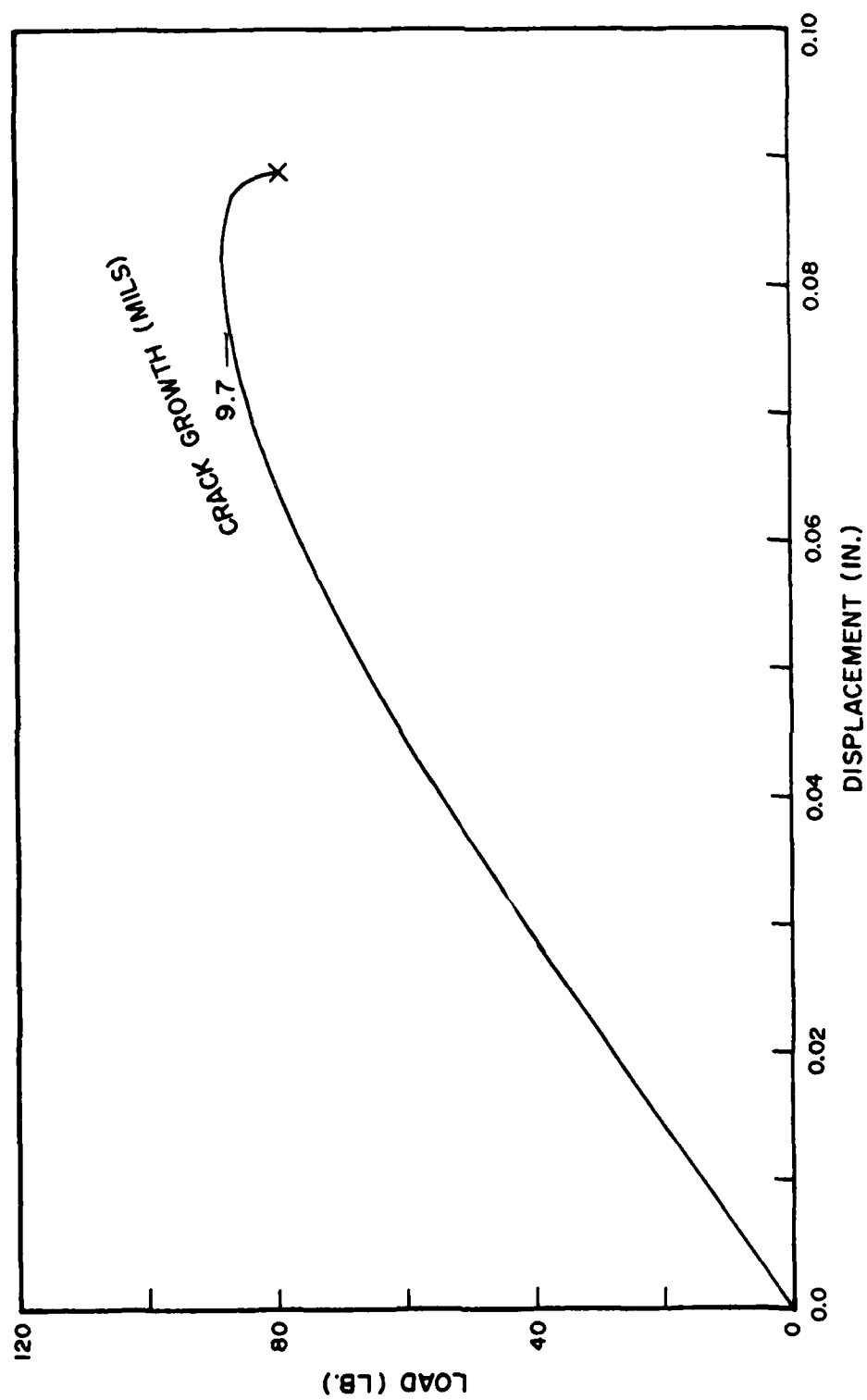


Figure A12. Load-Displacement Behavior of Specimen 22.

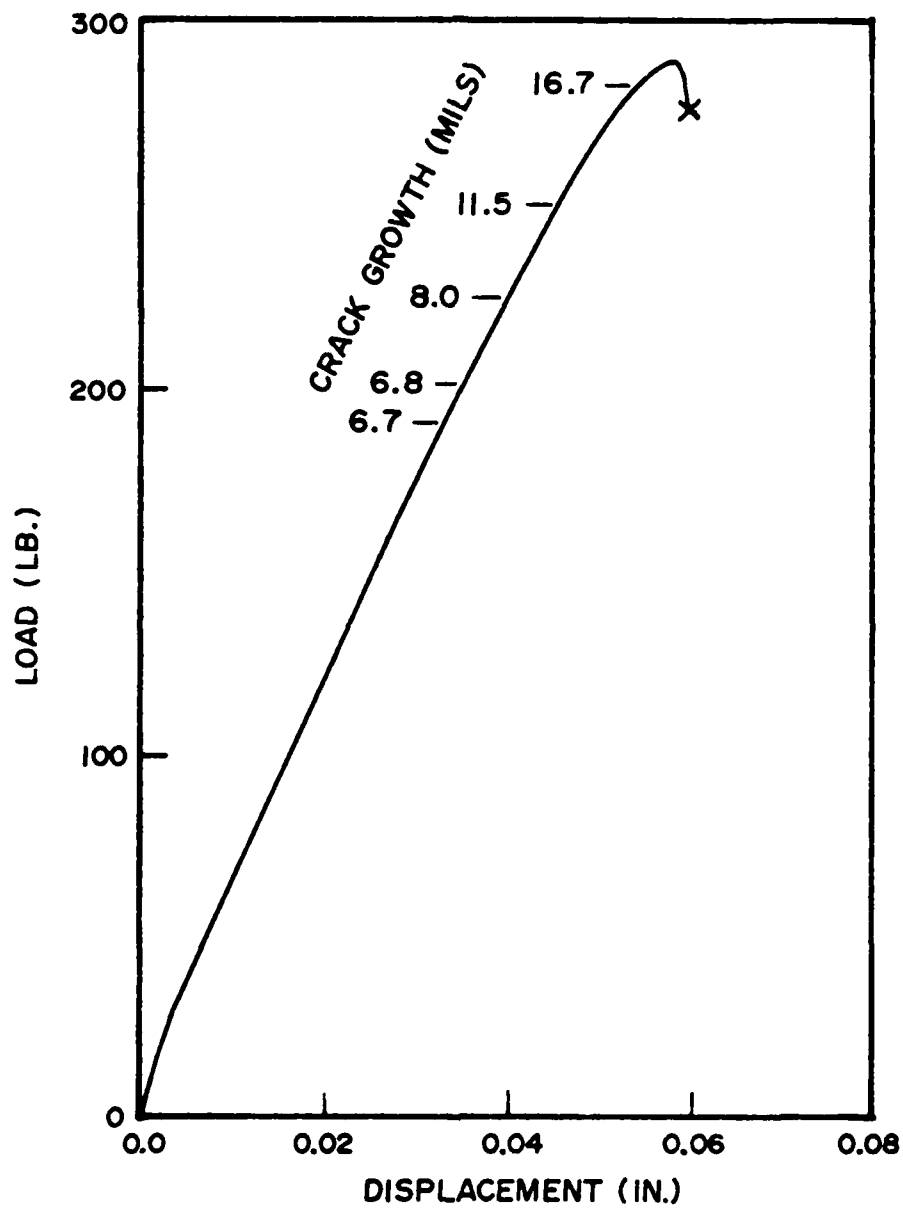


Figure A13. Load-Displacement Behavior of Specimen No. 23.

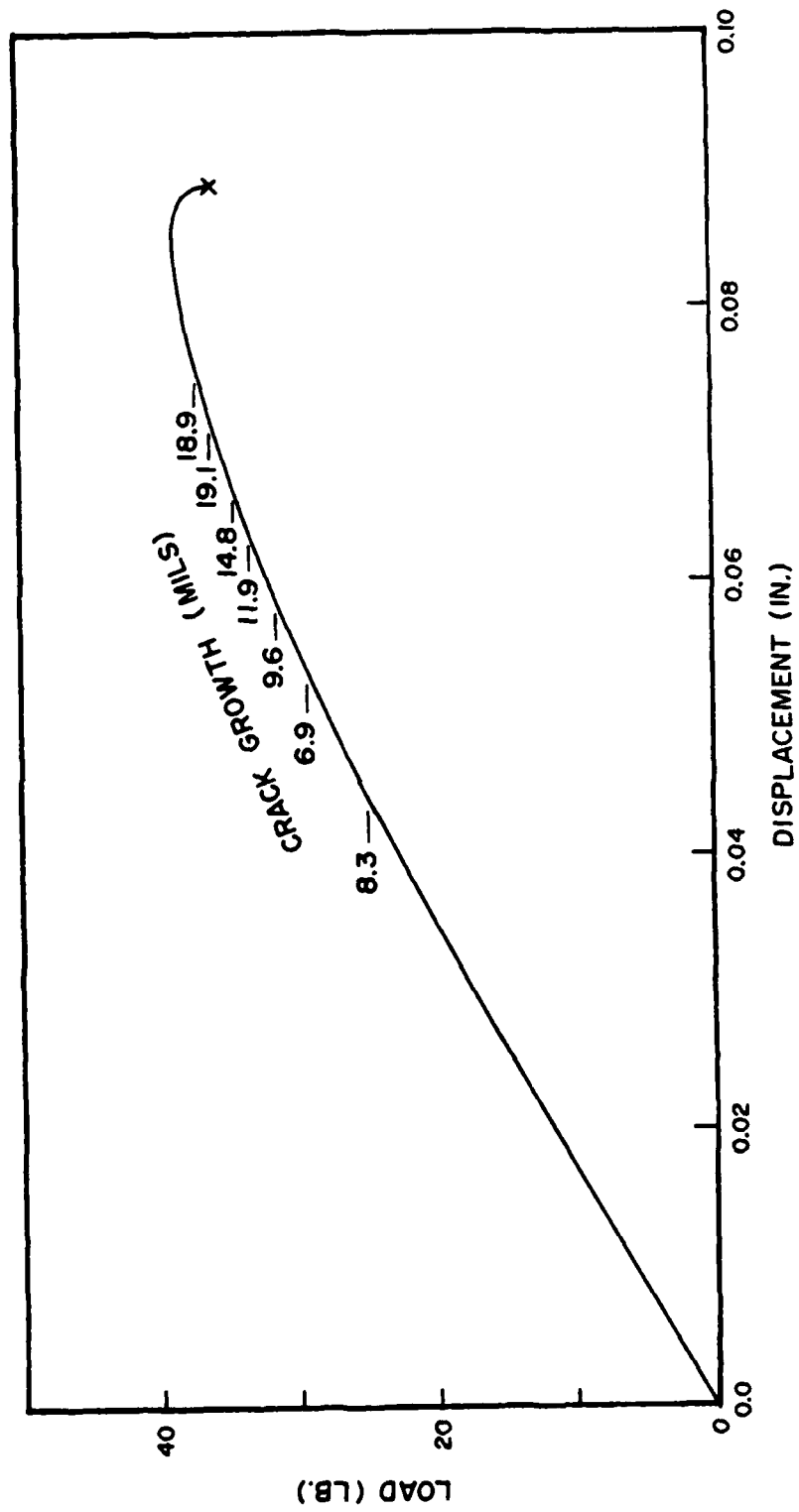


Figure A14. Load-Displacement Behavior of Specimen No. 24.



## APPENDIX B

### J VS. CRACK GROWTH FOR POLYCARBONATE

The values of  $J$  obtained by integration of the load vs. load-line-displacement results from three-point-bend specimens and the corresponding values of crack growth,  $\Delta a$ , measured from photographs are given in Tables B1-B13. The values of the stress-intensity factor,  $K$ , in each table were computed using the current load and the initial crack length. The height,  $W$ , for all specimens was nominally 1.01-in.

Plots of  $J$  vs.  $\Delta a$  using Cartesian coordinates for each specimen are shown in Figs. B1-B13. The linear line which begins at the origin and has the steeper slope is the blunting line,  $J = 2\sigma_f \Delta a$ , where  $\sigma_f$  is the flow stress. The second line, having the lesser slope, is a linear regression,  $J = b + m\Delta a$ , through data where  $\Delta a > 6$  mils, provided all subsequent crack growth is  $> 6$  mils. A linear regression was obtained for  $J$  vs. both crack growth and crack growth plus craze length for Specimen Nos. 10, 12, 15, and 21. These data which were used in the linear regression are also denoted in Tables B1-B13. In some photographs from Specimens 14, 20, and 24, the crack growth could not be determined accurately even though it was probably greater than 6 mils. Thus, crack-growth values are not given in the table and were not used in the linear regression.

Plots of  $J$  vs.  $\Delta a$  using log-log coordinates for each specimen are shown in Figs. B14-B26. The linear regression which made use of the same data,  $\Delta a > 6$  mils, as above would determine the constants  $C$  and  $m$  in the relationship  $J = C (\Delta a)^m$ .

Table B1

## CRACK-GROWTH DATA FOR SPECIMEN NO. 2

B = 0.998 in.

 $(a/W)_{init} = 0.698$ 

LOAD (lb)	K (psi $\sqrt{\text{in.}}$ )	J (psi-in.)	$\Delta a$		TOTAL (mils)
			CRACK (mils)	CRAZE (mils)	
52.75	1217.00	3.60	-	-	0.00
57.25	1321.00	4.25	-	-	1.00
62.00	1431.00	5.00	-	-	2.60
67.00	1545.00	5.80	-	-	2.50
71.75	1656.00	6.80	-	-	3.00
85.50	1973.00	9.80	-	-	6.00 *
94.50	2181.00	12.20	-	-	7.00 *
107.50	2481.00	16.00	-	-	10.50 *
119.25	2752.00	20.30	-	-	12.00 *
123.00	2839.00	21.70	-	-	14.50 *
133.00	3069.00	25.70	-	-	20.00 *
140.25	3237.00	32.00	-	-	30.00 *
142.25	3283.00	35.80	11.70	21.30	33.00 *
143.00	3300.00	37.50	15.40	21.60	37.00 *

\* Data used in linear regression.

Table B2

## CRACK-GROWTH DATA FOR SPECIMEN NO. 4

B = 0.500 in.

 $(a/W)_{init} = 0.693$ 

LOAD (lb)	K (psi $\sqrt{in.}$ )	J (psi-in.)	$\Delta a$		
			CRACK (mils)	CRAZE (mils)	TOTAL (mils)
2.50	112.40	0.00	-	-	0.00
5.50	247.30	.20	-	-	3.00
10.25	460.90	.60	-	-	2.60
20.00	899.40	2.00	-	-	4.25
24.50	1102.00	3.00	-	-	4.00
30.50	1372.00	4.75	-	-	6.25
40.00	1799.00	8.50	-	-	3.20
50.00	2248.00	13.70	-	-	3.60
60.00	2698.00	20.50	-	-	8.50 *
65.00	2923.00	24.70	-	-	13.50 *
68.00	3058.00	28.00	-	-	16.80 *
70.00	3148.00	30.00	-	-	18.60 *
71.75	3227.00	32.25	-	-	20.20 *
73.50	3305.00	35.50	-	-	27.10 *
74.25	3339.00	37.00	-	-	28.80 *
75.00	3373.00	40.00	-	-	33.20 *
74.00	3328.00	43.30	-	-	39.70 *
71.50	3215.00	44.00	-	-	47.25 *

\* Data used in linear regression.

Table B3

## CRACK-GROWTH DATA FOR SPECIMEN NO. 6

$$B = 0.498 \text{ in.}$$

$$(a/W)_{\text{init}} = 0.686$$

LOAD (lb)	K (psi $\sqrt{\text{in.}}$ )	J (psi-in.)	$\Delta a$		
			CRACK (mils)	CRAZE (mils)	TOTAL (mils)
4.25	185.40	0.00	-	-	6.50
14.50	532.60	.80	-	-	6.80
22.25	970.80	2.16	-	-	7.80
30.00	1309.00	4.17	-	-	8.60
35.50	1549.00	6.01	-	-	4.20
42.00	1832.00	8.52	-	-	6.00*
48.25	2105.00	11.80	-	-	8.80*
53.00	2312.00	14.40	-	-	10.60*
60.25	2629.00	19.30	-	-	13.60*
65.52	2858.00	23.60	-	-	19.00*
70.00	3054.00	28.50	-	-	24.40*
73.00	3185.00	32.10	-	-	28.00*
74.75	3261.00	35.30	-	-	33.90*
75.75	3305.00	37.70	-	-	35.80*
75.75	3305.00	40.50	-	-	43.80*
74.25	3240.00	41.70	-	-	49.90*
54.50	2378.00	42.90	-	-	116.00*
50.60	2208.00	46.30	-	-	140.00*

\* Data used in linear regression.

Table B4

## CRACK-GROWTH DATA FOR SPECIMEN NO. 10

$$B = 0.250 \text{ in.}$$

$$(a/W)_{\text{init}} = 0.782$$

LOAD (lb.)	K (psi $\sqrt{\text{in.}}$ )	J (psi-in.)	$\Delta a$		
			CRACK (mils)	CRAZE (mils)	TOTAL (mils)
1.30	196.00	.10	-	-	-
2.00	302.00	.20	-	-	-
3.00	453.00	.30	-	-	-
4.50	679.00	1.10	-	-	-
6.00	906.00	2.00	-	-	-
7.50	1132.00	3.50	-	-	-
9.00	1359.00	5.10	-	-	4.00
10.50	1585.00	7.00	-	-	6.00 *
12.00	1812.00	9.40	3.50	3.30	6.80 *
13.50	2038.00	12.20	4.40	5.30	9.70 *
14.60	2204.00	14.80	6.40	4.60	11.00 *
15.20	2295.00	16.30	7.50	4.40	11.90 *
15.90	2401.00	18.00	8.50	5.10	13.60 *
16.50	2491.00	19.70	9.00	5.70	14.70 *
17.10	2582.00	21.70	10.90	6.70	17.60 *
17.70	2672.00	23.70	13.00	7.30	20.30 *
18.30	2763.00	26.00	15.00	6.40	21.40 *
18.80	2839.00	28.70	17.30	6.70	24.00 *
19.30	2914.00	31.50	20.70	5.30	26.00 *
19.80	2990.00	34.70	22.50	7.60	30.10 *
20.10	3035.00	37.00	25.60	3.10	33.70 *
20.20	3050.00	38.50	28.70	7.40	36.10 *
20.30	3065.00	40.30	29.20	3.30	37.50 *
20.30	3065.00	43.20	30.20	7.90	38.10 *
20.20	3050.00	44.80	34.20	7.20	41.40 *
20.00	3020.00	46.00	36.40	7.00	43.40 *
19.80	2990.00	46.50	39.00	5.60	45.60 *
19.70	2974.00	47.50	39.70	8.20	47.90 *

\* Data used in linear regression.

Table B5

## CRACK-GROWTH DATA FOR SPECIMEN NO. 12

$$B = 0.248 \text{ in.}$$

$$(a/W)_{\text{init}} = 0.582$$

LOAD (lb.)	K (psi $\sqrt{\text{in.}}$ )	J (psi-in.)	$\Delta a$		
			CRACK (mils)	CRAZE (mils)	TOTAL (mils)
1.40	79.00	0.00	-	-	-
5.50	311.00	.10	-	-	-
10.00	556.00	.60	-	-	.90
15.20	860.00	1.90	-	-	2.30
20.20	1142.00	3.30	-	-	2.80
25.10	1420.00	5.30	-	-	4.60
28.70	1623.00	7.00	-	-	5.50
29.20	1651.00	7.50	-	-	6.50*
33.80	1912.00	9.90	3.20	5.60	8.80*
38.20	2160.00	13.00	4.80	5.40	10.20*
41.80	2354.00	15.80	6.90	7.00	13.90*
45.30	2562.00	18.90	8.10	8.30	16.40*
48.80	2760.00	22.50	11.30	8.00	19.30*
52.20	2952.00	26.50	15.80	7.40	23.20*
55.20	3122.00	30.50	18.70	9.30	27.00*
57.80	3269.00	34.20	23.00	7.50	30.50*

\* Data used in linear regression

Table B6  
CRACK-GROWTH DATA FOR SPECIMEN NO. 13

$B = 0.250 \text{ in.}$

$(a/W)_{\text{init}} = 0.681$

LOAD (lb)	K (psi $\sqrt{\text{in.}}$ )	J (psi-in.)	$\Delta a$		
			CRACK (mils)	CRAZE (mils)	TOTAL (mils)
2.00	159.70	0.00	-	-	-
3.00	254.60	.25	-	-	-
5.00	424.30	.50	-	-	2.80
10.00	848.50	1.75	-	-	4.70
12.60	1069.00	2.90	-	-	2.70
15.00	1273.00	4.25	-	-	5.50
17.50	1485.00	5.80	-	-	4.50
19.90	1689.00	7.60	-	-	4.70
23.50	1994.00	10.75	-	-	4.40
25.00	2121.00	12.25	-	-	6.10*
30.00	2546.00	18.40	-	-	7.30*
34.70	2944.00	26.00	-	-	12.00*
37.00	3140.00	30.75	-	-	13.80*
39.30	3335.00	37.70	-	-	18.30*
39.50	3352.00	39.25	-	-	20.00*
38.00	3224.00	41.00	-	-	26.60*
31.80	2698.00	41.75	-	-	71.60*

\* Data used in linear regression.

Table B7

## CRACK-GROWTH DATA FOR SPECIMEN NO. 14

$$B = 0.124 \text{ in.}$$

$$(a/W)_{\text{init}} = 0.785$$

LOAD (lb)	K (psi√in.)	J (psi-in.)	$\Delta a$		
			CRACK (mils)	CRAZE (mils)	TOTAL (mils)
2.00	621.70	1.00	-	-	0.00
2.90	901.50	2.25	-	-	1.70
4.00	1243.00	4.50	-	-	1.40
5.10	1585.00	7.25	-	-	1.60
6.00	1865.00	10.25	-	-	2.70
7.10	2207.00	14.75	-	-	4.20
8.00	2487.00	20.00	-	-	6.90 *
9.00	2793.00	27.75	-	-	-
9.60	2984.00	36.75	-	-	7.20 *
9.60	2984.00	40.00	-	-	10.10 *
9.60	2984.00	43.00	-	-	13.80 *
9.50	2953.00	47.00	-	-	19.50 *
9.50	2953.00	47.50	-	-	19.70 *
9.50	2953.00	48.00	-	-	21.60 *
9.45	2938.00	49.00	-	-	24.10 *
9.45	2938.00	50.00	-	-	25.00 *
9.40	2922.00	51.25	-	-	24.20 *
9.35	2906.00	52.00	-	-	29.80 *
9.20	2860.00	54.00	-	-	36.80 *
9.10	2829.00	55.50	-	-	39.30 *

\* Data used in linear regression.



Table B8

## CRACK-GROWTH DATA FOR SPECIMEN NO. 15

$$B = 0.125 \text{ in.}$$

$$(a/W)_{\text{init}} = 0.585$$

LOAD (lb.)	K (psi√in.)	J (psi-in.)	$\Delta a$		
			CRACK (mils)	CRAZE (mils)	TOTAL (mils)
1.40	159.00	0.00	-	-	-
5.00	557.00	.80	-	-	-
7.60	852.00	2.00	-	-	2.70
10.20	1157.00	3.70	-	-	4.20
12.70	1441.00	5.30	.30	4.60	4.90
15.00	1702.00	8.10	1.90	5.60	7.50 *
18.30	2075.00	12.70	4.60	6.60	11.20 *
20.40	2315.00	16.80	7.00	6.60	13.60 *
22.20	2519.00	19.00	9.60	7.90	17.50 *
23.60	2678.00	21.90	11.60	8.30	19.90 *
25.20	2859.00	25.90	12.50	9.80	22.30 *
25.90	2939.00	27.60	13.50	10.40	23.90 *
27.30	3097.00	32.00	17.20	12.10	29.30 *
28.30	3211.00	35.50	18.80	13.30	32.10 *
28.80	3258.00	39.00	26.10	13.90	40.00 *
28.60	3245.00	41.50	26.20	23.70	49.90 *
28.00	3177.00	42.10	25.50	32.60	58.10 *
27.90	3166.00	43.30	27.80	32.80	60.60 *
28.30	3211.00	46.30	26.40	40.30	66.70 *

\* Data used in linear regression.

Table B9

## CRACK-GROWTH DATA FOR SPECIMEN NO. 20

$$B = 0.123 \text{ in.}$$

$$(a/W)_{\text{init}} = 0.698$$

LOAD (lb)	K (psi√in.)	J (psi-in.)	$\Delta a$		
			CRACK (mils)	CRAZE (mils)	TOTAL (mils)
.80	149.90	0.00	-	-	0.00
2.00	374.80	.40	-	-	0.00
4.10	764.40	1.60	-	-	2.30
6.10	1143.00	3.80	-	-	4.00
8.00	1499.00	6.50	-	-	3.80
8.90	1663.00	8.10	-	-	5.20
9.60	1799.00	9.50	-	-	5.00
10.50	1963.00	11.30	-	-	6.60 *
12.00	2249.00	15.00	-	-	7.20 *
13.20	2474.00	18.50	-	-	12.20 *
14.00	2624.00	21.50	-	-	14.80 *
14.70	2755.00	24.50	-	-	18.10 *
15.20	2849.00	26.60	-	-	17.30 *
15.30	2857.00	27.50	-	-	20.90 *
15.50	2905.00	28.50	-	-	20.70 *
15.70	2942.00	29.50	-	-	22.90 *
15.90	2980.00	30.80	-	-	24.00 *
16.10	3017.00	32.00	-	-	27.50 *
16.50	3092.00	35.50	-	-	31.50 *
16.20	3035.00	41.00	-	-	38.50 *
16.20	3036.00	41.50	-	-	41.80 *
16.30	3055.00	43.50	-	-	41.30 *
16.40	3074.00	45.00	-	-	-
16.50	3092.00	46.00	-	-	50.00 *
16.60	3111.00	47.00	-	-	51.00 *
16.75	3139.00	48.80	-	-	59.30 *

\* Data used in linear regression.

AD-A121 178

A STUDY OF THE J-INTEGRAL METHOD USING POLYCARBONATE  
(U) SYSTEMS RESEARCH LABS INC DAYTON OH RESEARCH  
APPLICATIONS DIV H L BERNSTEIN AUG 82 AFWL-TR-82-4888  
F33615-79-C-5825 F/G 11/9

2/2

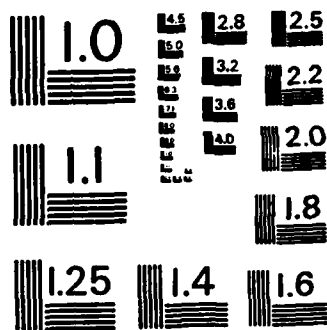
UNCLASSIFIED

NL

END

FORMED

DATE



MICROCOPY RESOLUTION TEST CHART  
NATIONAL BUREAU OF STANDARDS - 1963 - A

Table B10

## CRACK-GROWTH DATA FOR SPECIMEN NO. 21

$$B = 0.122 \text{ in.}$$

$$(a/W)_{\text{init}} = 0.806$$

LOAD (lb)	K (psi $\sqrt{\text{in.}}$ )	J (psi-in.)	$\Delta a$		
			CRACK (mils)	CRAZE (mils)	TOTAL (mils)
1.02	376.00	.20	-	-	3.10
1.02	376.00	.20	-	-	3.10
2.18	805.00	1.50	-	-	3.50
3.02	1115.00	3.00	-	-	5.80
3.84	1417.00	5.00	-	-	6.50
4.46	1646.00	6.90	-	-	6.40
5.16	1904.00	9.80	-	-	5.90
5.91	2181.00	13.50	-	-	8.10 *
6.42	2369.00	16.40	-	-	9.80 *
6.74	2487.00	18.50	-	-	11.50 *
6.93	2558.00	19.90	-	-	11.80 *
7.18	2650.00	21.70	8.60	5.10	14.70 *
7.40	2731.00	23.80	12.70	7.50	20.20 *
7.58	2797.00	25.50	11.80	8.70	20.50 *
7.77	2868.00	27.80	17.50	7.40	24.90 *
7.90	2916.00	29.50	19.00	7.40	26.40 *
8.06	2975.00	31.50	19.00	5.90	25.90 *
8.16	3011.00	33.40	22.30	7.30	29.60 *
8.26	3048.00	35.50	22.40	6.80	29.20 *
8.40	3100.00	36.80	23.00	9.30	32.30 *

\* Data used in linear regression.

Table B11

## CRACK-GROWTH DATA FOR SPECIMEN NO. 22

B = 0.990 in.

 $(a/W)_{init} = 0.763$ 

LOAD (lb.)	K (psi $\sqrt{\text{in.}}$ )	J (psi-in.)	$\Delta a$		
			CRACK (mils)	CRAZE (mils)	TOTAL (mils)
84.10	2827.00	29.40	-	-	4.40*
87.10	2928.00	34.60	-	-	9.70*
87.90	2955.00	36.90	-	-	13.00*
88.00	2957.00	39.40	-	-	18.30*
86.80	2918.00	40.60	-	-	21.30*

\* Data used in linear regression.

Table B12

## CRACK-GROWTH DATA FOR SPECIMEN NO. 23

B = 1.014 in.

 $(a/W)_{init} = 0.538$ 

LOAD (lb)	K (psi $\sqrt{in.}$ )	J (psi-in.)	$\Delta a$		
			CRACK (mils)	CRAZE (mils)	TOTAL (mils)
28.50	337.50	.25	-	-	0.00
121.00	1433.00	5.50	-	-	3.10
131.00	1551.00	6.50	-	-	2.56
141.00	1670.00	7.75	-	-	2.38
151.00	1788.00	8.75	-	-	2.53
161.00	1907.00	9.80	-	-	3.45
170.50	2019.00	10.50	-	-	3.25
180.00	2132.00	12.50	-	-	4.44
190.50	2256.00	14.10	-	-	6.67 *
201.00	2380.00	15.75	-	-	6.84 *
225.00	2665.00	20.75	-	-	8.00 *
250.50	2967.00	25.75	-	-	11.53 *
282.50	3346.00	35.00	-	-	16.75 *

\* Data used in linear regression.

Table B13

## CRACK-GROWTH DATA FOR SPECIMEN NO. 24

$$B = 0.495 \text{ in.}$$

$$(a/W)_{\text{init}} = 0.795$$

LOAD (lb.)	K (psi $\sqrt{\text{in.}}$ )	J (psi-in.)	$\Delta a$		
			CRACK (mils)	CRAZE (mils)	TOTAL (mils)
25.00	2093.00	11.50	-	-	6.30
29.30	2453.00	16.40	-	-	6.90 *
31.50	2637.00	19.70	-	-	9.60 *
32.60	2729.00	21.40	-	-	9.50 *
33.40	2795.00	23.20	-	-	11.90 *
34.00	2847.00	24.00	-	-	12.80 *
34.60	2897.00	25.40	-	-	14.80 *
35.10	2939.00	26.50	-	-	13.40 *
36.20	3031.00	28.90	-	-	19.10 *
37.30	3123.00	32.20	-	-	18.90 *
37.90	3173.00	34.00	-	-	-
38.20	3198.00	35.20	-	-	-
38.80	3249.00	36.50	-	-	24.20 *
38.90	3257.00	38.00	-	-	28.20 *
38.90	3257.00	40.00	-	-	32.20 *
38.50	3223.00	40.80	-	-	33.70 *

\* Data used in linear regression.



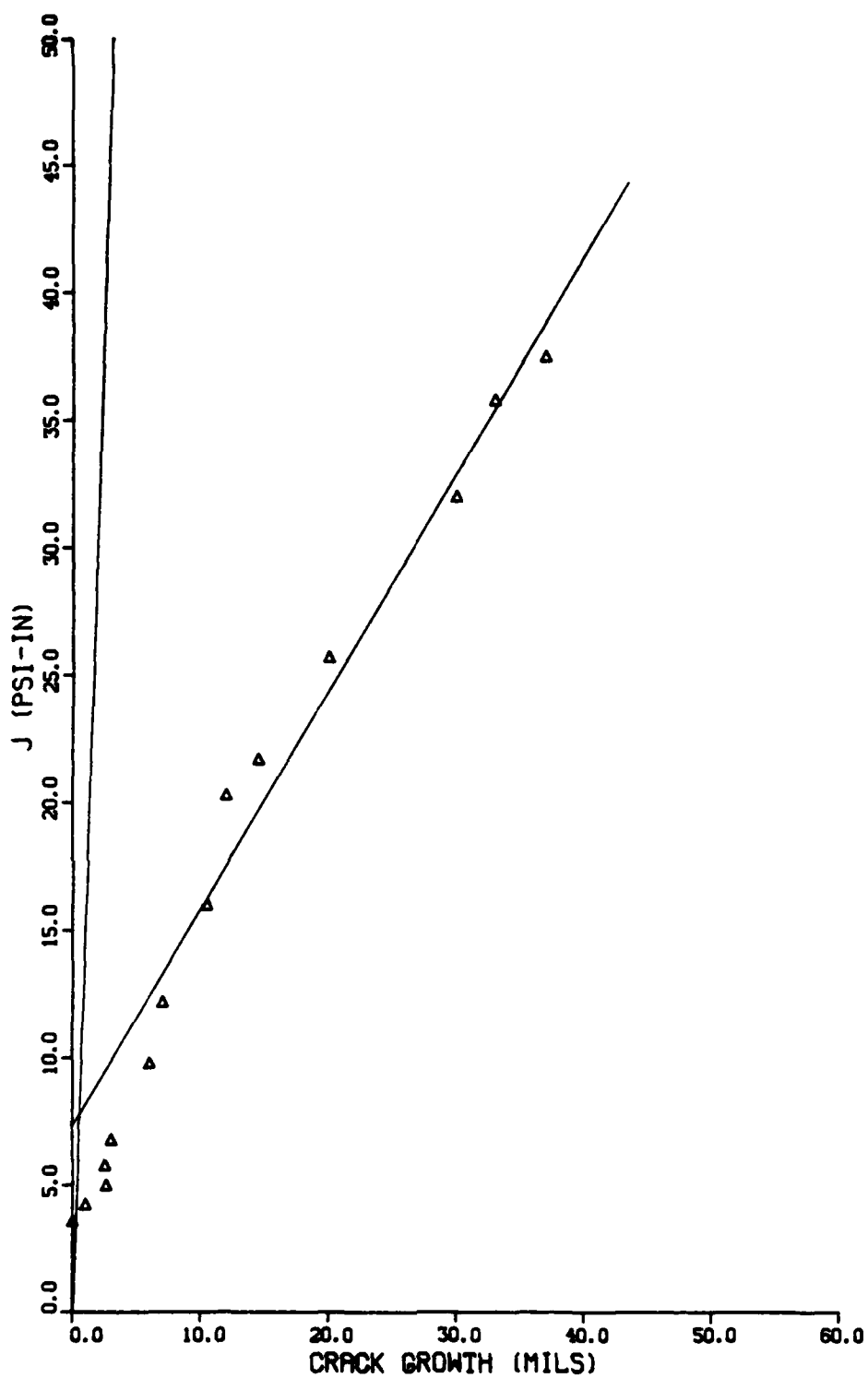


Figure B1. Plot of Crack-Growth Behavior as a Function of J using Linear Coordinates for Specimen No. 2.

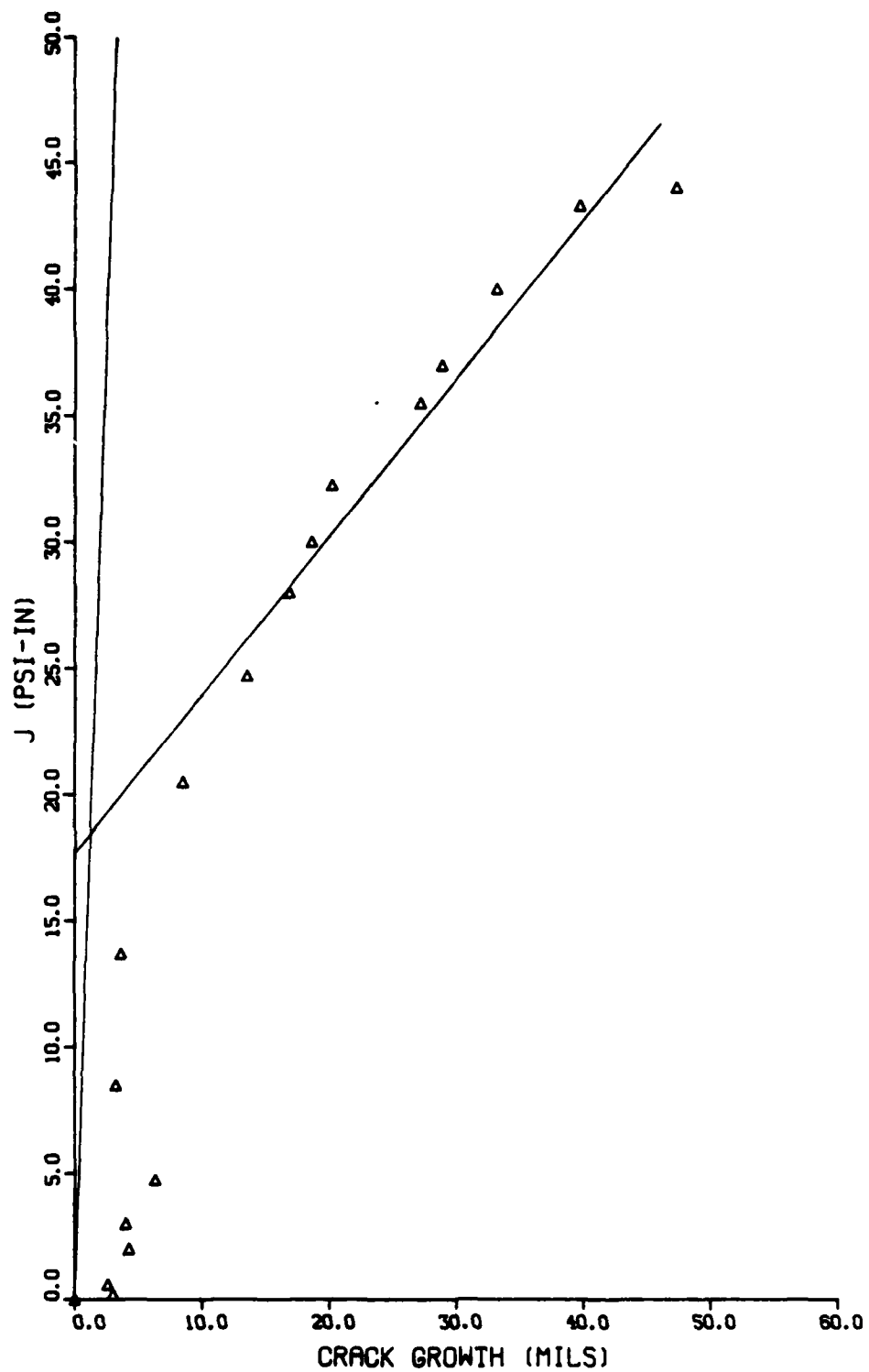


Figure B2. Plot of Crack-Growth Behavior as a Function of J using Linear Coordinates for Specimen No. 4.

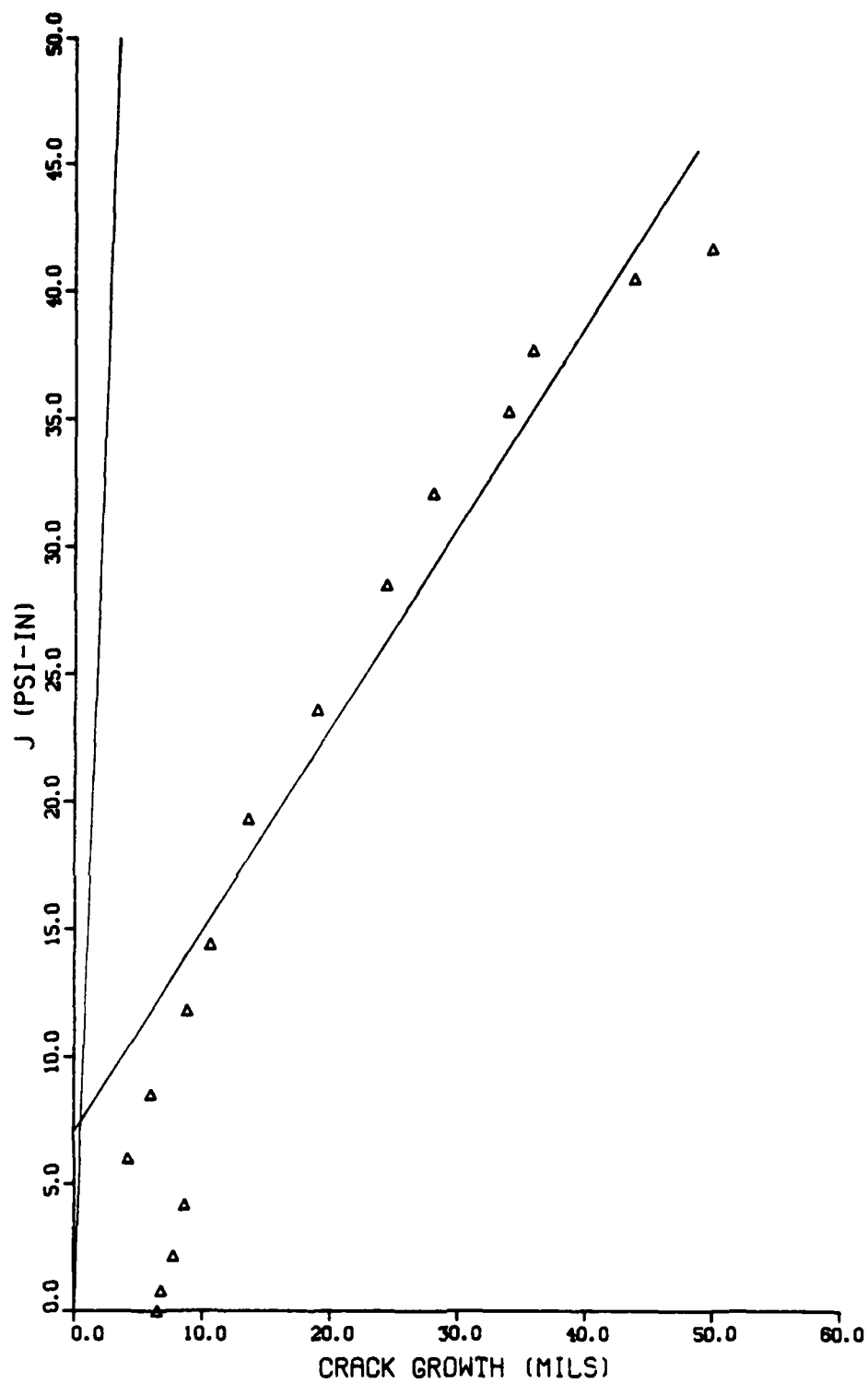


Figure B3. Plot of Crack-Growth Behavior as a Function of J using Linear Coordinates for Specimen No. 6.

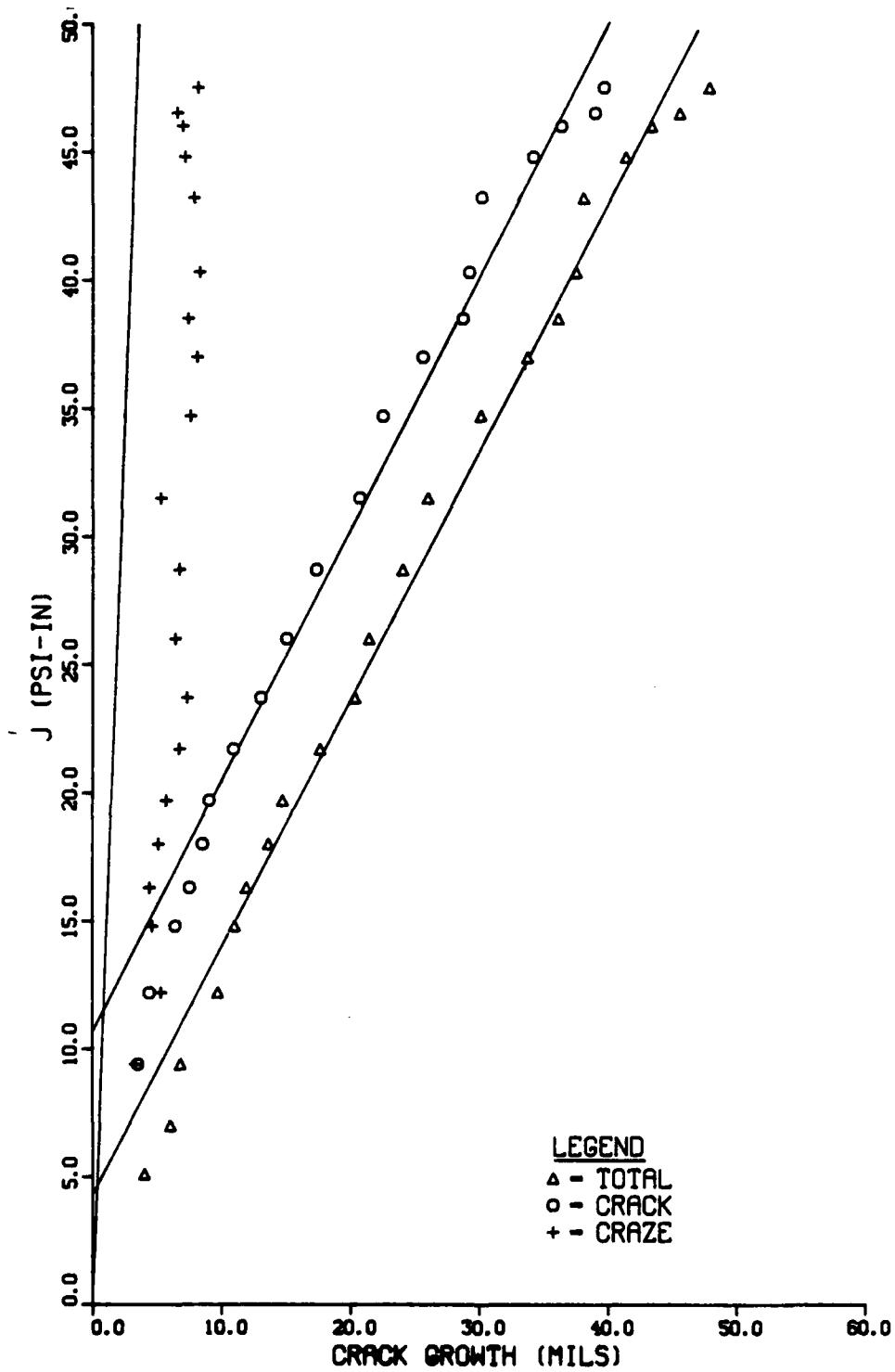


Figure B4. Plot of Crack-Growth Behavior as a Function of J using Linear Coordinates for Specimen No. 10.

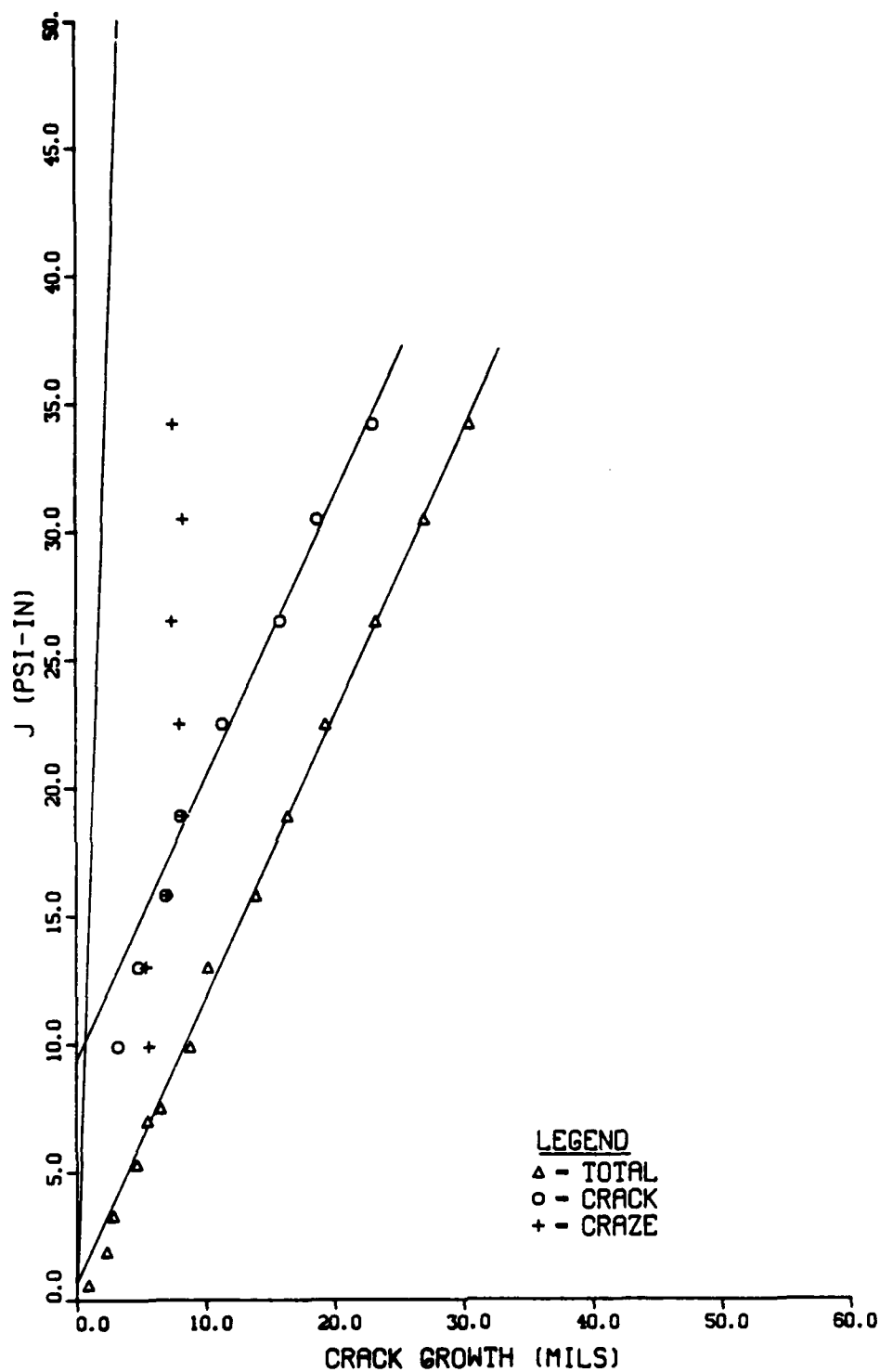


Figure B5. Plot of Crack-Growth Behavior as a Function of J using Linear Coordinates for Specimen No. 12.

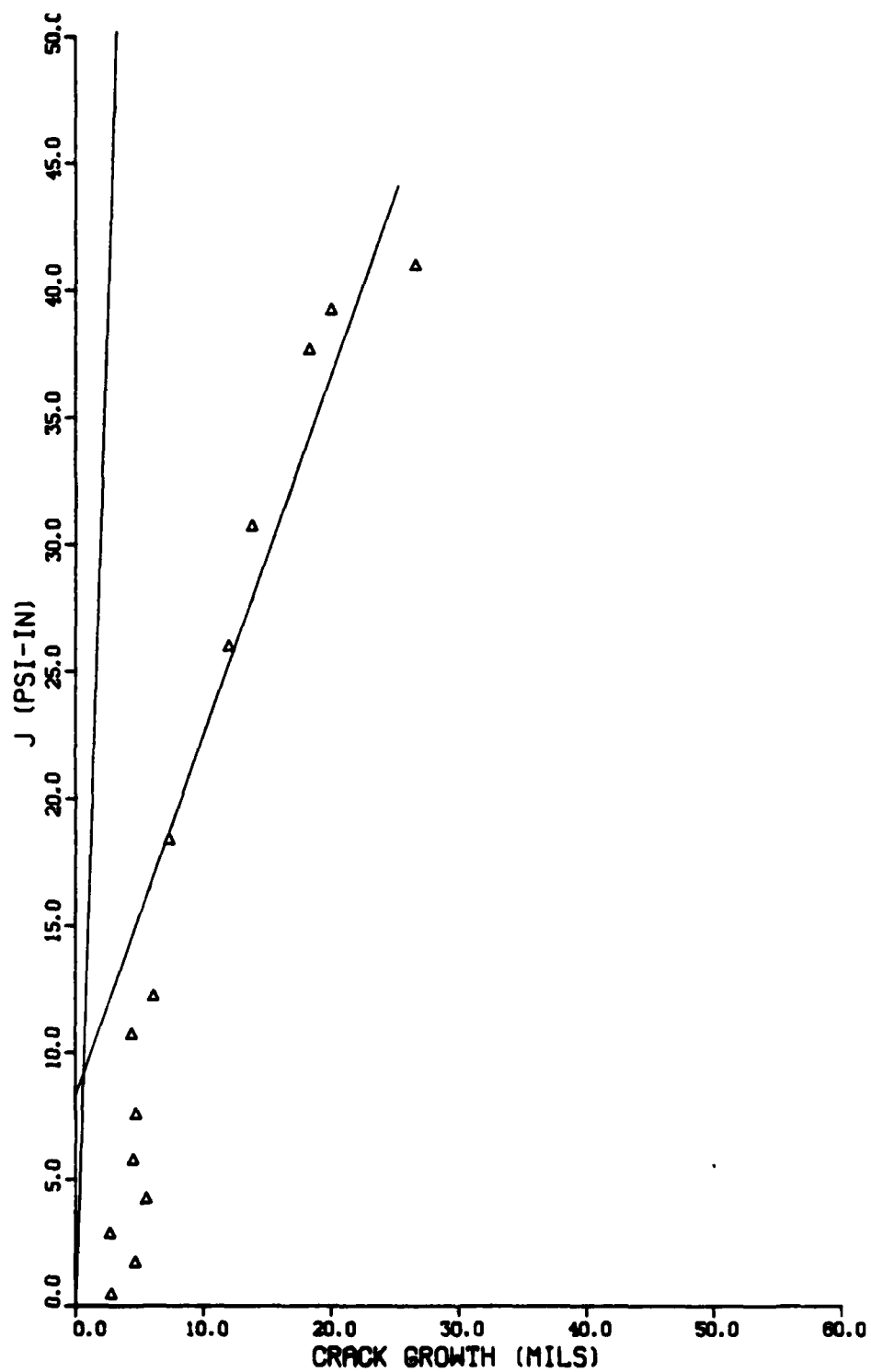


Figure B6. Plot of Crack-Growth Behavior as a Function of J using Linear Coordinates for Specimen No. 13.

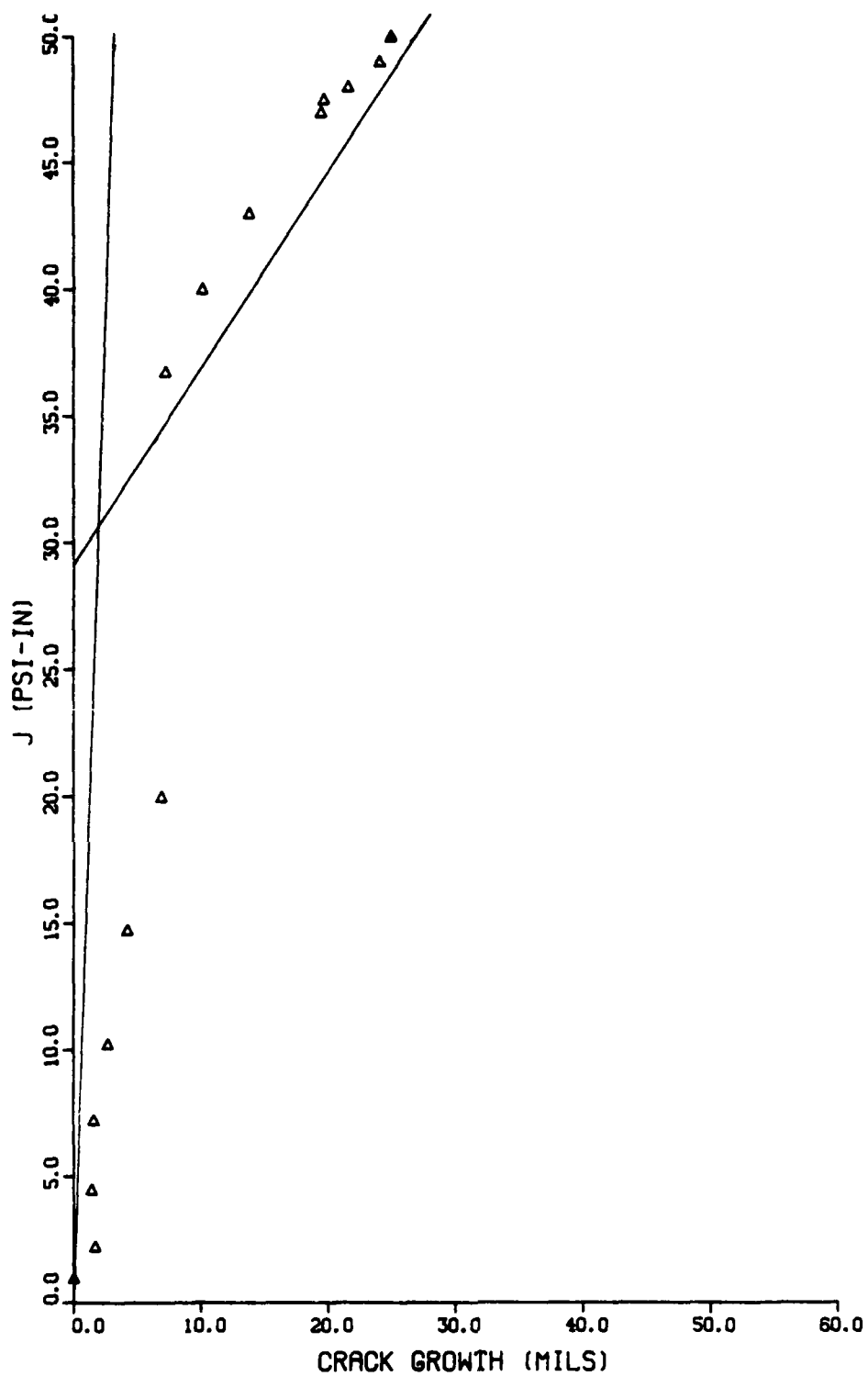


Figure B7. Plot of Crack-Growth Behavior as a Function of J using Linear Coordinates for Specimen No. 14.

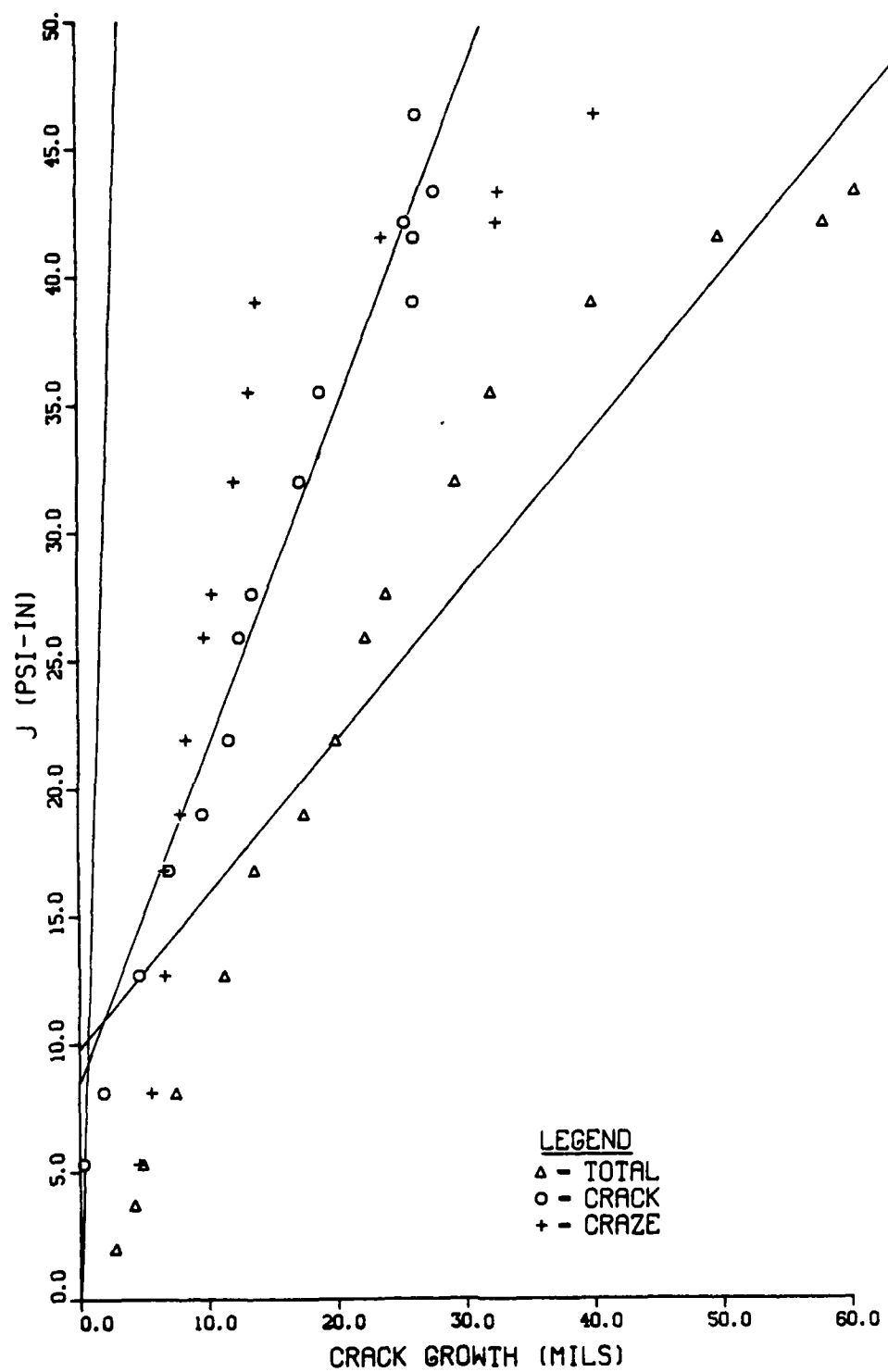


Figure B8. Plot of Crack-Growth Behavior as a Function of J using Linear Coordinates for Specimen No. 15.



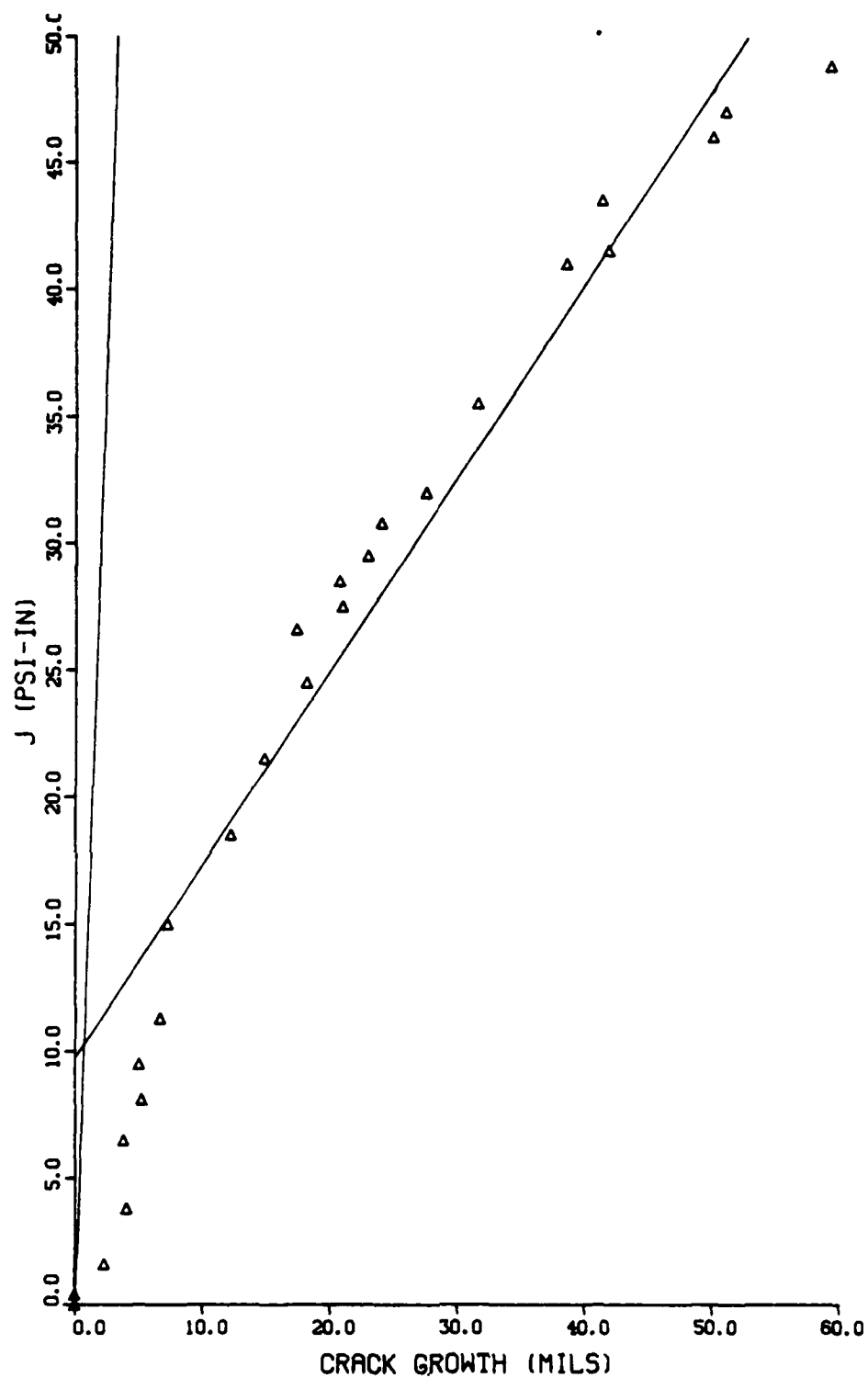


Figure B9. Plot of Crack-Growth Behavior as a Function of J using Linear Coordinates for Specimen No. 20.

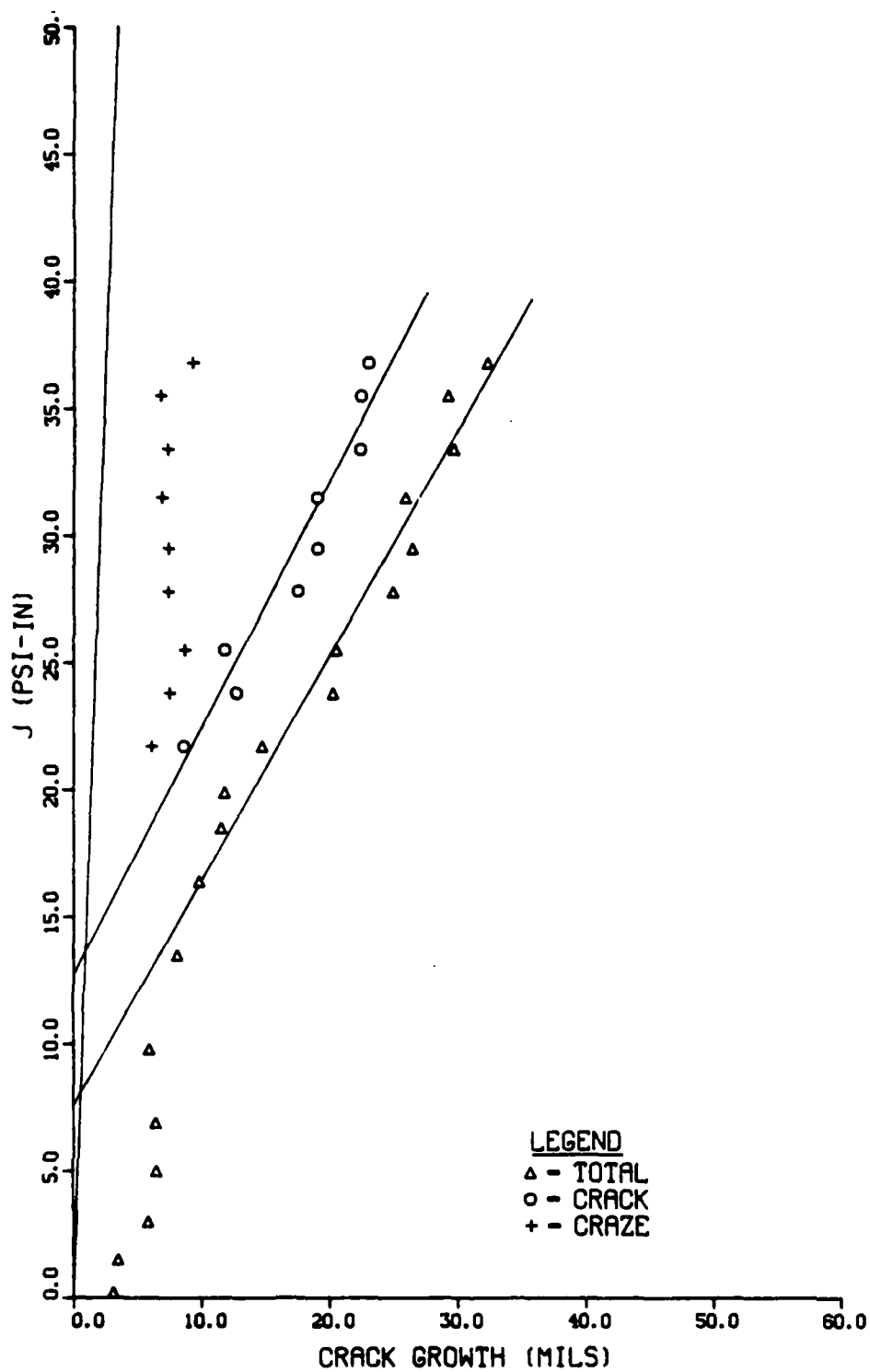


Figure B10. Plot of Crack-Growth Behavior as a Function of J using Linear Coordinates for Specimen No. 21.

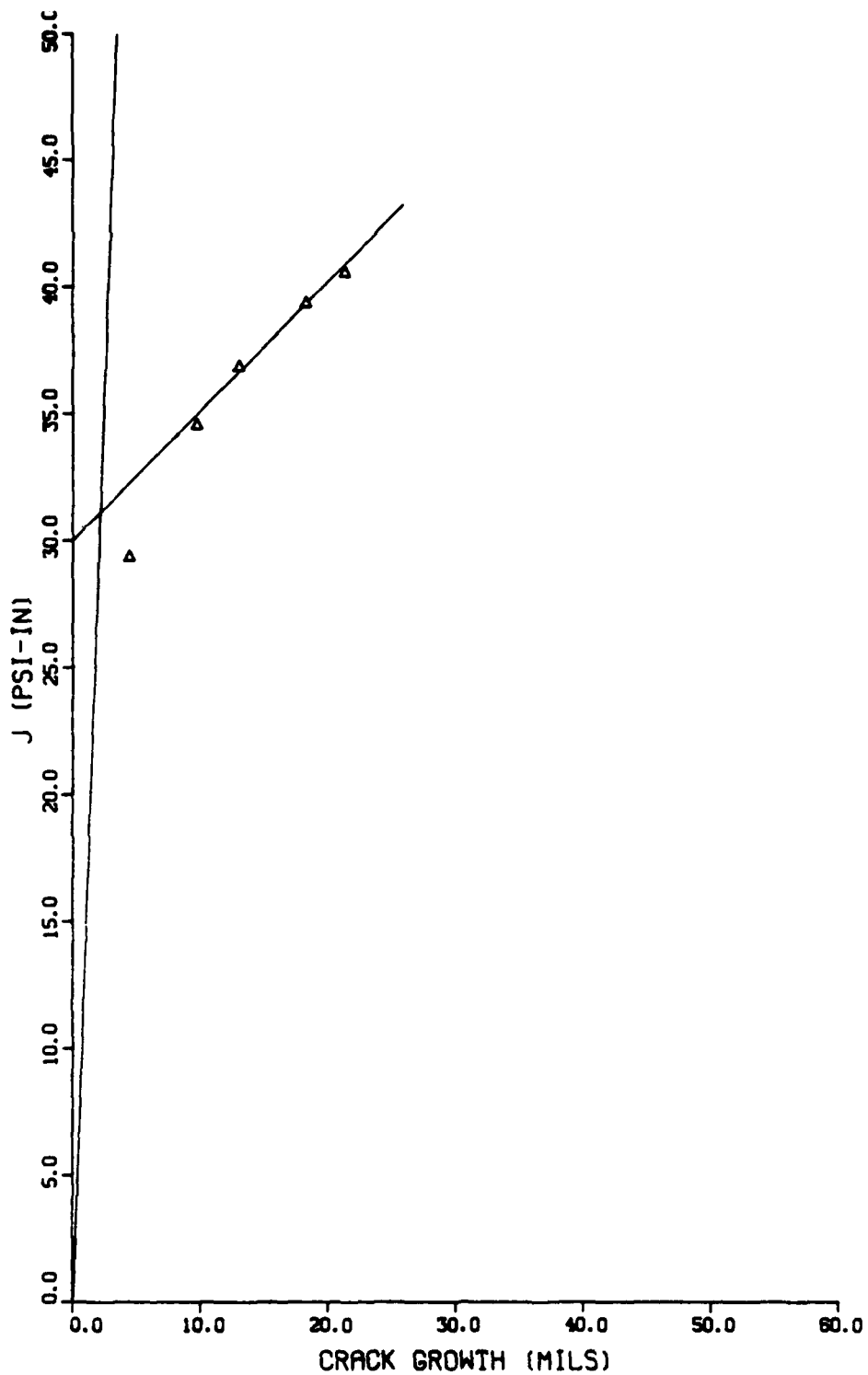


Figure B11. Plot of Crack-Growth Behavior as a Function of J using Linear Coordinates for Specimen No. 22.

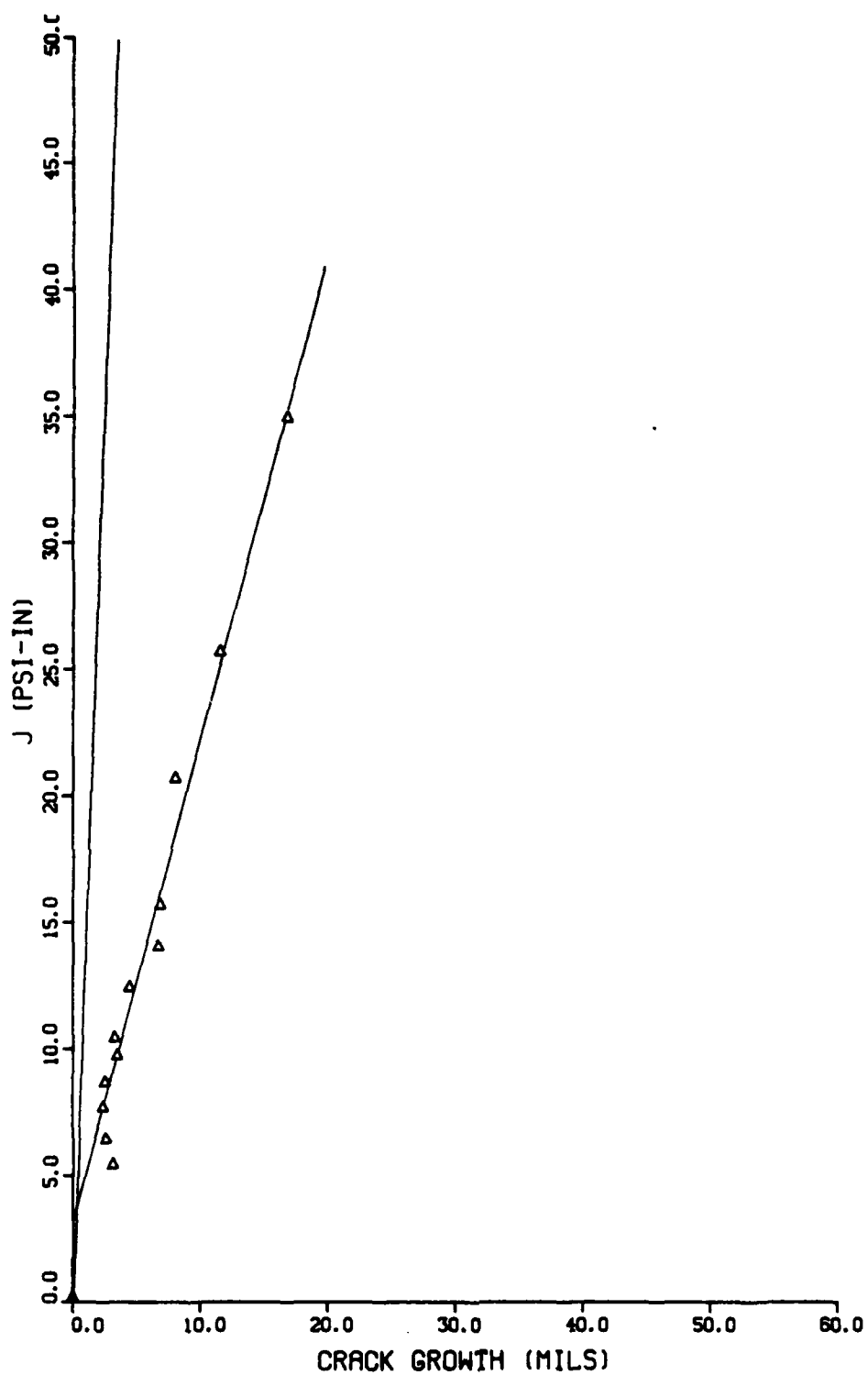


Figure B12. Plot of Crack-Growth Behavior as a Function of J using Linear Coordinates for Specimen No. 23.

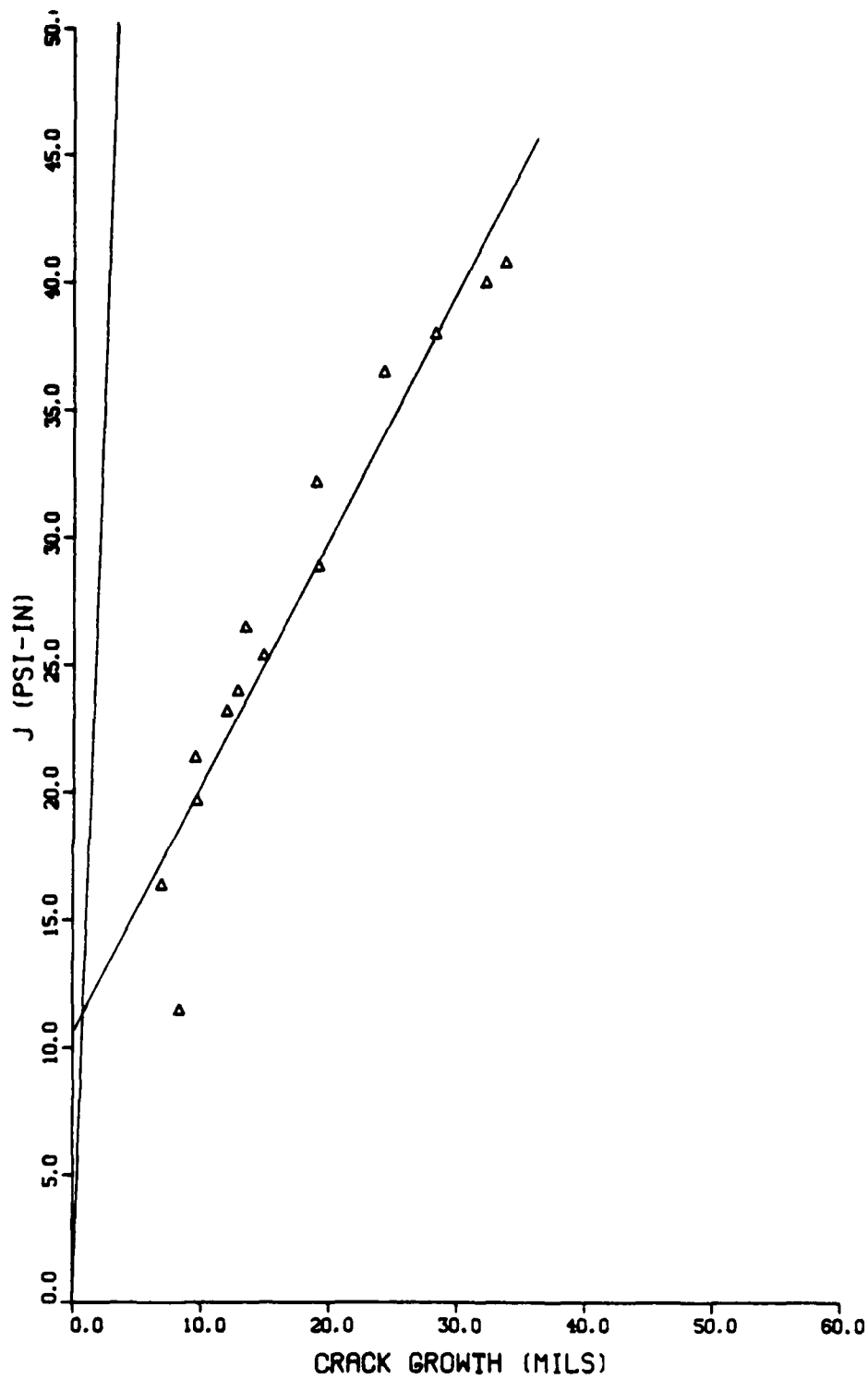


Figure B13. Plot of Crack-Growth Behavior as a Function of J using Linear Coordinates for Specimen No. 24.

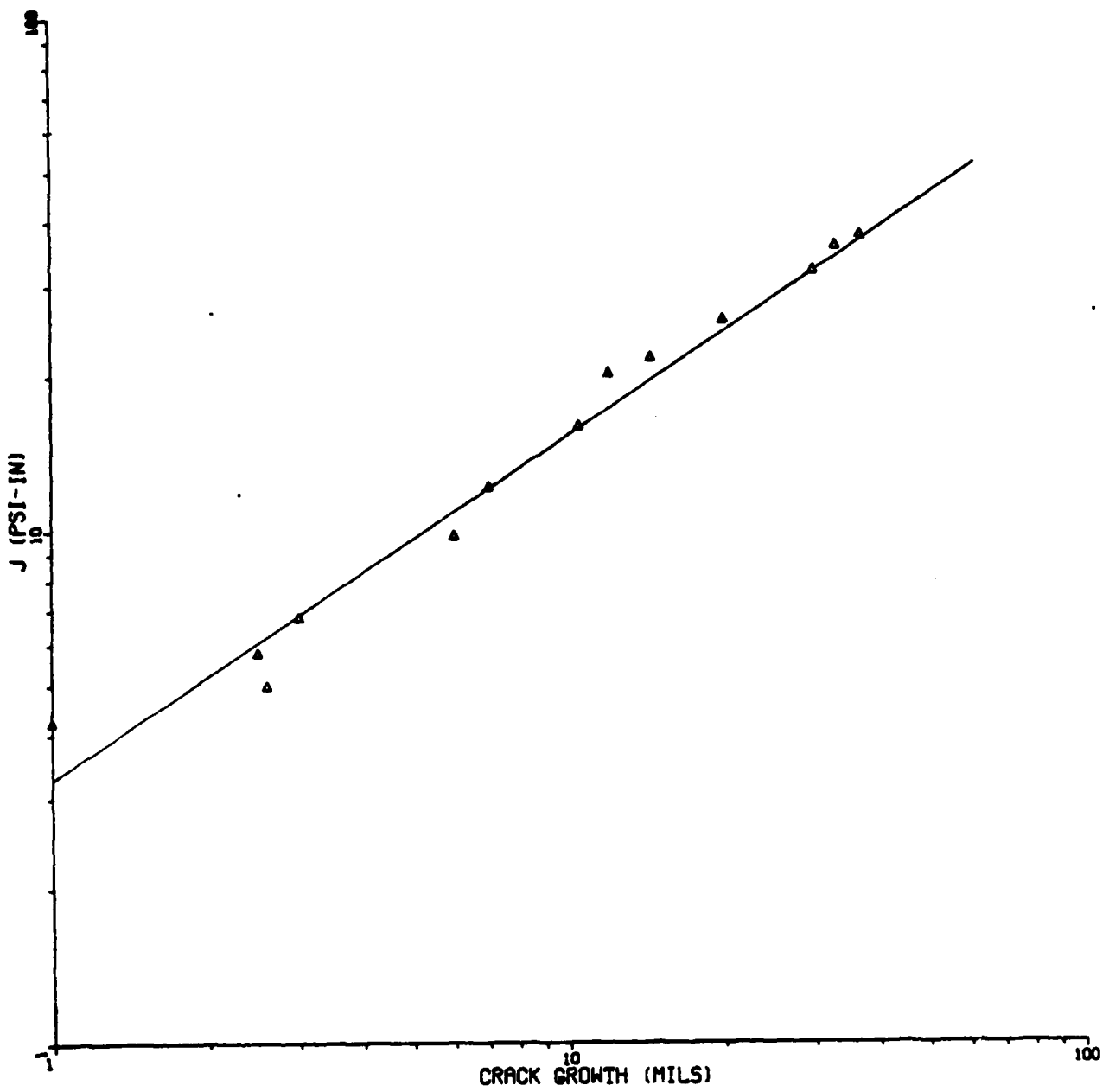


Figure B14. Plot of Crack-Growth as a Function of J  
using Logarithmic Coordinates for Specimen No. 2.

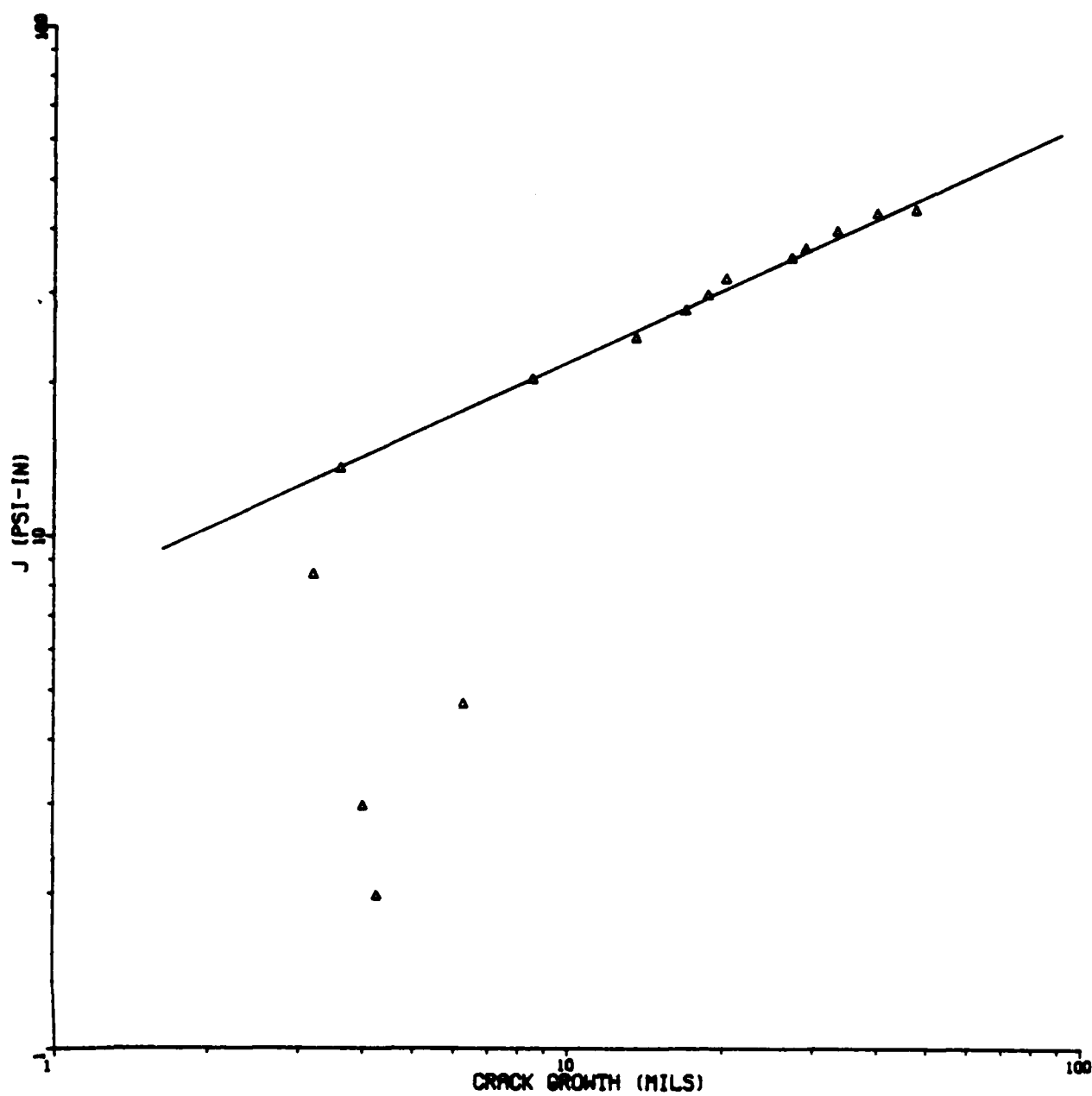


Figure B15. Plot of Crack-Growth as a Function of J using Logarithmic Coordinates for Specimen No. 4.

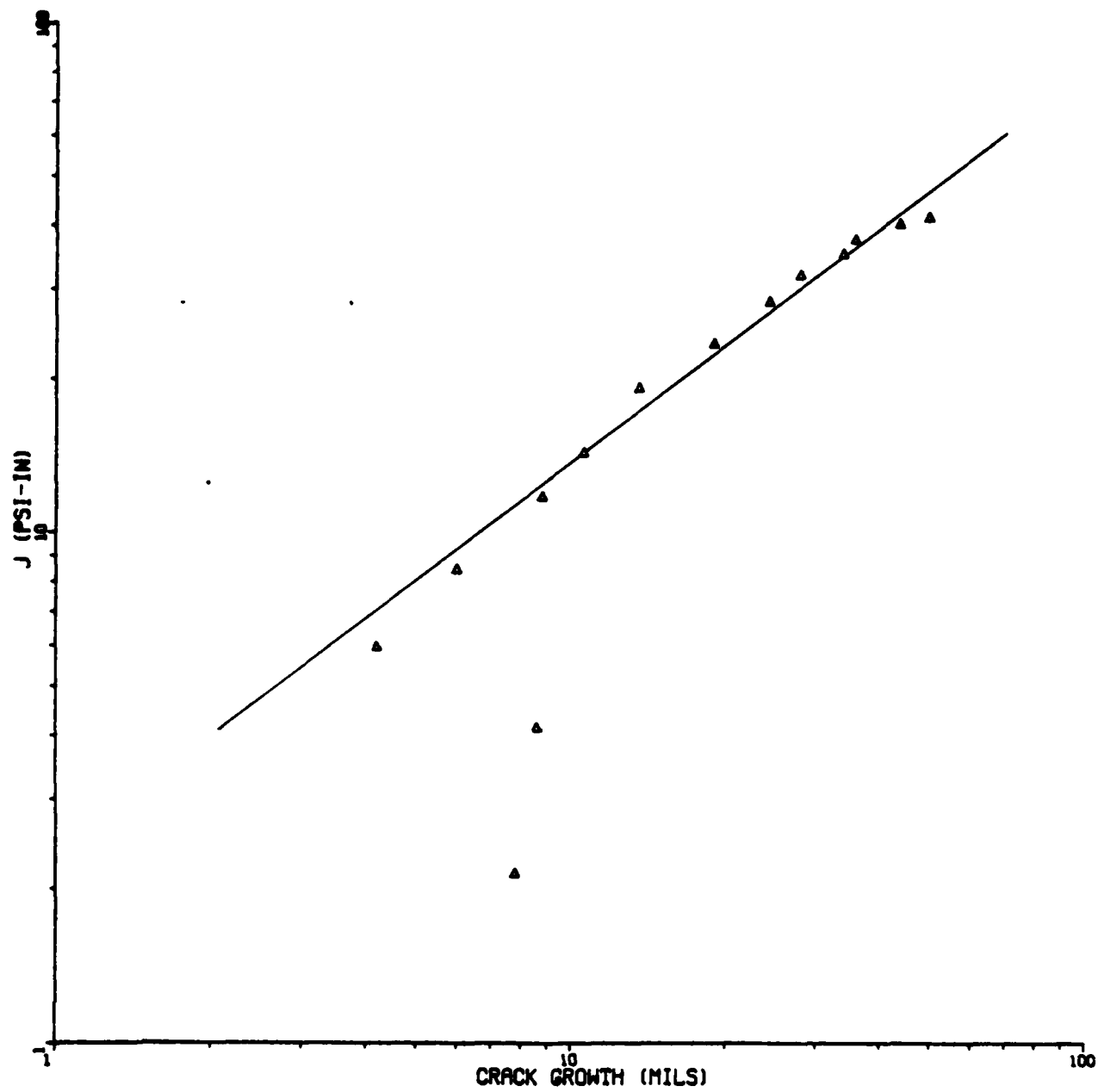


Figure B16. Plot of Crack-Growth as a Function of J using Logarithmic Coordinates for Specimen No. 6.



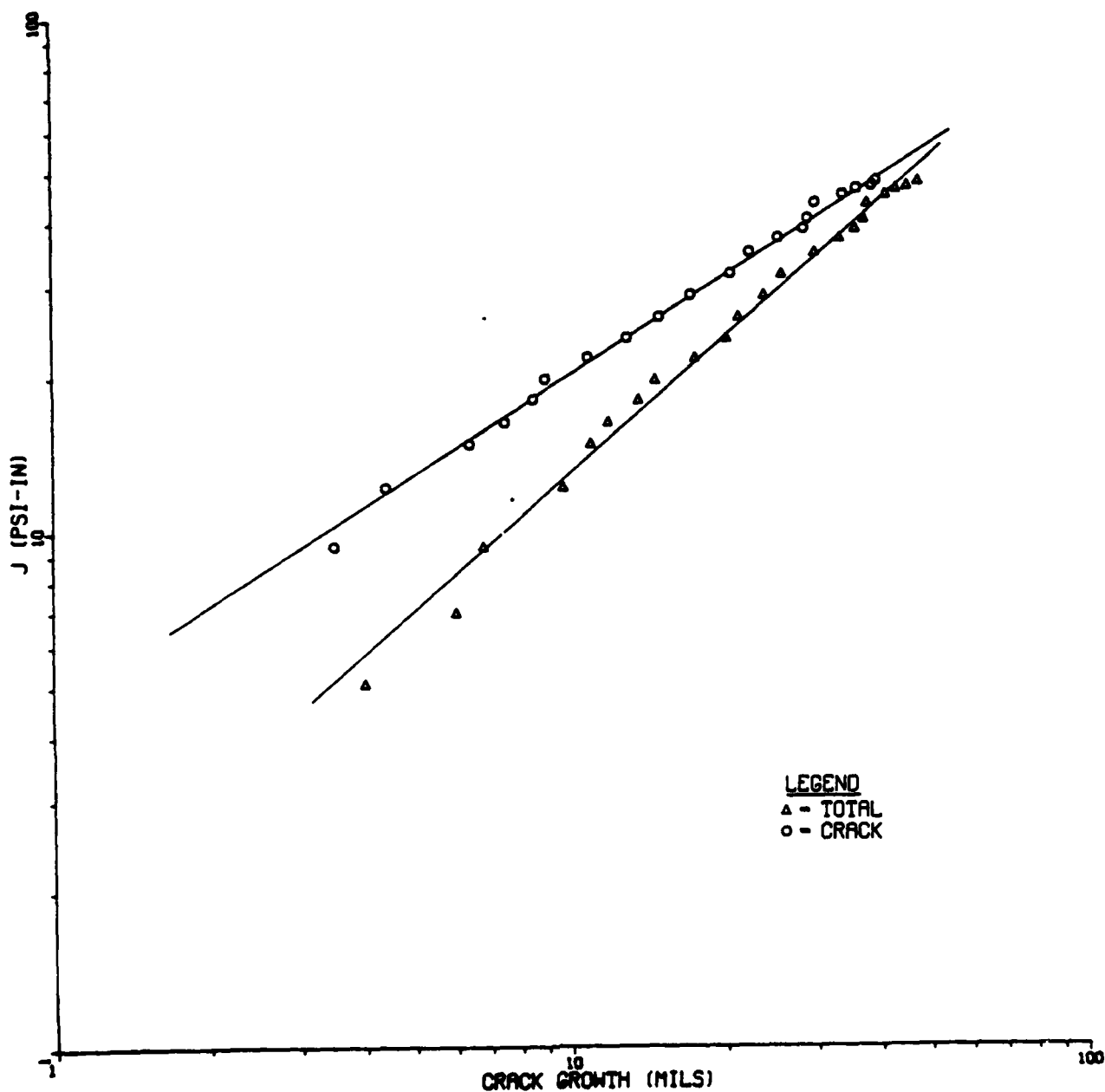


Figure B17. Plot of Crack-Growth as a Function of J using Logarithmic Coordinates for Specimen No. 10.

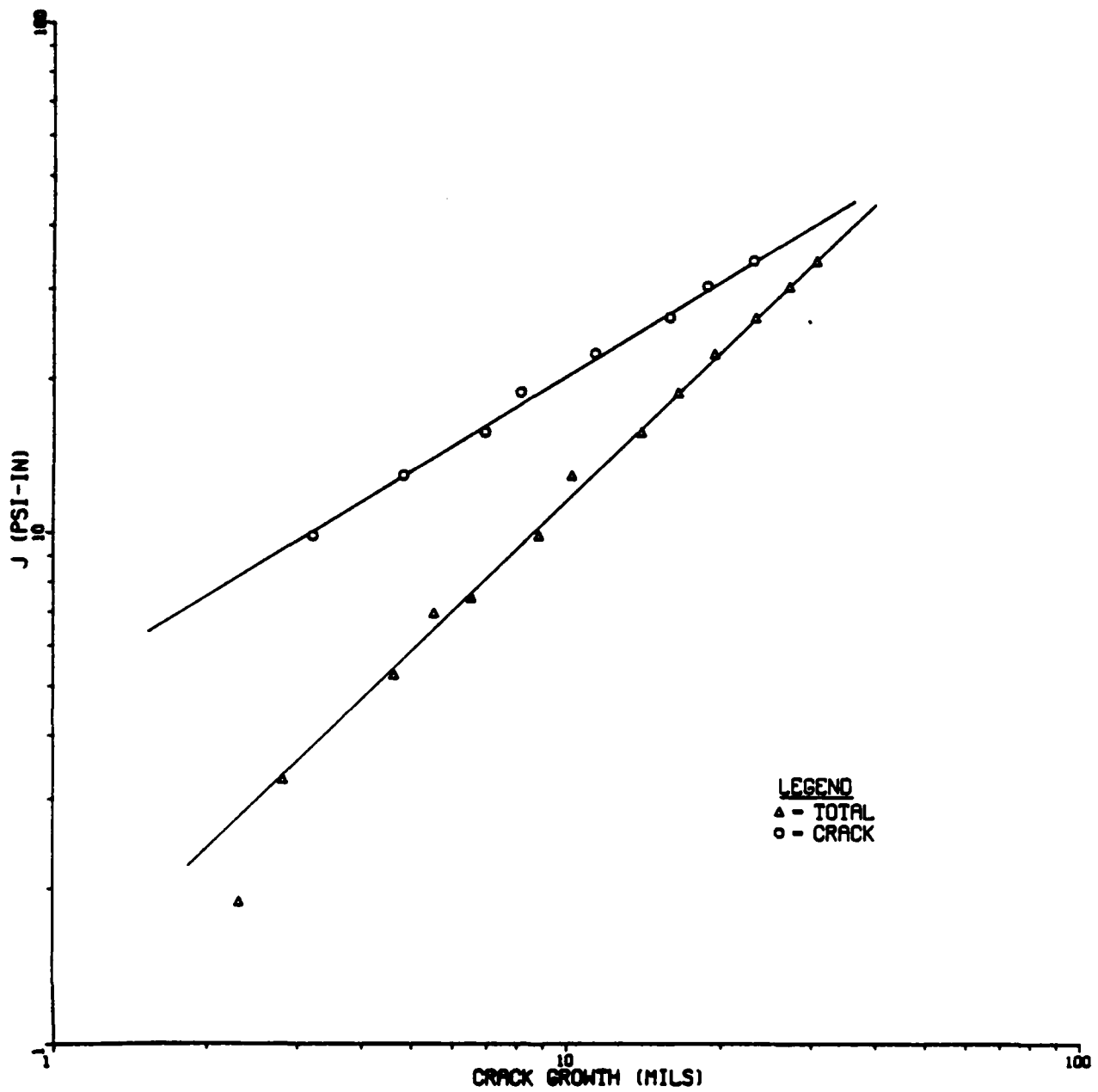


Figure B18. Plot of Crack-Growth as a Function of J using Logarithmic Coordinates for Specimen No. 12.

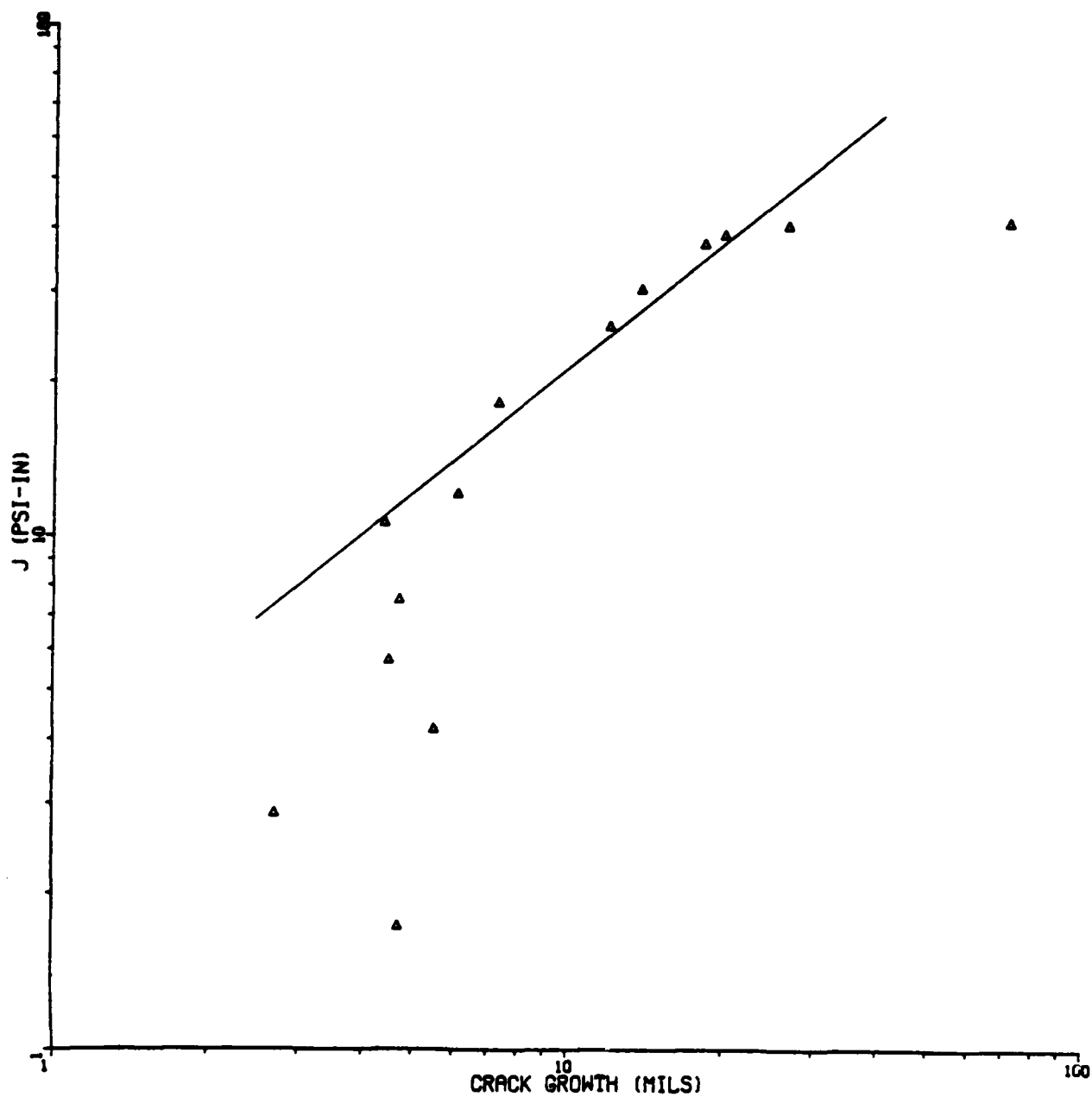


Figure B19. Plot of Crack-Growth as a Function of J using Logarithmic Coordinates for Specimen No. 13.

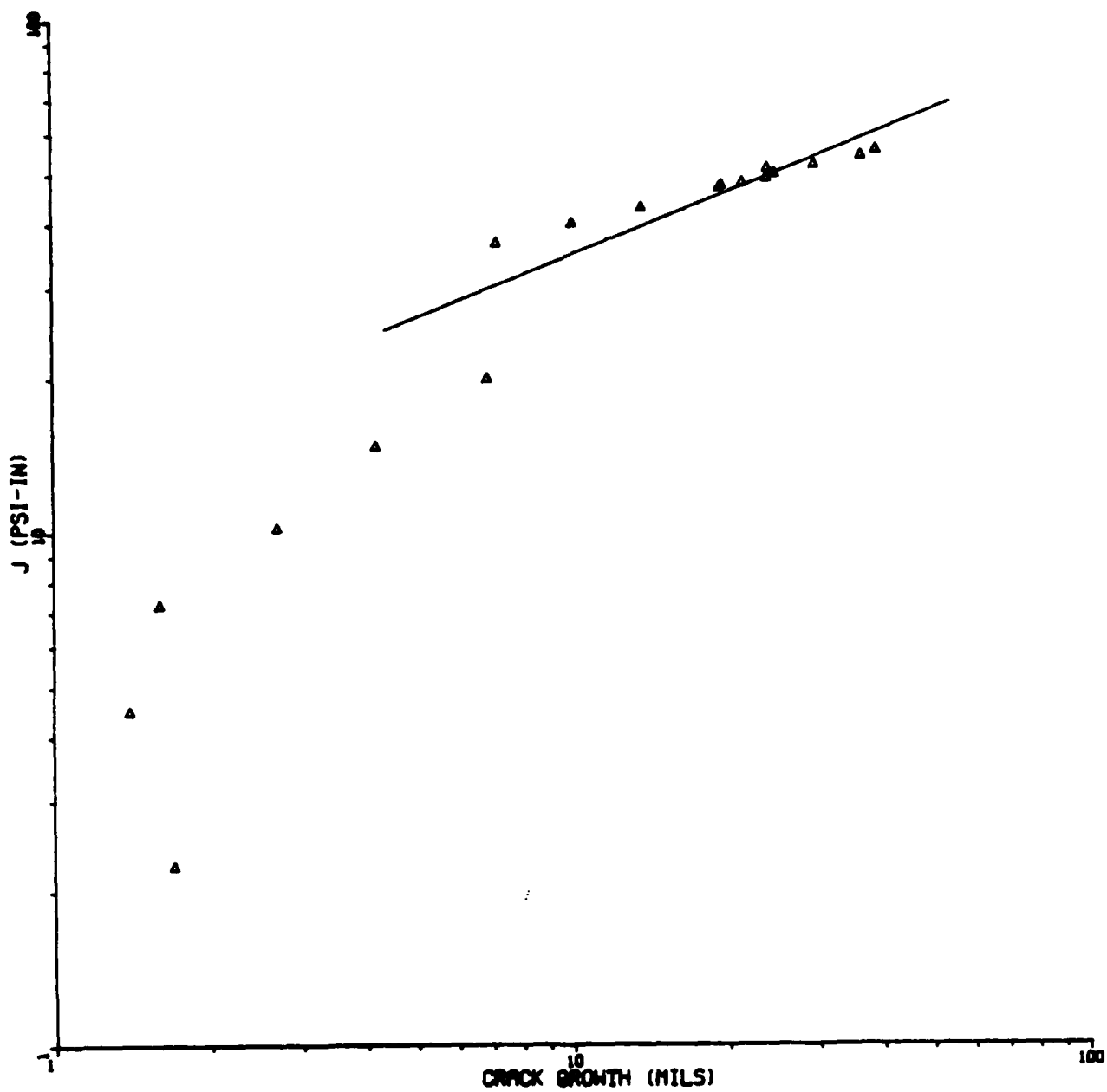


Figure B20. Plot of Crack-Growth as a Function of J using Logarithmic Coordinates for Specimen No. 14.

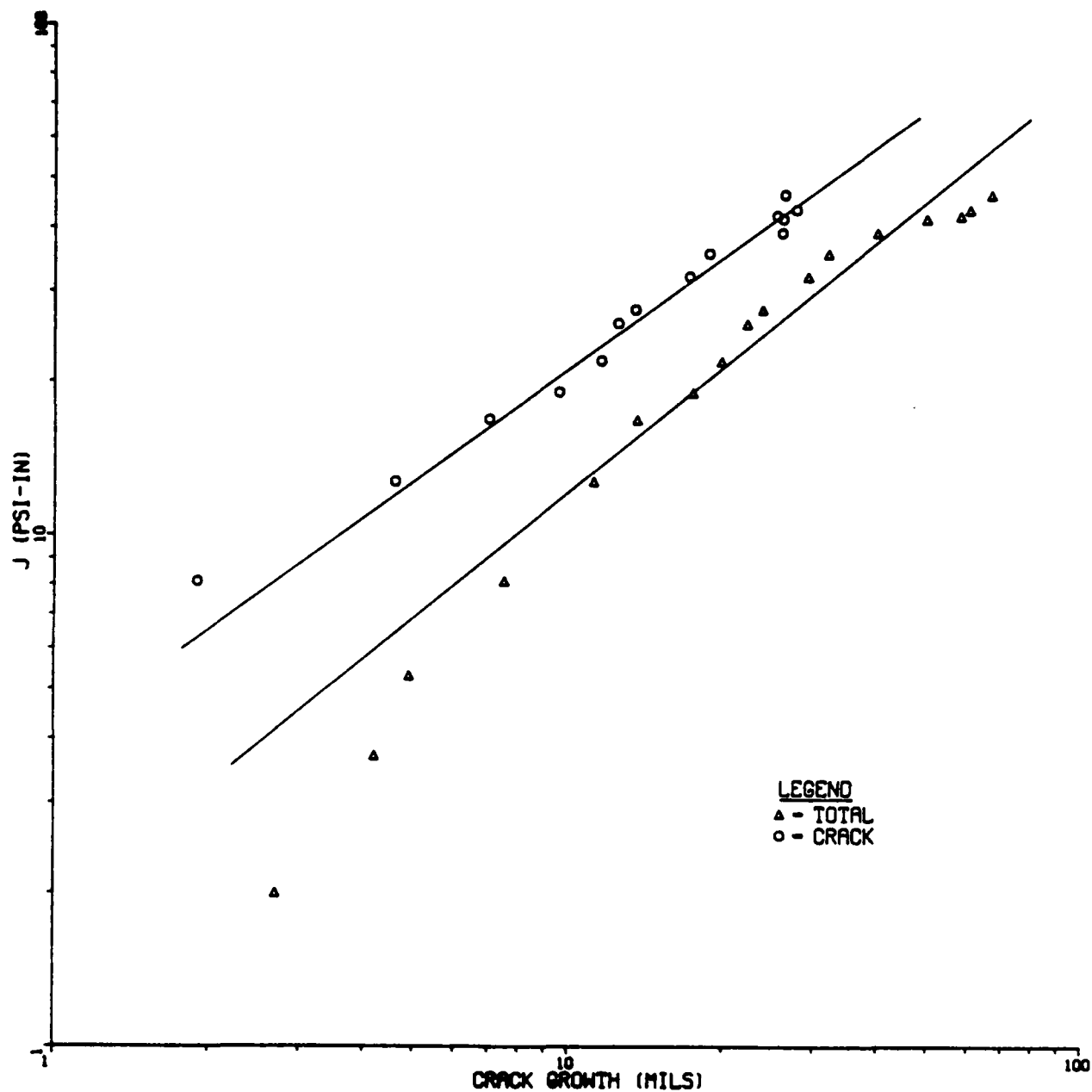


Figure B21. Plot of Crack-Growth as a Function of J using Logarithmic Coordinates for Specimen No. 15.

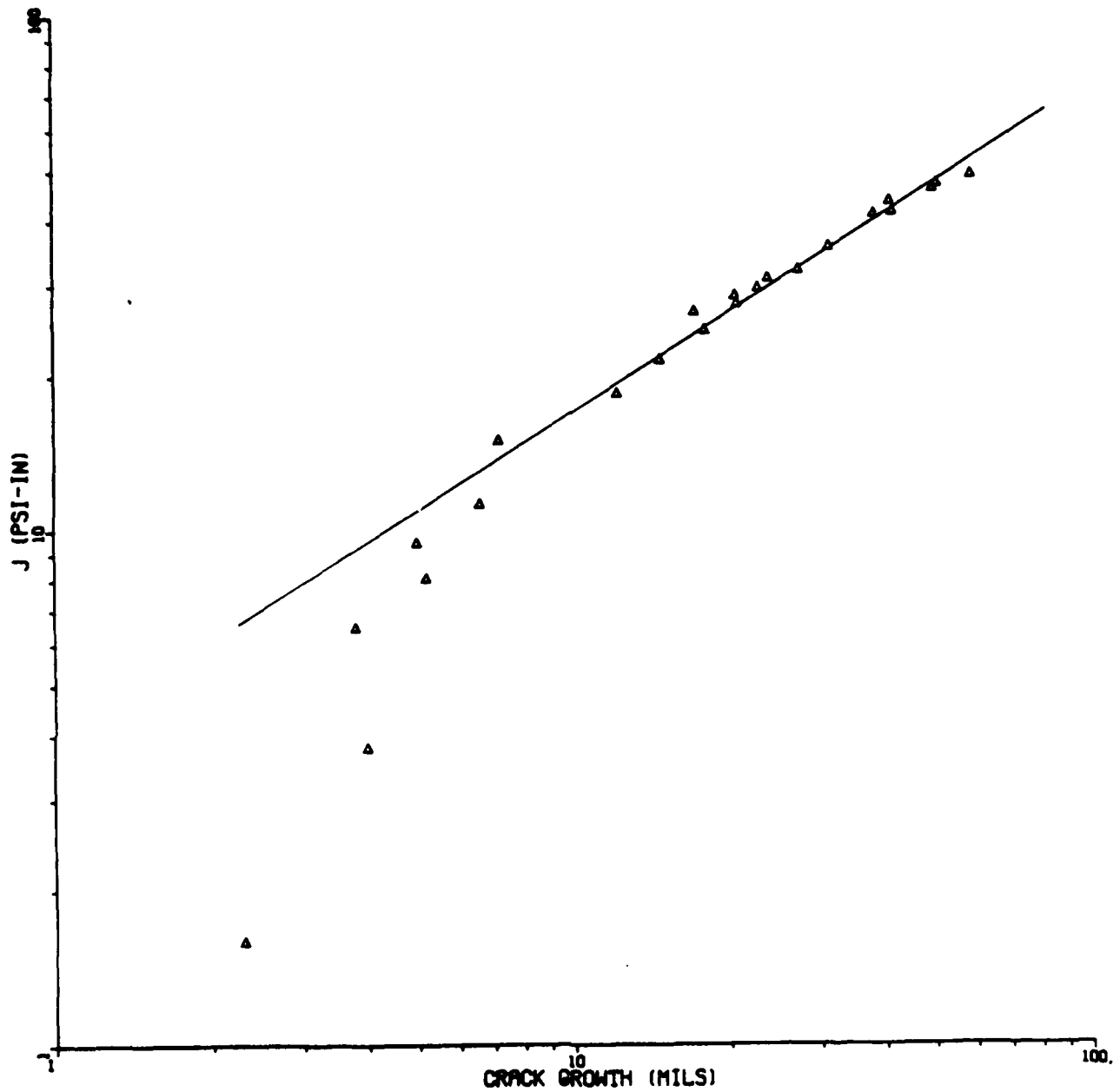


Figure B22. Plot of Crack-Growth as a Function of J using Logarithmic Coordinates for Specimen No. 20.

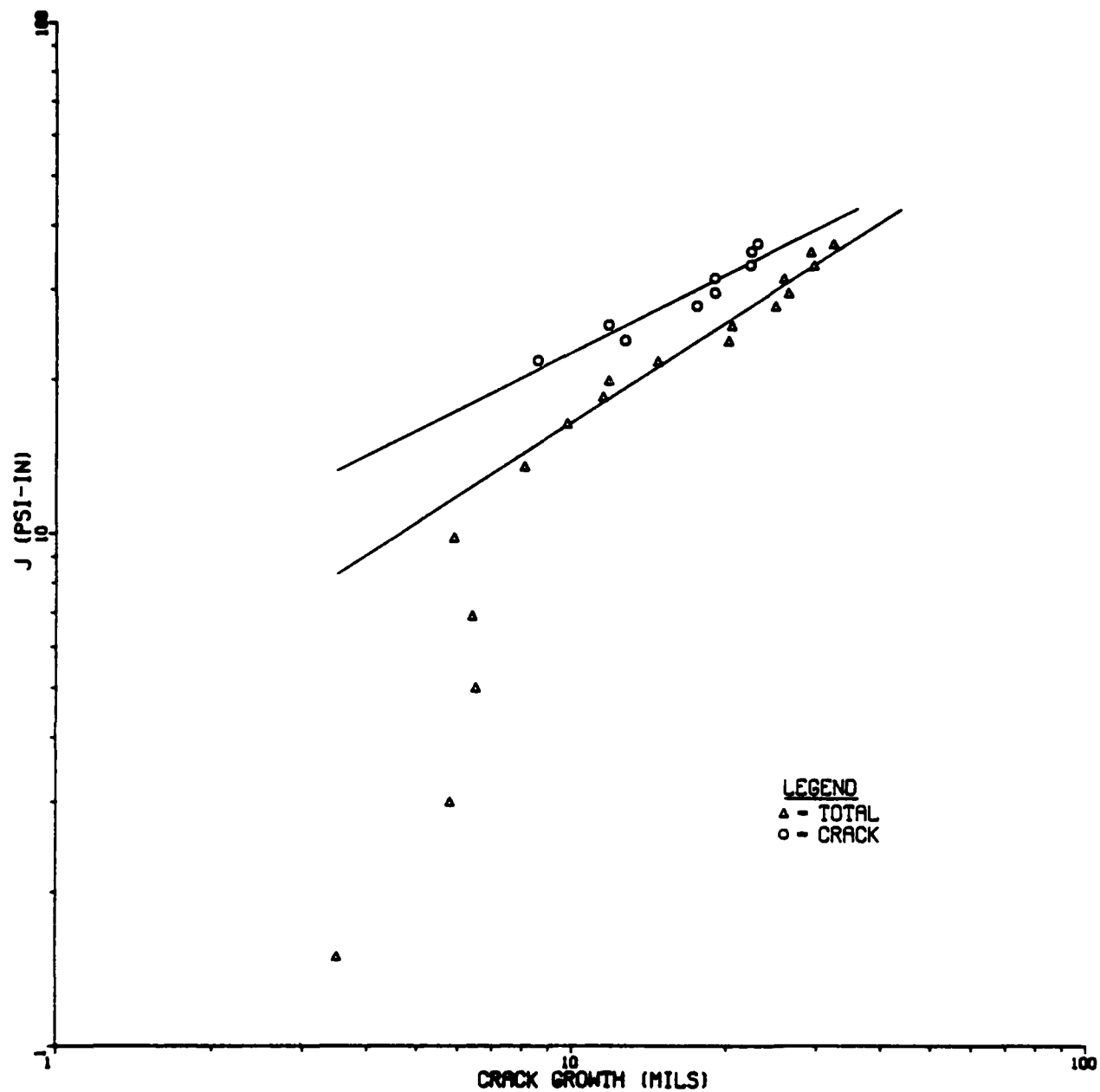


Figure B23. Plot of Crack-Growth as a Function of J using Logarithmic Coordinates for Specimen No. 21.

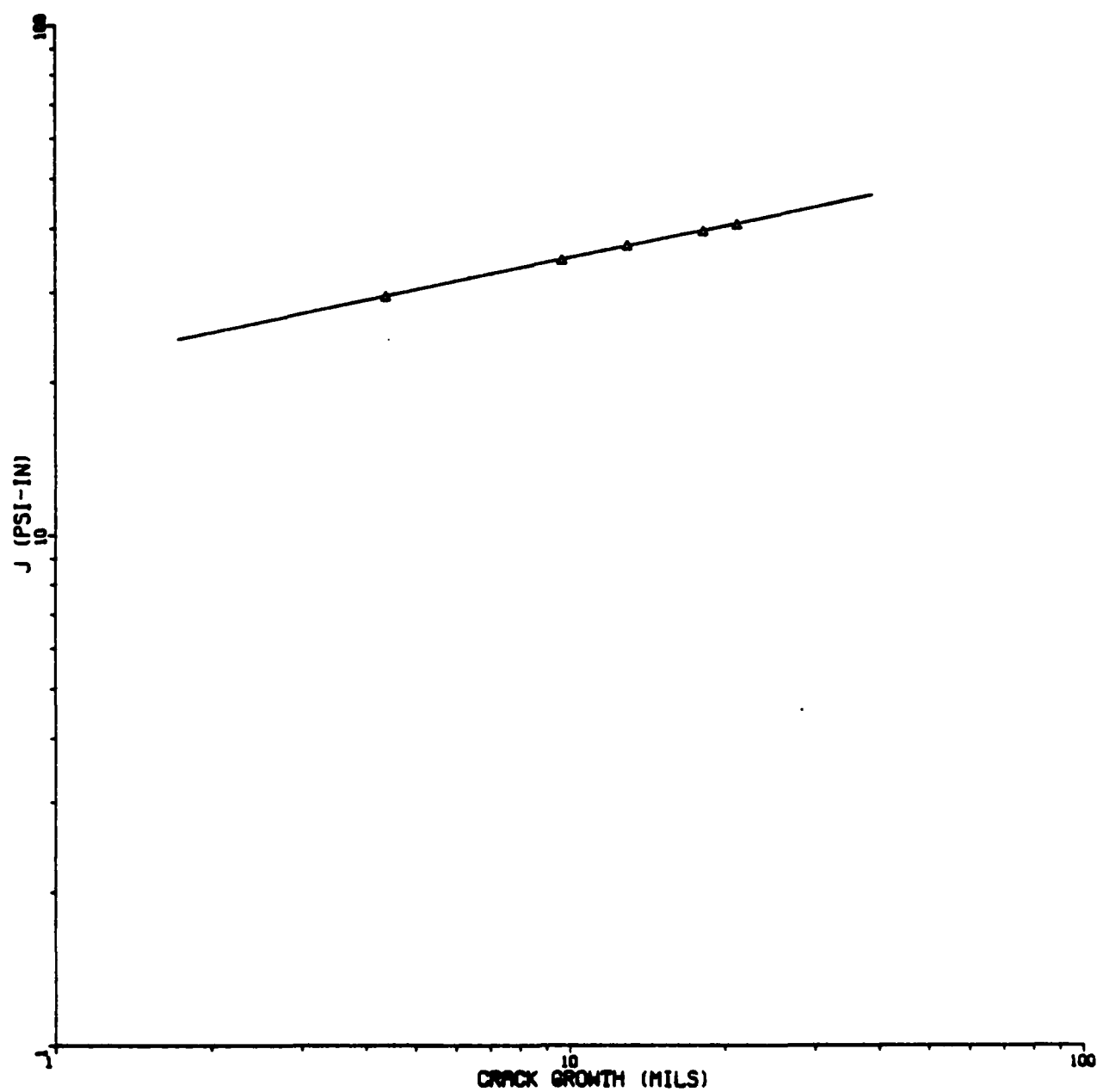


Figure B24. Plot of Crack Growth as a Function of J using Logarithmic Coordinates for Specimen No. 22.



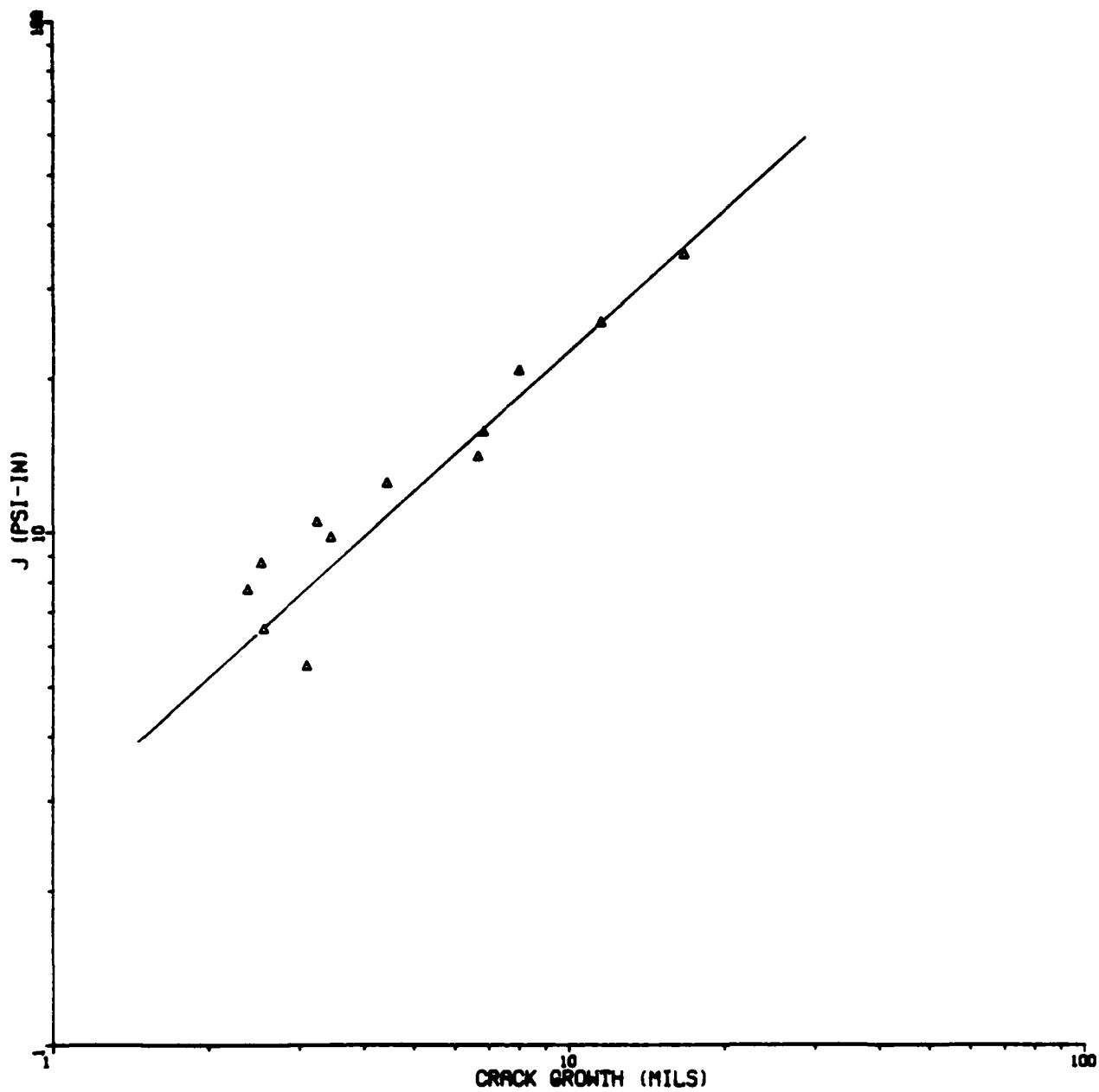


Figure B25. Plot of Crack-Growth as a Function of J using Logarithmic Coordinates for Specimen No. 23.

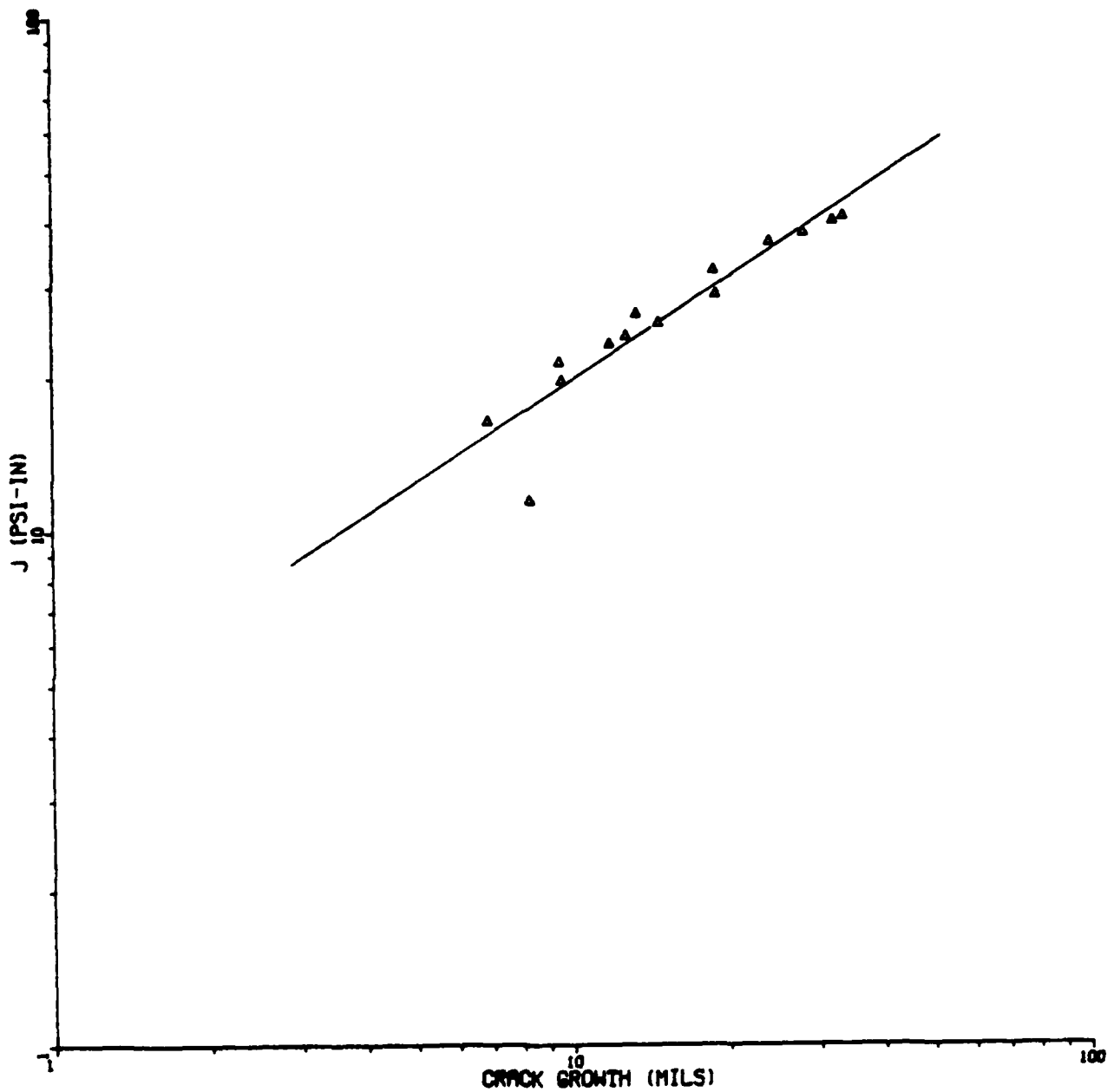


Figure B26. Plot of Crack-Growth as a Function of J using Logarithmic Coordinates for Specimen No. 24.

## APPENDIX C

### DATA ON THE LITERATURE ON J VALUES AND CRACK GROWTH

Data in the literature on J values and crack growth for various materials are plotted using linear and log-log coordinates.

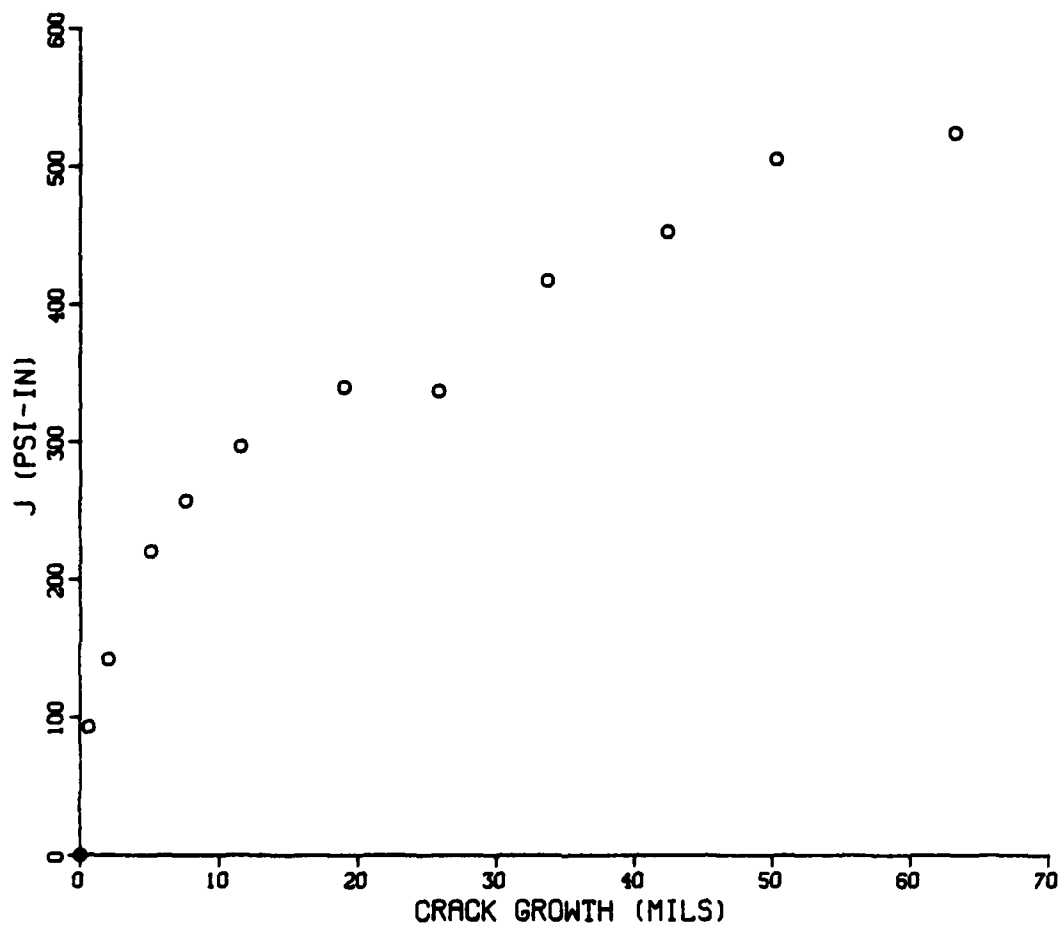


Figure C1(a). Plot of Crack-Growth as a Function of J for 5083-0 Aluminum (Refs. 16, 25): Cartesian Coordinates.

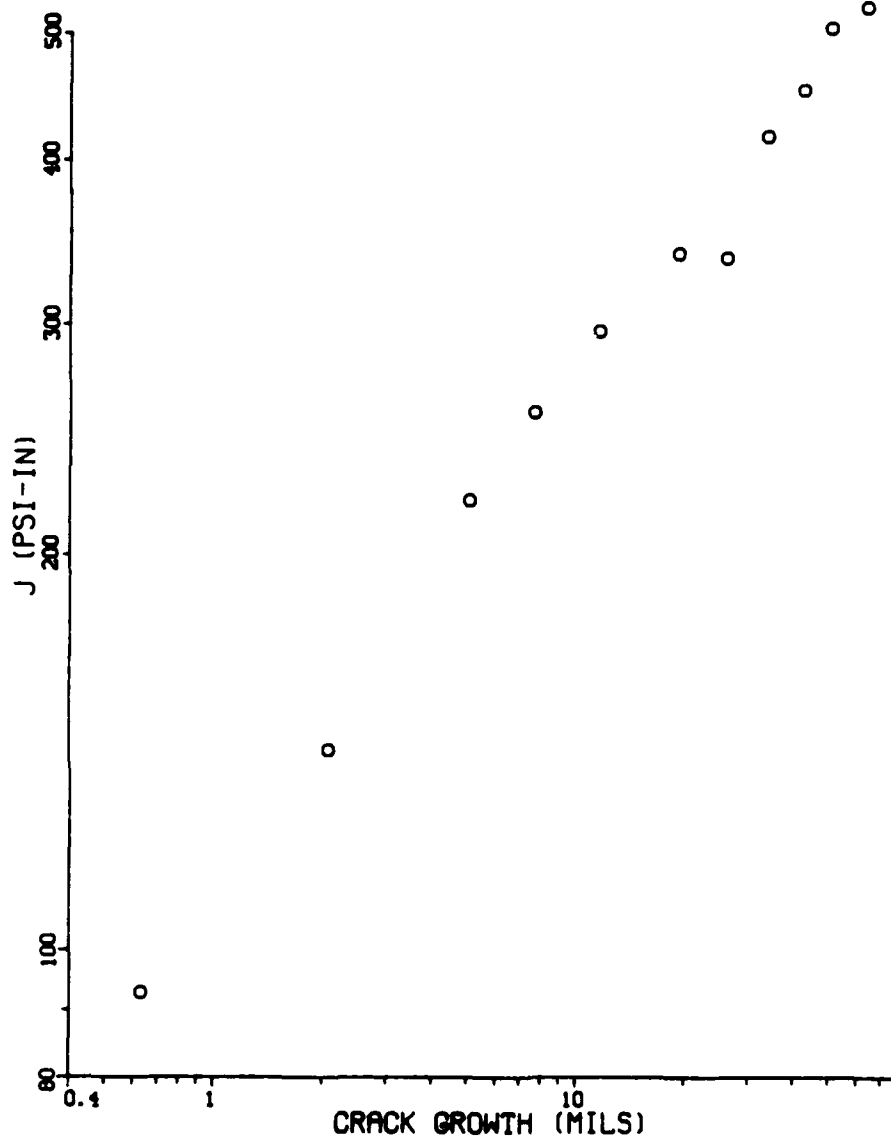


Figure C1(b). Plot of Crack-Growth as a Function of J for 5083-0 Aluminum (Refs. 16, 25): Log-Log Coordinates.

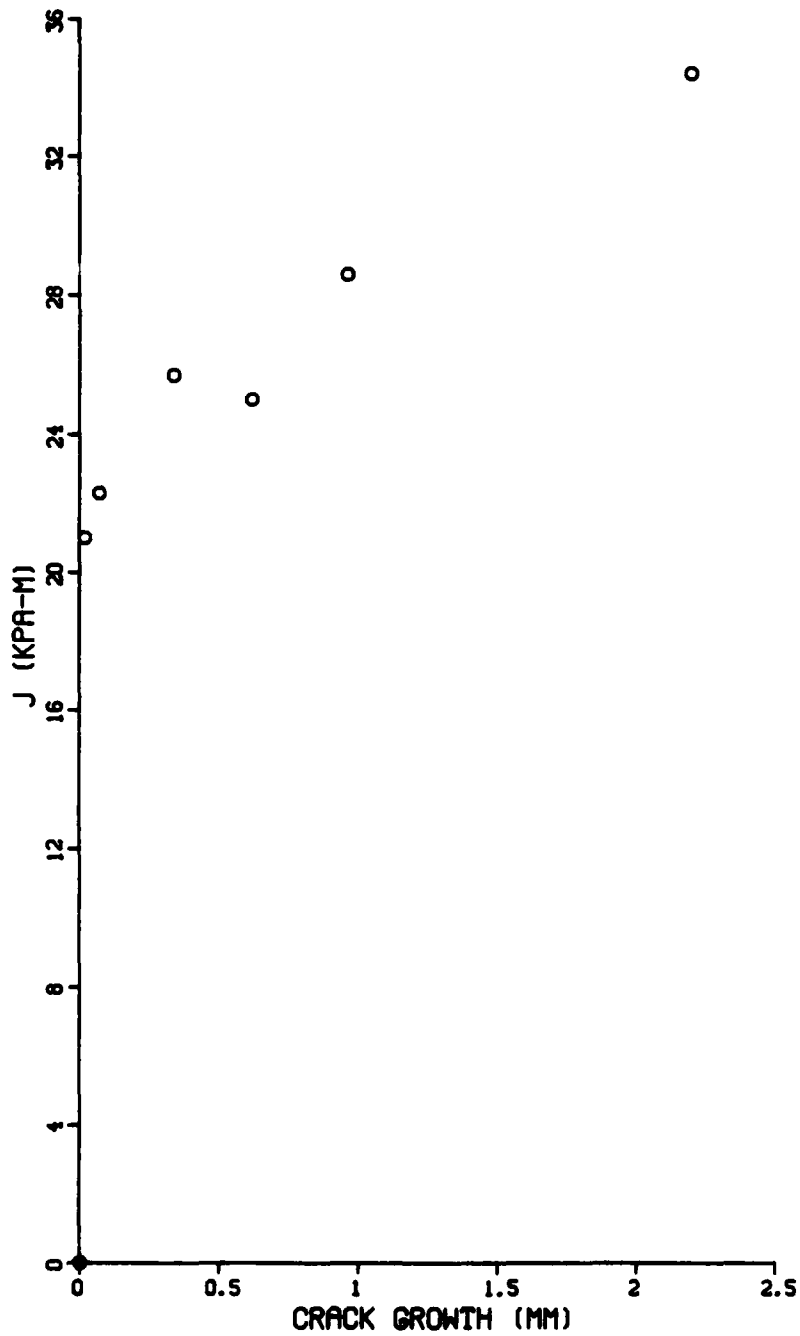


Figure C2(a). Plot of Crack-Growth as a Function of J  
for 7005-T6351 Aluminum (Ref. 10):  
Cartesian Coordinates.

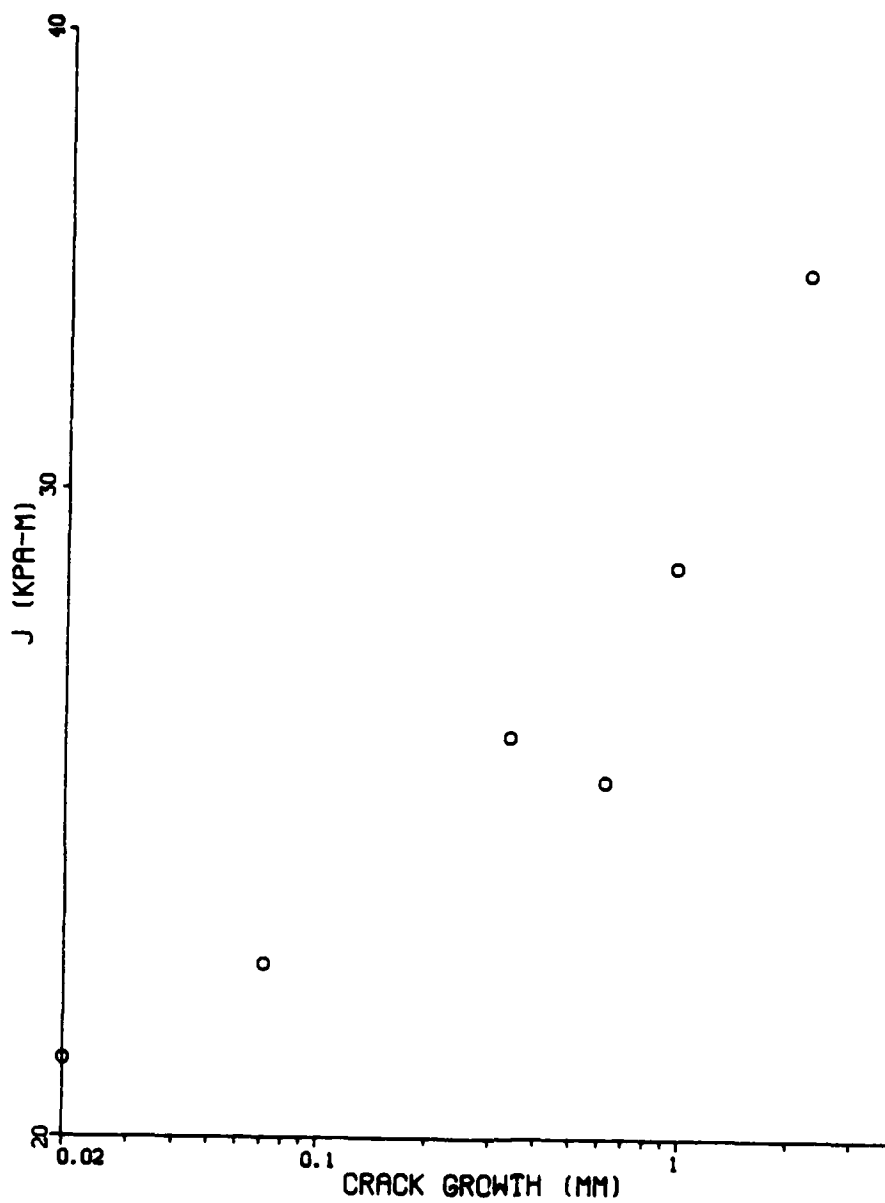


Figure C2(b). Plot of Crack-Growth as a Function of J for 7005-T6351 Aluminum (Ref. 10): Log-Log Coordinates.

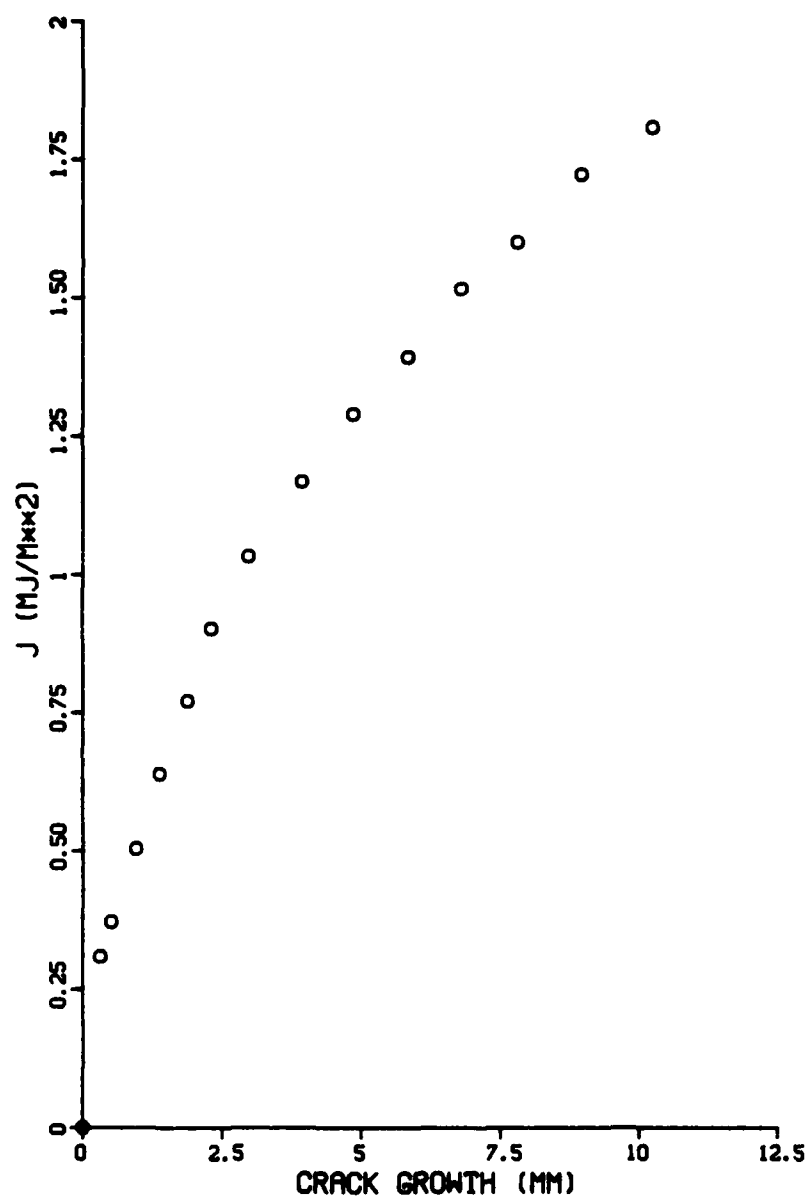


Figure C3(a). Plot of Crack-Growth as a Function of J for A533B Steel (Ref. 17): Cartesian Coordinates.



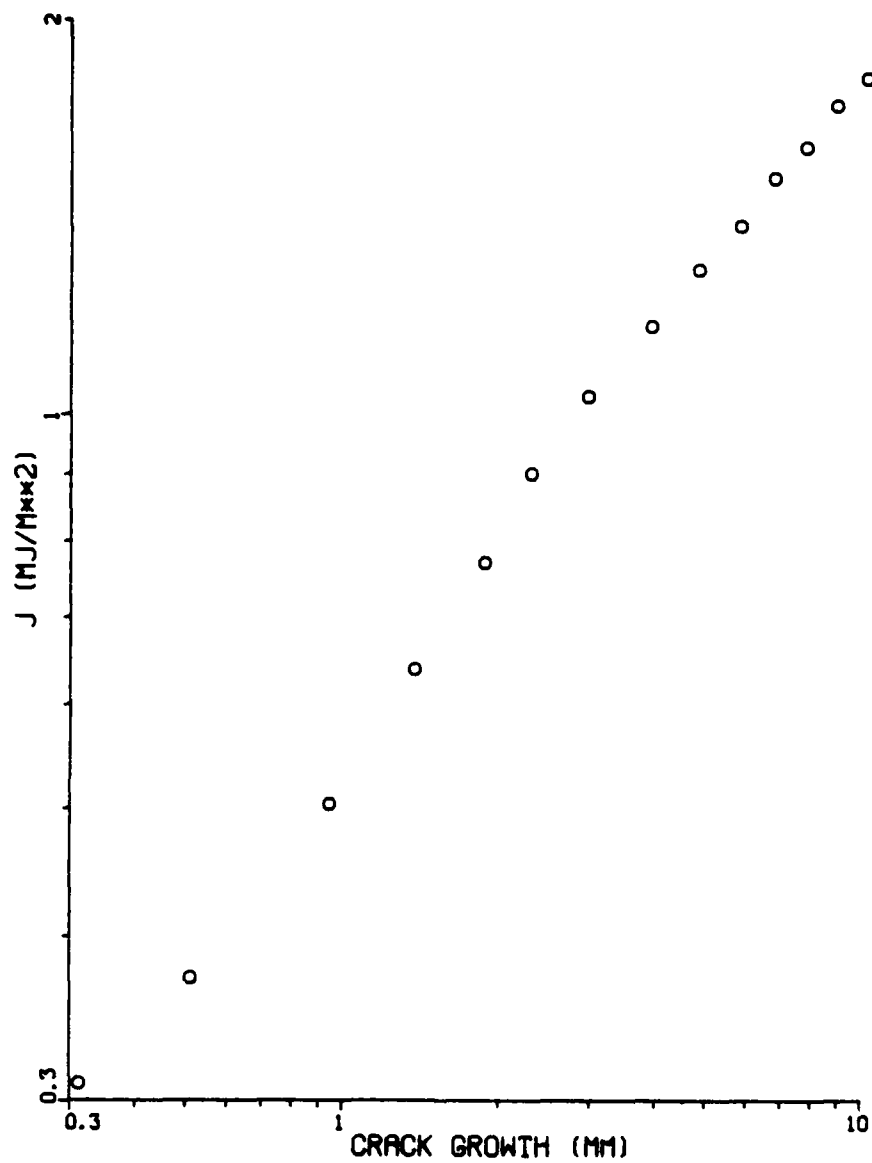


Figure C3(b). Plot of Crack-Growth as a Function of J for A533B Steel (Ref. 17): Log-Log Coordinates.

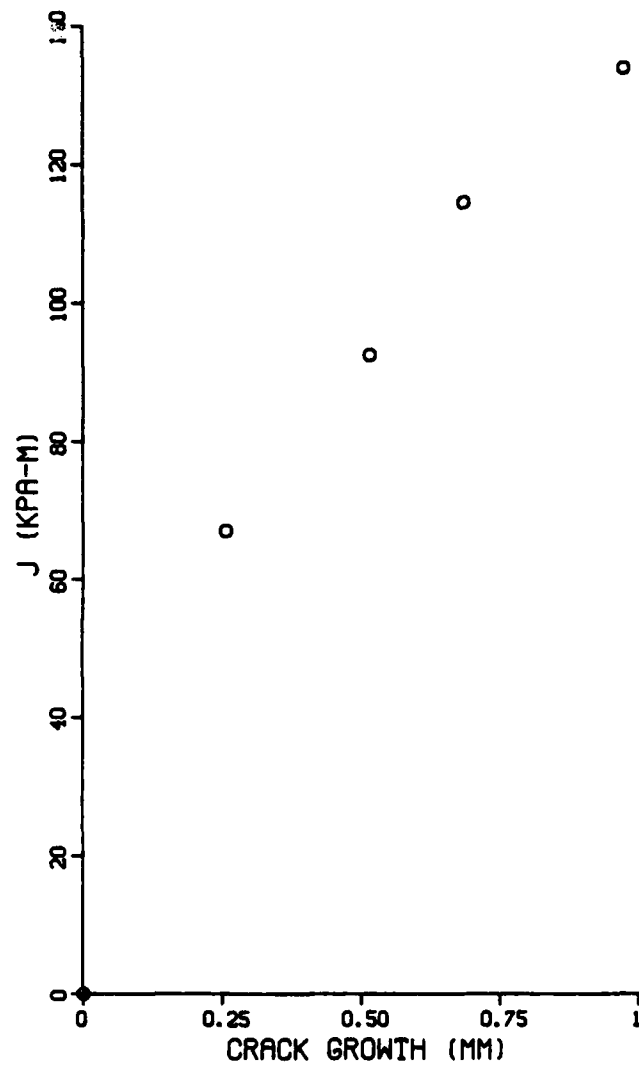


Figure C4(a). Plot of Crack-Growth as a Function of J for Ti-7Al-2Cb-1Ta Titanium (Ref. 19): Cartesian Coordinates.

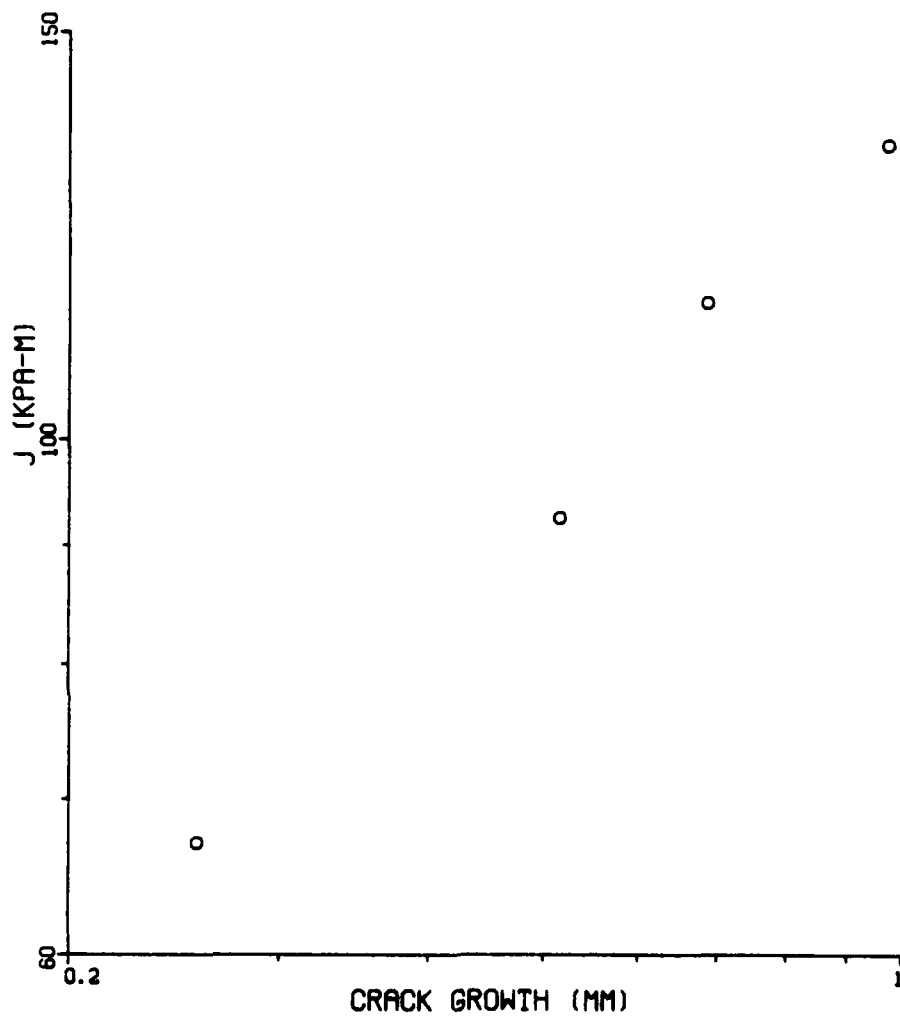


Figure C4 (b). Plot of Crack Growth as a Function of J for Ti-7Al-3Cb-1Ta Titanium (Ref. 19): Log-Log Coordinates.

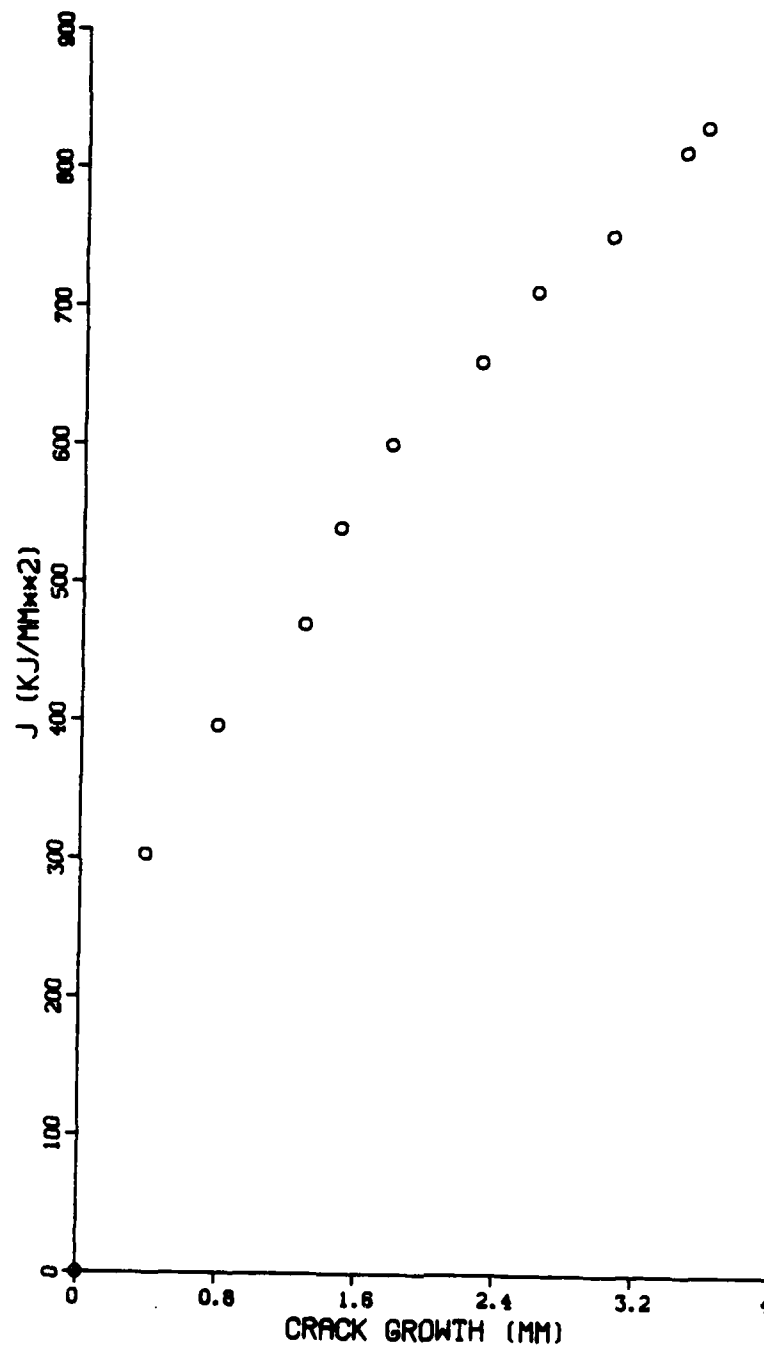


Figure C5(a). Plot of Crack Growth as a Function of J for A533B Steel (Ref. 14): Cartesian Coordinates.

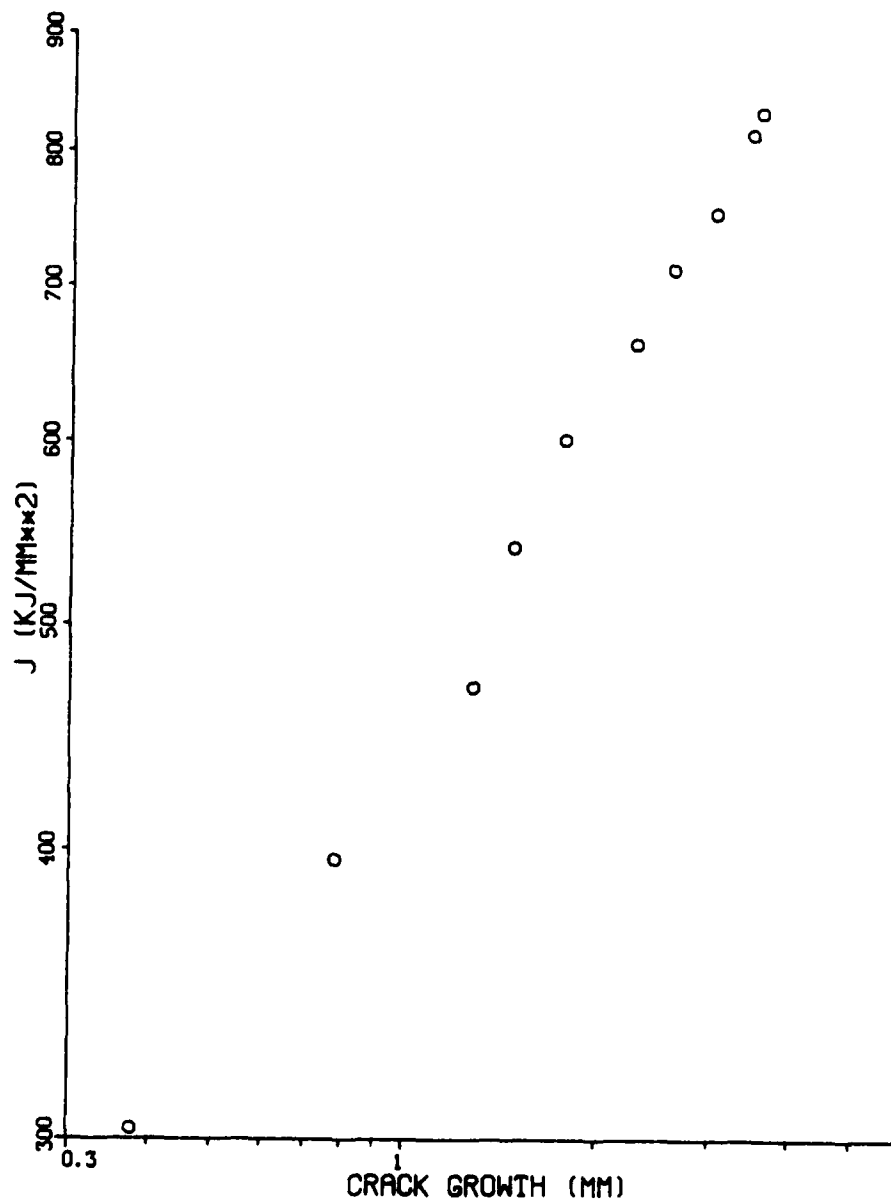


Figure C5(b), Plot of Crack Growth as a Function of J for A533B Steel (Ref. 14): Log-Log Coordinates.

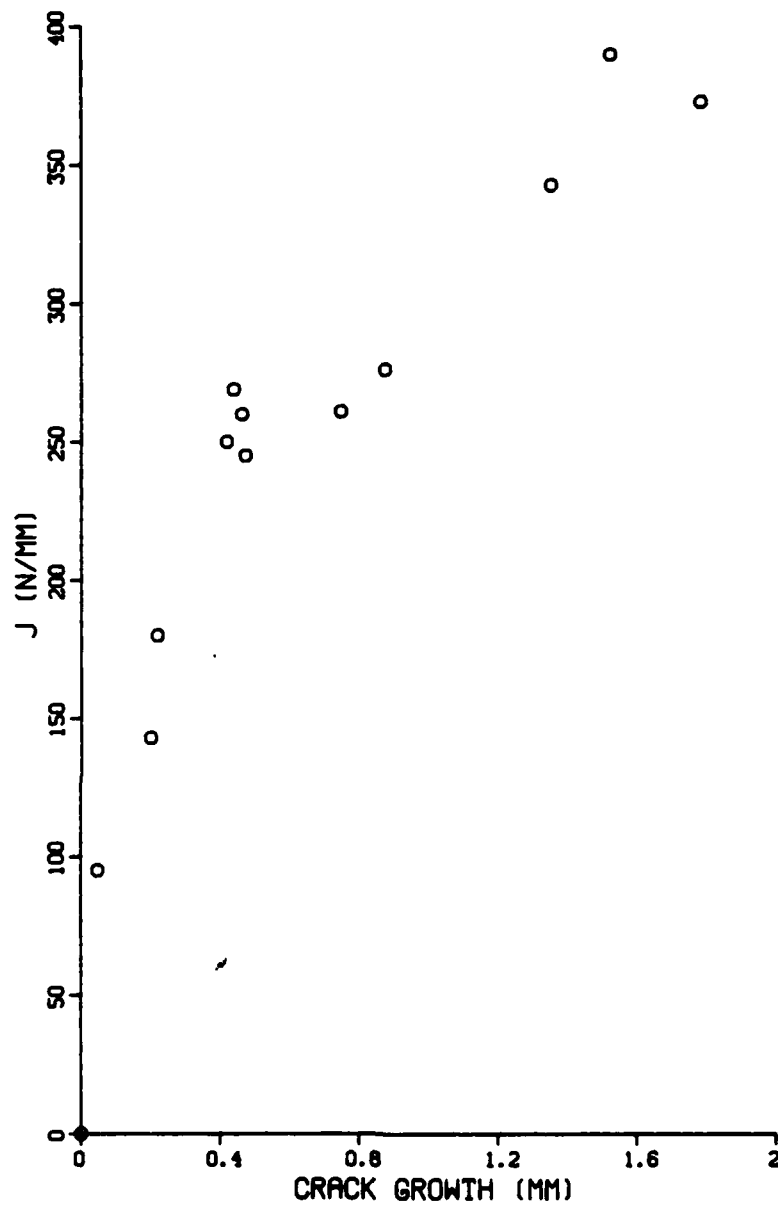


Figure C6(a). Plot of Crack-Growth as a Function of J for Ni-Cr-Mo Steel (Ref. 18): Cartesian Coordinates.

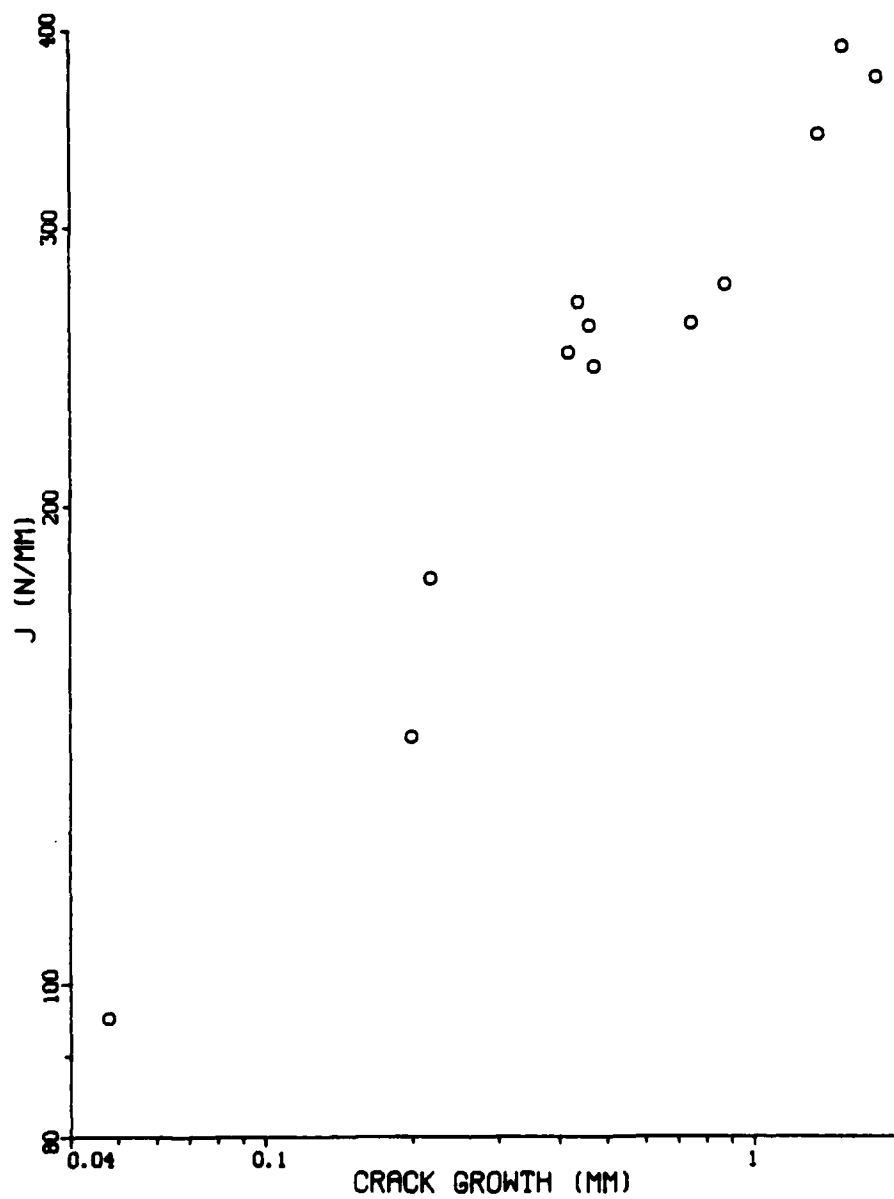


Figure C6(b). Plot of Crack-Growth as a Function of J for Ni-Cr-Mo Steel (Ref. 18): Log-Log Coordinates.